Dissertation

submitted to the

Combined Faculty of Natural Sciences and Mathematics

of Heidelberg University, Germany

for the degree of

Doctor of Natural Sciences

Put forward by

Moritz Drescher

Born in Konstanz, Germany

Oral examination: 30 July 2020

Dynamics of a Strongly Interacting Impurity in a Bose-Einstein Condensate

Referees: Priv.-Doz. Dr. Tilman Enss

Prof. Dr. Thomas Gasenzer

Zusammenfassung

Das Bose-Polaron-Problem befasst sich mit einem Fremdteilchen in einem Bose-Einstein-Kondensat und ist ein Repräsentant des allgemeinen Konzepts eines Teilchens im Medium. Die vorliegende Doktorarbeit behandelt die Theorie der Bose-Polaronen mit Schwerpunkt auf dem Bereich starker Wechselwirkung zwischen Fremdteilchen und Kondensat, der den Übergang zwischen attraktiver und repulsiver Streuung entlang einer Streuresonanz bildet. Wir behandeln den Fall eines schweren Fremdteilchens in einem idealen Kondensat analytisch, um detaillierte Erkenntnisse über die Entstehung der Vielteilchenphysik aus der Zweiteilchenphysik zu gewinnen, und leiten die exakte Lösung der Zeitentwicklung her. Das wechselwirkende Bosegas wird mit der verbreiteten Bogoliubov-Methode behandelt, was zu einer Theorie führt, die über das klassische Fröhlich-Modell der Polaronen hinausgeht. Für starke Wechselwirkung stellt sich heraus, dass die Bogoliubov-Beschreibung nicht länger anwendbar ist und wir leiten eine neue Theorie stark deformierter Kondensate in Form einer nicht-lokalen Erweiterung der Gross-Pitaevskii-Theorie her. Der gebundene Zustand zwischen Fremdteilchen und Boson, den es für repulsive Wechselwirkung gibt, erweist sich als verantwortlich für langlebige Oszillationen in verschiedenen Observablen wie der Anzahl vom Fremdteilchen angezogener Bosonen, dem Tan-Kontakt und dem Dichteprofil des Kondensats um das Fremdteilchen. In Letzterem ist ein bemerkenswerter Halo reduzierter Dichte zu sehen, der periodisch eine Dichte von Null in einem festgelegten Abstand zum Fremdteilchen erreicht. Polaron-Trajektorien zeigen, dass sich das Fremdteilchen für attraktive Wechselwirkung letztendlich wie ein freies Quasiteilchen mit höherer effektiver Masse bewegt, während für repulsive Wechselwirkung Oszillationen in der Geschwindigkeit auftreten, die zu Stop-and-Go-Verhalten führen. Nahe der Im-Medium-Resonanz wird ein dynamischer Übergang von repulsivem zu attraktivem Polaron beobachtet.

Abstract

The Bose polaron problem is concerned with an impurity particle moving through a Bose-Einstein condensate, which is an instance of the general concept of a particle in medium. This dissertation investigates the theory of the Bose polaron with a focus on the region of strong coupling between impurity and condensate that marks the transition between attractive and repulsive scattering processes as a scattering resonance is crossed. We use an analytical study of a heavy impurity in an ideal condensate to obtain detailed insights on the emergence of many-body physics from two-body physics and derive the exact solution of the time evolution. The interacting Bose gas is treated by the widely-adopted Bogoliubov method, which results in a theory beyond the classical Fröhlich description of polarons. At strong coupling, the Bogoliubov description is found to be no longer applicable and a new theory for strongly deformed condensates is derived in the form of a non-local extension of Gross-Pitaevskii theory. We find that the impurity-boson bound state that exists for repulsive coupling is responsible for long-lived coherent oscillations in a number of observables, such as the number of bosons attracted by the impurity, Tan's contact and the density profile of the condensate around the impurity. The latter exhibits a remarkable depletion halo, which periodically reaches zero density at a certain distance to the impurity. Polaron trajectories show that the impurity eventually moves like a free quasi-particle with enhanced effective mass for attractive coupling and present velocity oscillations on the repulsive side, leading to stop-and-go motion. Close to the in-medium resonance, a dynamical transition from a repulsive to an attractive polaron is observed.

Contents

Chapter 1

Introduction

When a quantum mechanical particle moves through a medium, it may interact with the elementary excitations of the medium in such a way that the combination of particle and excitations forms a single quasi-particle. This concept is of a very general nature and occurs in a broad range of physical contexts: An electron moving through an ionic crystal lattice displaces the surrounding ions and polarises the lattice. The resulting quasi-particle, the polaron, is the elementary charge carrier in these crystals. An impurity atom moving through an ultracold gas becomes "dressed" with phononic excitations, a situation which allows for highly controllable experiments. The general concept of a particle immersed in a medium includes fundamental effects such as the Higgs mechanism and even the quantum mechanical vacuum may serve as a medium: the dressing of electrons by virtual phonons results in renormalised electron properties and the Lamb shift. The connection to ultracold gas experiments has been drawn recently, by measurement of the *phononic Lamb shift* of trapped atoms, with a surrounding Bose-Einstein condensate (BEC) serving as *synthetic vacuum* [Ren+16].

The concept of polarons was first introduced by Pekar and Landau [Lan33; Pek46b; Pek46a; Pek47; Pek48; LP48] in the context of electrons moving through a crystal lattice. They realised that the present theory of conductivity was insufficient in that it considered the lattice ions as fixed, giving rise to a static periodic potential for the conduction electrons. In reality, the ions are displaced by the presence of the electrons. At first, it was hypothesised that by this displacement, an effective potential for the electron would be created in which it would come to rest, so that the electron would be caught in a trap of its own making, an effect known as self-localisation. It turned out that the electron is never fully trapped but that it keeps moving, dragging the lattice polarisation along with it. The ensemble of the electron and the lattice deformations around it can be described as a quasi-particle with a higher effective mass than an electron: a dressed electron which was called polaron by Pekar.

The concept of dressing a particle moving through a medium with quasi-particle excitations and the question of self-localisation have found their generalisation in different areas of physics. A rather new field

of study investigates ultracold quantum gases as medium, in which individual impurity atoms or ions of a different species or different internal state become dressed by elementary excitations of the surrounding gas. Depending on whether the gas consists of fermions or bosons, one speaks of a Fermi or Bose polaron, respectively. The great interest that these systems attract originates in the high amount of control that is available in ultracold gas experiments. While for the classical solid-state polaron, the strength of interactions is fixed by nature, the discovery of Feshbach resonances enables experiments in which the coupling can be controlled by a magnetic field. The high values that can be reached by this method enable the investigation of new regimes for which interesting effects had been predicted already by works on the solid-state polaron.

The Fermi polaron has been intensively studied in the context of the unitary Fermi gas and the BEC-BCS crossover [Zwe12]. Here, the two spin states of a fermionic atom species form a bipartite atomic mixture in a natural way. If such a gas is partly polarised, the mixture becomes unbalanced and in the limit of strong imbalance, the physics of individual particle in a medium dominates the behaviour.

In a bosonic gas, impurities are usually particles of a different atom species or different isotopes. The increased tendency of bosons towards collective behaviour promises new and interesting effects. A competition occurs between two entirely different points of view: On one hand, an impurity in a low-density gas will always have only a limited number of host atoms in its vicinity and the few-body physics should dominate the behaviour. On the other hand, bosons are not favourable for localisation into separate regions of space, but form a condensate of macroscopic size, which interacts with the impurity as a single collective mode.

In this dissertation, we follow the route to understand this competition, to gain insights on the effect of a medium on a particle and, conversely, to understand how a condensate reacts to a strong local perturbation.

1.1 Related Works and Summary of Results

Many aspects of the Bose polaron have already been studied theoretically and some experiments have achieved the realisation of the Bose polaron. This section lists previous works on the topic and summarises the new results that this dissertation contributes to the field.

We start with some of the most relevant classical works on polaron physics.

- In 1933, Landau [Lan33] observed that when electrons move through a crystal lattice with defects, they may be either scattered off or enter bound states. His theory is highly relevant for a large number of effects, for example colour centres in crystals, but also polarons where lattice defects are introduced by the electrons themselves.

- Pekar [Pek46a; Pek46b; Pek47; PD48; Pek48] realised the necessity to account for lattice deformations by conduction electrons and

introduced the polaron as elementary charge carrier. A particularly important work is the joint paper of Landau and Pekar [LP48].

- Lee, Low, Pines [LLP53] and Fröhlich [Frö54] introduced a second-quantised formulation and the famous Fröhlich Hamiltonian that is widely used in polaron physics and still topic of theoretical developments. A review was given by Devreese and Alexandrov [DA09].
- In [LLP53], a canonical transformation, the LLP transformation, was presented that its applicable to many situations of particles in medium.
- Feynman [Fey55] derived a particularly successful treatment of the Fröhlich Hamiltonian by path integrals. His method has been adapted to many polaronic contexts.

For the Bose polaron, experimental realisation became possible only recently. The following results were obtained.

- By means of tightly confined atoms weakly coupled to a BEC, the effect of the bath on the impurity particles was investigated [Sce+13; Ren+16] and the *phononic Lamb shift* was measured.
- With strongly imbalanced two-component mixtures in presence of a magnetic field tuned to a Feshbach resonance, RF spectra and polaron energies were measured at strong coupling [Hu+16; Jør+16; Peñ+19; Yan+20].
- Rydberg atoms as impurities in BECs were realised in [Cam+18].
- Recently, the coherence dynamics in presence of a Feshbach resonance was measured [Sko+20].

Theoretically, the Bose polaron attracts significant attention in recent times.

- The first investigation of an impurity in a BEC dates back to 1961 [Gir61] and was directly motivated by the advances in solid-state polaron physics that had been made.
- Interest renewed when the experimental realisation of Bose polarons came within reach. Many early works focused on the concept of self-trapping by describing the BEC density variation via the Gross-Pitaevskii equation to which a separate impurity wave function is coupled [AP04; CT06; KB06; BBJ08; BBT13; MPS05; Tak+19]. The resulting spatial density distributions of impurity and bosons provide information on the impurity localisation for weak coupling.
- A direct connection to the classical solid-state polaron can be drawn by describing the Bose polaron via a Fröhlich-type Hamiltonian, which can be derived from a Bogoliubov-description of the BEC when the impurity-boson (IB) coupling is small.

  - A variety of methods has been developed for the Fröhlich Hamiltonian and quasi-particle properties such as the effective mass and the energy have been computed [ST06; HW09; Tem+09; Cas+11; CTD12; Sha+14; Gru+15; Gru16; KL16; Shc+16a].
  - Polaron trajectories were obtained in [DK13; Gru+18].
  - A different method was presented in [Lam+17], where the impurity motion was described as quantum Brownian motion with a memory kernel.
  - Dynamics of decoherence, correlations and entanglement between impurity and bath were investigated by [Nie+19] and [Boy+19].
  - [Vli+15] *et al.* employed diagrammatic Monte Carlo methods and found a discrepancy to results obtained from Feynman's approach for the Bose polaron, even though the approaches agree well for the acoustic polaron.
  - For a review of the Fröhlich Hamiltonian in the context of the Bose polaron we refer to [GD16].

- Numerically exact quantum Monte Carlo calculations [PG15] provide insights on the ground state properties, including the energy and effective mass as well as density profiles of the condensate around the impurity.

- Finite-temperature results are limited in number and predict a qualitative change in the impurity's properties when the critical temperature is crossed [Bou14; SSD16; SZC17; Lev+17; Gue+18]. Cooling dynamics were investigated in [LWF18].

- The possibility of many-body bound states and Efimov physics has been investigated with variational wave functions with a limited number of excitations [LPB15; SZC17; Shi+18; Yos+18]. Such states with two or more excitations are able to include the three-body (four-body, etc.) physics in full detail in regions where not more excitations are expected.

- [SL15] found that also rotational properties of the impurity are renormalised by the medium.

- A different method consisting of a multi-layer multi-configuration time-dependent Hartree method was presented in [Mis+19].

- At stronger IB coupling, the description of the impurity-BEC system by the Fröhlich polaron becomes inaccurate as was first observed in [RS13]. Instead, second-order terms in the IB coupling that arise in the Bogoliubov description need to be taken into account. This also allows for the existence of a bound state, which is absent in the Fröhlich model. The resulting model was adopted in an number of works [RS13; LD14; CLB15; GAD17; Sch+18].

  - [VHZ15] compute time-dependent impurity density profiles for the case of an ideal BEC.
  - [Shc+16b] compute the resulting RF spectrum across a Feshbach resonance.
  - Three regimes of qualitatively different dynamical behaviour were found in [Gru+17; KL18]: between the weak-to-intermediate-coupling attractive and repulsive regions, a dynamically unstable region was found within the approximations employed.

- In 1D, additional effects such as quantum flutter [MZD12] occur and special techniques may be employed [VH17; Cat+12], which, however, do not carry over to higher dimensions.

This dissertation makes the following new contributions. The essential results are published in [DSE19; DSE20].

- An analytical study of an infinite-mass impurity and an ideal BEC improves the understanding of the relation between the two-body physics between impurity and one boson and the many-body physics of impurity and BEC. Qualitative differences in the time-evolution are explained as being related to many-body bound states and to the zero-energy mode taking a role similar to a bound state. This leads to oscillations that can be seen in a large class of observables. The many-body spectrum is explained in terms of contributions from the different parts of the two-body spectrum.

- A moving impurity is considered in a framework which allows for stronger coupling than preceding works and in particular for accessing both sides of a resonance. The repulsive side is found to exhibit particularly interesting trajectories.

- Within the same approach, dynamical density profiles are computed which provide intuitively accessible information on the polaron formation.

- The number of bosons attracted by the impurity is used to quantify the polaron size as it evolves in time for a wide range of couplings.

- An analytical argument shows how the oscillations found for the non-interacting Bose gas remain stable and undamped in an interacting gas described by Bogoliubov theory. A formula for the computation of the frequencies is derived.

- It is argued that the dynamical instability found in [Gru+17] at strong coupling is inherent to Bogoliubov theory and not related to a specific ansatz. This shows the necessity to find a new theoretical treatment when the deformation of the BEC by a near-resonantly interacting impurity becomes too large.

- We provide such a treatment by deriving a new non-local extension to Gross-Pitaevskii theory. The resulting theory remains stable at all couplings across a resonance.

- In the course of deriving this treatment, we prove a general theorem about expectation values of operators with respect to Jastrow functions.

- We analyse the strong-coupling region between attractive and and repulsive side and find that close to the critical point, a transition occurs also dynamically in that initial repulsive features vanish in favour of attractive ones.

- We find that the range of the interaction potentials, in addition to the scattering length, becomes important as the condensate deformation is increased and, in particular, that it sensitively affects the position of the in-medium resonance.

1.2 Outline

The remainder of this introduction contains short outlines of the main chapters and an overview over notational conventions. The ensuing main text is organised in two parts.

In part I, we review background knowledge required for the understanding of the following. This is mostly elementary and we shall try to focus on those points, which directly connect to points made in the results section of the dissertation. Three topics are covered: *(i)* Basic concepts of scattering theory with a focus on the zero-energy scattering state, which is of great importance to the impurity-BEC problem, and on the contact potential, which we will employ frequently and whose peculiarities must be well-understood. *(ii)* The successful and widely adopted theories of the Bose gas that Bogoliubov theory (BT) and Gross-Pitaevskii theory (GPT) constitute. *(iii)* The Lee-Low-Pines (LLP) transformation as a general technique for particles in media is discussed and applied to the Bose polaron. This chapter introduces the general problem treated in part II.

Part II is the main part of this work and contains the new techniques and results developed and obtained. It is structured in three chapters with the following contents.

Heavy Impurity in an Ideal BEC

In the first chapter, we treat the *a priori* simple case of an infinitely heavy impurity and a non-interacting Bose gas. It is solved exactly by a product state ansatz in terms of two-body (impurity-boson) eigenstates. Despite its simplicity, many important properties of the Bose polaron can already be understood within this framework. For the case of an impurity-boson contact potential, we will be able to solve the time evolution analytically. By means of a numerically exact RF spectrum, the relation between the spectral properties of the two-body system on one hand and those of the many-body system on the other hand are discussed.

The Bose Polaron in Bogoliubov Approximation

The second chapter makes use of the widely adopted Bogoliubov description of the condensed Bose gas.

By using a Hamiltonian, which goes beyond the classical Fröhlich Hamiltonian from solid state physics (c.f. [RS13]), the dynamics of both the attractive and the repulsive side of a scattering resonance are investigated. The mean-field solution and the different qualitative regions (see [Gru+17]) are reviewed. Of the above-mentioned results, this chapter contains the computation of polaron trajectories, dynamical density profiles and boson numbers as well as the analytical treatment of oscillations and the discussion on the applicability of Bogoliubov theory at very strong coupling.

The Strong-Coupling Bose Polaron: A Non-Local Extension of Gross-Pitaevskii Theory

Previous technical developments allowed to extend the tractable parameter region of the Bose polaron problem by developing new methods to treat the Fröhlich and beyond-Fröhlich Hamiltonians. Yet the region of strongest coupling that marks the transition from attractive to repulsive coupling across a resonance remained inaccessible. In the third chapter, we develop the new technique that is able to fill this gap. It contains the theorem on Jastrow functions and its proof, the non-local extension of Gross-Pitaevskii theory and the results obtained with it, which are the transition across a resonance and the dependence of the in-medium shift of the resonance on the potential range.

1.3 Notation and Conventions

The following conventions are employed throughout.

- Units in which $\hbar = 1$ are used.
- Vectors are written in bold, their absolute values non-bold.
- Position and momentum arguments to functions are frequently written as subscripts. Subscripts are also used for indicating integration variables, where integration is understood to be performed over a three-dimensional volume $\mathscr{V}$:

$$\int_{\boldsymbol{x},\boldsymbol{y}} f_{\boldsymbol{x}} g_{\boldsymbol{y}} \delta^3_{\boldsymbol{x}-\boldsymbol{y}} = \int_{\mathscr{V}} \mathrm{d}^3\boldsymbol{x} \int_{\mathscr{V}} \mathrm{d}^3\boldsymbol{y}\, f(\boldsymbol{x}) g(\boldsymbol{y}) \delta^3(\boldsymbol{x}-\boldsymbol{y}).$$

- For momentum space discussions, it is usually assumed that volume is infinite and momentum space thus continuous. Integrals are denoted by $\fint$, which indicates division by $(2\pi)^d$:

$$\fint_{\boldsymbol{k}} f_{\boldsymbol{k}} = \int_{\mathbb{R}^3} \frac{\mathrm{d}^3\boldsymbol{k}}{(2\pi)^3} f(\boldsymbol{k}).$$

A superscript Λ indicates a momentum cutoff in the context of a contact potential:

$$\fint_{\boldsymbol{k}}^{\Lambda} \cdot = \fint_{\boldsymbol{k}} \cdot f(k/\Lambda)$$

with a cutoff function f. If volume is explicitly assumed finite, integral symbols are interpreted as scaled sums:

$$\fint_{\boldsymbol{k}} f_{\boldsymbol{k}} = \frac{1}{\mathscr{V}} \sum_{\boldsymbol{k}} f_{\boldsymbol{k}}$$

and

$$(2\pi)^3 \delta^3_{\boldsymbol{k}-\boldsymbol{q}} = \mathscr{V} \delta_{\boldsymbol{k},\boldsymbol{q}}.$$

- $\mathscr{F}$ denotes the Fourier transform operator, scaled such as to represent transformation from position to momentum or from frequency to time.

$$(\mathscr{F} f)(\boldsymbol{k}) = \int_{\boldsymbol{x}} e^{-i\boldsymbol{k}\cdot\boldsymbol{x}} f(\boldsymbol{x}) \qquad (\mathscr{F}^{-1} g)(\boldsymbol{x}) = \fint_{\boldsymbol{k}} e^{i\boldsymbol{k}\cdot\boldsymbol{x}} g(\boldsymbol{k})$$
$$(\mathscr{F} A)(t) = \int_{\mathbb{R}} \mathrm{d}\omega\, e^{-i\omega t} A(\omega) \qquad (\mathscr{F}^{-1} S)(\omega) = \fint_{\mathbb{R}} \mathrm{d}t\, e^{i\omega t} S(t).$$

- $\hat{a}^{(\dagger)}$ are the field operators of the bosonic bath. We use the same symbol for position and momentum space representations (to be distinguished by argument name) and independently of whether the argument is continuous or discrete:

$$\hat{a}_{\boldsymbol{k}} = \int_{\boldsymbol{x}} e^{-i\boldsymbol{k}\cdot\boldsymbol{x}} \hat{a}_{\boldsymbol{x}}$$
$$[\hat{a}_{\boldsymbol{x}}, \hat{a}^\dagger_{\boldsymbol{y}}] = \delta^3(\boldsymbol{x}-\boldsymbol{y})$$
$$[\hat{a}_{\boldsymbol{k}}, \hat{a}^\dagger_{\boldsymbol{q}}] = (2\pi)^3 \delta^3(\boldsymbol{k}-\boldsymbol{q}).$$

  $\hat{b}^{(\dagger)}$ are the Bogoliubov mode (phonon) operators; $\hat{c}^{(\dagger)}$, $\hat{d}^{(\dagger)}$ other operators obtained through canonical transformations of $\hat{a}^{(\dagger)}$ in specific contexts.

  The boson vacuum is denoted by $|0\rangle$, the vacuum state for different modes by $|0_{\hat{b}}\rangle$ etc.

  For a single-particle wave function $\psi(\boldsymbol{x})$, we will occasionally define the creator of a particle in this state $\hat{\psi}^\dagger = \int_{\boldsymbol{x}} \psi_{\boldsymbol{x}} \hat{a}^\dagger_{\boldsymbol{x}}$.

- $\bar{z}$ denotes the complex conjugate of z, $A^\dagger$ the adjoint of A.

- $\mathrm{He}\, A = (A + A^\dagger)/2$ and $\mathrm{Ah}\, A = (A - A^\dagger)/2i$ are the hermitian and anti-hermitian part of an operator.[1] Note that both are hermitian operators.

[1] For a normal operator A, this corresponds to $\mathrm{Re}\, A$ and $\mathrm{Im}\, A$ as defined by functional calculus. For non-normal A, however, common calculation rules for "Re" and "Im" may fail, as in $\mathrm{He}(\hat{a}\,\mathrm{He}(\hat{a})) \neq \mathrm{He}(\hat{a})\,\mathrm{He}(\hat{a})$.

- Juxtaposed multiplication has higher precedence than division, as in $p^2/2m$.
- $\mathbb{1}(\textit{condition}) = 1$ if *condition* fulfilled, 0 else.

Some more specialised shortening notations are used in specific contexts and explained there.

1.3.1 Common Symbols and Abbreviations

The following abbreviations are used often:

- BEC: Bose-Einstein condensation
- IB: Impurity-boson
- BB: Boson-boson
- BT: Bogoliubov theory
- GP, GPT, GPE: Gross-Pitaevskii (theory, equation)
- RF: Radio-frequency (spectroscopy)
- UV: Ultraviolet (in the sense of high momentum in integrals)
- LLP: Lee-Low-Pines
- LSY: Lieb-Seiringer-Yngvason

In formulae, indices I and B stand for impurity and bosons, respectively, as in the impurity position $\boldsymbol{x}_\mathrm{I}$. The following symbols are encountered frequently:

- $a_\mathrm{IB}, a_\mathrm{BB}$: IB and BB scattering lengths.
- $m_\mathrm{I}, m_\mathrm{B}, m_\mathrm{red}$: Masses of impurity and boson and their reduced mass $m_\mathrm{red}^{-1} = m_\mathrm{I}^{-1} + m_\mathrm{B}^{-1}$. In the chapter on scattering theory, m_red is a general reduced mass, which can also mean the BB reduced mass in applications.
- $V^\mathrm{IB}, V^\mathrm{BB}, v^\mathrm{IB}, v^\mathrm{BB}, V^\mathrm{ext}$: Interaction potentials in position space (V) and momentum space (v); external potential.
- N: Number of bosons.
- $\mathscr{V}$: Volume, often taken to be $\mathbb{R}^3$.
- n, n_0: Density of Bose gas and condensate density.

Other symbols are defined in their contexts.

Part I

Background

Chapter 2

Scattering Theory

The theory of two-body quantum mechanics, known as scattering theory, is of a double significance for the impurity-BEC problem.

(i) The properties of a low-density gas alone are dominated by two-body processes, such that scattering theory is fundamental for the theory of ultracold gases in general. In the Bose polaron problem, the two-body physics thus occurs in the form of *boson-boson* (BB) scattering processes. For an ultracold gas, only the low-energy states are important. Their effect can be characterised by a single number, the scattering length, while further details of the potential become unimportant.

(ii) Similarly, for the behaviour of an impurity in a gas, the two-body physics of the impurity and a single bath particle is important. This is particularly true when the bath particles are bosons, since then, the eigenstates of a single bath particle in vicinity of the impurity can be occupied by multiple bosons and even macroscopically. Hence the significance of the *impurity-boson* (IB) scattering for the problem. Since a low-temperature Bode gas is condensed in the zero-momentum mode, also the zero-energy mode of the IB scattering problem will be central.

In this chapter, we review basic concepts of scattering theory with a focus on the zero-energy mode and discuss the example of a square-well potential. Then, a particular choice of potential, the contact potential, is treated in detail. It will be employed widely in part II. Even though the material is mostly elementary, this constitutes the largest chapter of the background part. The reason for this is that even some of the most interesting features of the Bose polaron already have a direct correspondence in the IB scattering problem.

Further information on scattering theory can be found in textbooks, e.g. [Thi13; RS79]. Elementary properties in the context of the Bose gas are given in [Yng14; Lie+05]. The contact potential is treated in detail in [Alb+88].

2.1 Definition of the Scattering Length

The general two-body Hamiltonian for particles of masses m_1 and m_2 is

$$H = -\frac{\Delta_{\boldsymbol{x}_1}}{2m_1} - \frac{\Delta_{\boldsymbol{x}_2}}{2m_2} + V(\boldsymbol{x}_1 - \boldsymbol{x}_2)\,,$$

acting on wave functions $\psi \in L^2(\mathbb{R}^3 \times \mathbb{R}^3)$ subject to

$$\psi(\boldsymbol{x}_1, \boldsymbol{x}_2) = \begin{cases} \psi(\boldsymbol{x}_2, \boldsymbol{x}_1) & \text{for identical Bosons} \\ -\psi(\boldsymbol{x}_2, \boldsymbol{x}_1) & \text{for identical Fermions} \\ \text{arbitrary} & \text{for distinguishable particles.} \end{cases}$$

Transforming to centre-of-mass and relative coordinates, the eigenfunctions take a product form $\psi(\boldsymbol{x}_1, \boldsymbol{x}_2) = \Psi(\boldsymbol{R})\phi(\boldsymbol{r})$ with $\boldsymbol{R} = \frac{\boldsymbol{x}_1 m_1 + \boldsymbol{x}_2 m_2}{m_1 + m_2}$, $\boldsymbol{r} = \boldsymbol{x}_1 + \boldsymbol{x}_2$ and

$$\begin{aligned} -\frac{\Delta_{\boldsymbol{R}}}{2(m_1+m_2)}\Psi(\boldsymbol{R}) &= E_1\Psi(\boldsymbol{R}) \\ \Big(-\frac{\Delta_{\boldsymbol{r}}}{2m_{\text{red}}} + V(\boldsymbol{r})\Big)\phi(\boldsymbol{r}) &= E_2\phi(\boldsymbol{r}) \end{aligned} \tag{2.1}$$

where m_{red} is the reduced mass, $m_{\text{red}}^{-1} = m_1^{-1} + m_2^{-1}$, and

$$H\Psi \otimes \phi = (E_1 + E_2)\Psi \otimes \phi\,.$$

Scattering theory is concerned only with the relative wave function ϕ and we will assume $E_1 = 0$ in the following. The symmetry condition turns to

$$\phi(-\boldsymbol{r}) = \begin{cases} \phi(\boldsymbol{r}) & \text{for identical Bosons} \\ -\phi(\boldsymbol{r}) & \text{for identical Fermions} \\ \text{arbitrary} & \text{for distinguishable particles.} \end{cases}$$

In particular, the relative wave function for Fermions cannot be spherically symmetric, i.e. there is no s-wave scattering between identical Fermions.

In the context of ultracold gases, one is interested in the low-lying part of the spectrum of the relative Hamiltonian, which consists of

- the bound states, i.e. the normalisable states with negative energy.
- the low-energy scattering states, i.e. tempered distributions that are not L^2-functions but fulfil the eigenvalue equation for some energy $E > 0$.

Unless one is dealing with identical fermions, the lowest energies can be obtained for spherically symmetric (s-wave) states, which have no rotational energy. In this case, the Laplacian can be reduced to its s-wave part, $\Delta = r^{-1}\partial_r^2 r$. This formula is valid only for the regular and not for the distributional Laplacian, but (2.1) implies that ϕ has no pole at zero if V is a regular potential[1]. This implication must now be imposed

[1] This is different for the contact potential, which will be discussed in section 2.3

explicitly, or one would get additional and wrong solutions. For the s-wave states, it is convenient to define $u = r\phi$ which thus fulfils $u(0) = 0$. The Schrödinger equation then turns into

$$\left(-\frac{\partial^2}{\partial r^2} + V - E\right) u = 0\,.$$

2.1.1 Zero-Energy Solution and Scattering Length

The low-energy scattering states are, in fact, determined by the zero-energy state u_0,

$$(-\partial_r^2 + V)u_0 = 0\,, \tag{2.2}$$

alone. Often, it is referred to only as *the* scattering state and equation (2.2) as *the* scattering equation, implying energy zero. It will turn out to be central for the impurity-BEC problem.

If we assume, for simplicity, that the potential has a finite range r_V, the scattering solution outside the ball of this radius (denoted B_{r_V}) must be of the form

$$u_0(r > r_V) = const \cdot (r - a)\,. \tag{2.3}$$

The constant a is called the **(s-wave) scattering length**. It completely quantifies the scattering solution for distances larger than the potential range while telling little about smaller distances. In an ultracold gas, the potential range is the smallest length scale by far, typically around 1-10 nm compared to the mean-particle distance of more than 100 nm. In such a situation, only the long-range behaviour is important and the properties of the gas are universally determined by the scattering length, independent of the details of potential.

For purely repulsive potentials $V > 0$, the scattering length is always positive and smaller than r_V. For attractive potentials, it may be positive or negative and take arbitrarily large absolute values.

For a general potential, u_0 approaches the form in equation (2.3) as $r \to \infty$ and the scattering length is defined by [Yng14]

$$a = \lim_{r\to\infty} r - \frac{u_0(r)}{u_0'(r)}\,. \tag{2.4}$$

Except for some specific potentials, it is impossible to compute a exactly, since this involves solving the second-order differential equation (2.2)[2].

2.1.2 Low-Energy States and Scattering Phase

The non-zero- but low-energy s-wave scattering states fulfil, again assuming a finite potential range r_V,

$$u_k(r) = const \cdot \sin(kr + \delta_k) \qquad (r > r_V)$$

[2] In fact, a first-order equation is sufficient: defining $\alpha(r) = r - u/u'$, α fulfils $\alpha' = V(r)(r-\alpha)^2$ with initial condition $\alpha(0) = 0$ and $\alpha(\infty) = a$. From this, one may also see that the potential is required to decay somewhat faster than r^{-3} to obtain a well-defined scattering length: for $V \sim r^{-3}$, one would get $\alpha' \sim r^{-1}$ and logarithmic divergence.

with a constant δ_k, the **scattering phase**, and energy $E = k^2/2m_{\text{red}}$. δ_k constitutes a shift of the wave compared to the case without potential: there, only $\delta_k = 0$ is possible due to the boundary condition at $r = 0$. For low energies, $k \approx 0$, we may obtain a relation to the scattering length by assuming that the boundary conditions at r_V vary continuously with k:

$$\frac{u_0(r_V)}{u_0'(r_V)} \approx \frac{u_k(r_V)}{u_k'(r_V)} .$$

The left-hand side is $r_V - a$, the right-hand side is

$$\frac{\sin(kr_V + \delta_k)}{k\cos(kr_V + \delta_k)} = \frac{\sin(\delta_k) + kr_V\cos(\delta_k) + \mathcal{O}(k^2)}{k\cos(\delta_k) + \mathcal{O}(k^2)} = \frac{\tan(\delta_k)}{k} + r_V + \mathcal{O}(k) ,$$

from which we get

$$a = \lim_{k\to 0} -\frac{\tan(\delta_k)}{k} .$$

This is another common definition of the scattering length. It shows that a (and therefore u_0) determines the entire low-energy scattering behaviour. Note that for $a > 0$, the wave functions u_k are shifted away from the centre (repulsive scattering) while for $a < 0$, they are shifted inwards (attractive scattering).

2.1.3 The Born Approximation

There exists an expansion of the scattering length in powers of the interaction potential V, that can be used approximatively when $\max_x V(x)$ is small, i.e. when v is sufficiently flat. It relies on comparing a scattering state ϕ_k with the corresponding state ϕ_k^0 of the free Hamiltonian $H_0 = -\Delta/2m_{\text{red}}$.

Assume first, that the volume Ω is finite, such that the scattering states are normalisable. By A' we denote the generalised inverse of a (non-invertible) matrix A, that projects out the subspace where A cannot be inverted before inverting it on the remaining subspace. It fulfils $A'A = AA' = 1 - \mathcal{P}_{\ker A}$ where $\mathcal{P}_{\ker A}$ is the projector onto the nullspace (kernel) of A. Applying the generalised inverse of $H_0 - E$ to the stationary Schrödinger equation for $E > 0$,

$$(H_0 - E)\,|\phi_k\rangle = -V\,|\phi_k\rangle ,$$

we get

$$(1 - |\phi_k^0\rangle\langle\phi_k^0|)\,|\phi_k\rangle = -(H_0 - E)'V\,|\phi_k\rangle .$$

We refer to $(H_0 - E)'$ as Green's operator[3] $G_0(E)$. Since $|\phi_k\rangle$ and $|\phi_k^0\rangle$ are scattering states that differ only locally, it is clear that $\langle\phi_k^0|\phi_k\rangle \to 1$ as $\Omega \to \infty$. This leads to the *Lippmann-Schwinger equation*

$$|\phi_k\rangle = |\phi_k^0\rangle - G_0(E)V\,|\phi_k\rangle .$$

[3]This essentially corresponds to $(G^+ + G^-)/2$ in terms of the retarded and advanced Green operators $G^\pm = G(E \pm i\epsilon)$.

Iterating this equation yields the *Born series*

$$|\phi_k\rangle = |\phi_k^0\rangle - G_0(E)V\,|\phi_k^0\rangle + (G_0(E)V)^2\,|\phi_k^0\rangle + \dots\,,$$

an expansion in powers of V. If it is broken off after the linear term, one speaks of the *Born approximation*.

To obtain the scattering length from it, we need to look at $E = 0$: Here, $G_0(0) = -2m_{\mathrm{red}}\Delta'$ is given by, by spectral decomposition,

$$(G_0(0)f)(\boldsymbol{x}) = \lim_{\epsilon\searrow 0}\int_{k>\epsilon}\frac{\mathrm{d}^3\boldsymbol{k}}{(2\pi)^3}\int\mathrm{d}^3\boldsymbol{y}\,\frac{2m_{\mathrm{red}}}{k^2}e^{i\boldsymbol{k}\cdot(\boldsymbol{x}-\boldsymbol{y})}f(\boldsymbol{y})\,.$$

The ϵ projects out the zero mode as required by the generalised inverse. Provided that f is continuous in momentum space at $k = 0$, the limit can be taken and the momentum integral executed:

$$(G_0(0)f)(\boldsymbol{x}) = \int\mathrm{d}^3\boldsymbol{y}\,\frac{2m_{\mathrm{red}}}{4\pi|\boldsymbol{x}-\boldsymbol{y}|}f(\boldsymbol{y})\,.$$

From $a = \lim_{r\to\infty} r(1-\phi_0(r))$ and $\phi_0^0(r) = 1$, we thus obtain

$$\begin{aligned} a &= \lim_{r\to\infty} -r\sum_{n=1}^{\infty}((-G_0(0)V)^n 1)(r) \\ &= \frac{2m_{\mathrm{red}}}{4\pi}\int\mathrm{d}^3\boldsymbol{r}\,V(r)\sum_{n=0}^{\infty}((-G_0(0)V)^n 1)(r)\,. \end{aligned}$$

For small V, the series may be broken off after the first term, yielding the *Born approximation for the scattering length*:

$$a \approx \frac{2m_{\mathrm{red}}}{4\pi}\int\mathrm{d}^3\boldsymbol{r}\,V(r)\,. \tag{2.5}$$

It should be pointed out here, that this approximation is not valid for *weak* potentials in the sense of a small scattering length, but rather when $V(r)$ is small for every r, i.e. for *flat* potentials. For instance, a hard sphere potential with radius a (i.e. $V(r<a) = \infty$, $V(r>a) = 0$) has also scattering length a, but above integral diverges even for small a.

2.2 The Square-Well Potential

A simple exactly solvable model is that of a square well,

$$V(r) = \begin{cases} V_0 & \text{if } r < r_V \\ 0 & \text{if } r > r_V\,. \end{cases}$$

We shall solve it here explicitly. This allows us to demonstrate the basic properties of the scattering length and to point out a feature that will be relevant for the impurity-BEC problem. Also, we make use of it in the next section to construct the contact interaction as the limit $r_V \to 0$.

The eigenvalue equation can be solved inside and outside B_{r_V}, the ball of radius r_V, independently before matching slope and value of the wave function (or, simpler, of $u(r)$) at r_V.

Bound States Bound states can, of course, occur only for $V_0 < 0$. For $E < 0$ the only solution outside B_{r_V} is

$$u_B(r > r_V) = const \cdot \exp(-\kappa r)$$

with $\kappa > 0$ and $E = -\kappa^2/2m_{\text{red}}$. The other formal solution, $\exp(+\kappa r)$, makes little physical sense and is, besides that, not a tempered distribution. Inside B_{r_V}, $u(0) = 0$ is required, such that

$$u_B(r < r_V) = const \cdot \sin(q_B r)\,.$$

where $-V_0 + E = q_B^2/2m_{\text{red}}$. If we had $E < V_0$, q_B would be imaginary and the sin would really be a sinh. But it is clearly impossible to match slope and value of the monotonically growing sinh with that of a decaying exponential. Matching u_B'/u_B at r_V as well as the energies yields the equations, from which the binding energies can be obtained:

$$E = -\frac{\kappa^2}{2m_{\text{red}}} = V_0 + \frac{q_B^2}{2m_{\text{red}}} \tag{2.6a}$$

$$\frac{u_B(r_V)}{u_B'(r_V)} = -\frac{1}{\kappa} = \frac{\tan(q_B r_V)}{q_B}\,. \tag{2.6b}$$

The number of solutions and therefore bound states depends on the potential depth V_0. The minimum depth to allow for at least one is obtained by setting $\kappa = 0$, which yields $2m_{\text{red}}|V_0|r_V^2 = \frac{\pi^2}{4}$.

Scattering Length For the zero-energy scattering equation, we have outside B_{r_V}

$$u_0(r > r_V) = const \cdot (r - a)$$

and inside

$$u_0(r < r_V) = const \cdot \sin(q_0 r)$$

where $q_0^2/2m_{\text{red}} = -V_0$ (for $V_0 > 0$, u_0 can still be chosen real by adjusting the constant). Matching boundary conditions yields

$$\frac{u_0(r_V)}{u_0'(r_V)} = r_V - a = \frac{\tan(q_0 r_V)}{q_0}\,,$$

and we obtain the scattering length

$$a = r_V \left(1 - \frac{\tan(q_0 r_V)}{q_0 r_V}\right)\,. \tag{2.7}$$

Note that this is indeed always real. The relation is shown in figure 2.1. One can see that for repulsive potentials, the scattering length is always positive and smaller than r_V. For $V_0 = \infty$, the hard-sphere potential, one obtains $a = r_V$; this can be a useful model potential for repulsive scattering. For attractive potentials, on the other hand, a can take arbitrarily large values and changes its sign whenever the number of bound states that is allowed by the potential changes. For

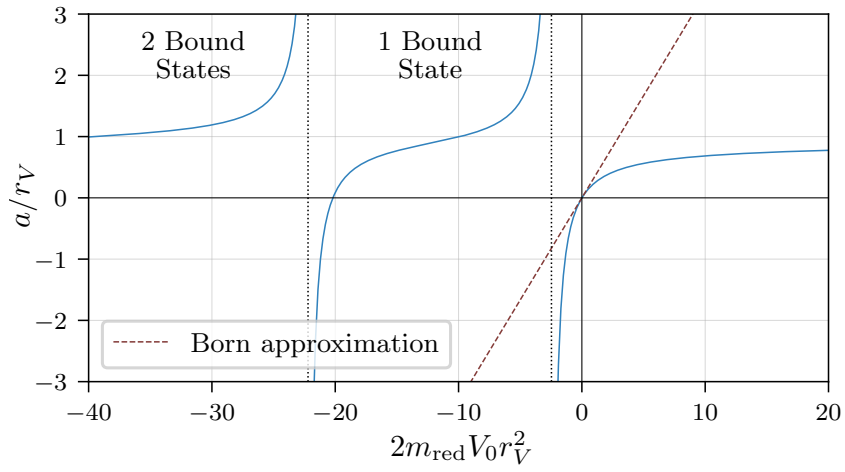

Figure 2.1: Scattering length of a square well potential as function of potential height V_0 and radius r_V. In comparison the Born approximation, valid for small values of V_0.

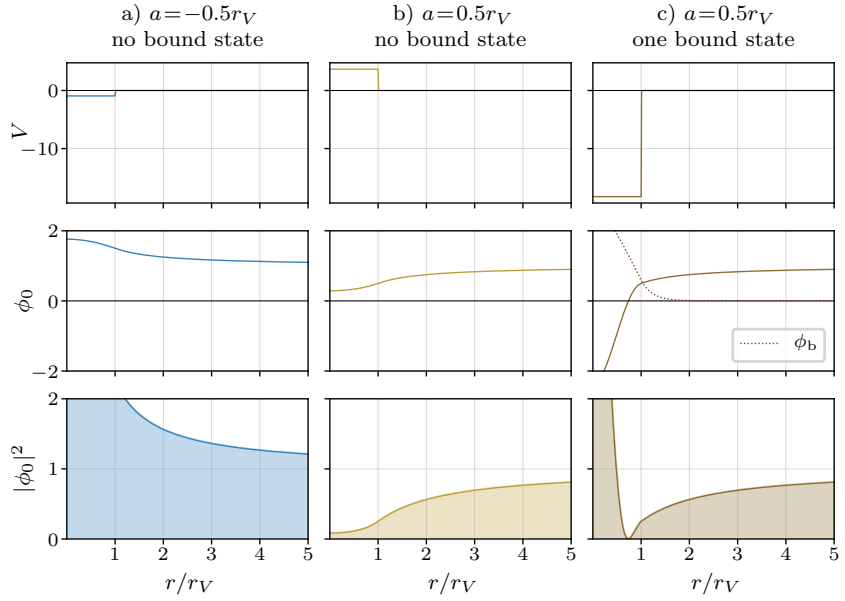

Figure 2.2: Potential shape, scattering solution and corresponding particle density for three different potential depths with the same absolute value of the scattering length. Note that the scattering states for $a = 0.5r_V$ are identical for $r > r_V$, but very different for $r < r_V$. In a) and b), the scattering solution is the ground state while in c), a bound state exists (red dotted line).

three particular values, the scattering solution is shown in figure 2.2. The behaviour is simple in the cases a) and b) when no bound state exists: the particles attract or repel each other, leading to an increased or reduced absolute value of the relative wave function. Case c), however, is more interesting since here, the potential is attractive but the scattering length is positive. For $r > r_V$, the scattering solution is the same as for the repulsive potential b). At small distances, however, it crosses zero, leading to a remarkable density profile where the probability of finding the two particles at a certain distance between a and r_V is zero. Note that for $a > r_V$, the zero-crossing is precisely at $r = a$ and therefore outside the potential range.

For the two-body problem, this peculiarity in the scattering solution is of little interest. After all, it is just a formal solution and no physical, normalisable state, and then, it is not even the ground state. But for the

impurity-BEC problem, the zero-energy scattering solution will prove central as will be shown in the next chapters.

Scattering Phase Similarly, we get for the scattering equation with non-zero energy

$$u_k(r > r_V) = const \cdot \sin(kr + \delta_k)$$
$$u_k(r < r_V) = const \cdot \sin(q_k r)$$

with $q_k^2/2m_{\text{red}} = -V_0 + k^2$ and the boundary condition turns into

$$\frac{u_k(r_V)}{u_k'(r_V)} = \frac{\tan(kr_V + \delta_k)}{k} = \frac{\tan(q_k r_V)}{q_k}\,, \tag{2.8}$$

from which δ_k can be determined (again, the right-hand side is real even if q_k is imaginary).

2.3 The Contact Potential

Motivated by the separation of scales in an ultracold gas and the universal dependence of its properties on the scattering length, one may ask if it is possible to take the range of the interaction potentials to zero while increasing their height in such a way, that the scattering length is kept fixed. Such zero-range effective potentials are called *point interactions* or *contact potentials*. One candidate would be, for example, the delta function. In finding such a contact potential, one would forget about all the unimportant details of the potential shapes and make the theoretical description simpler and more universal. It turns out that this is possible under conditions that are different depending on the dimensionality. In 3d, the situation is as follows:

- There is no purely repulsive contact potential, i.e. with positive scattering length and no bound states. After all, for a positive potential $V > 0$ of range r_V, the scattering length can be no larger than the potential range, such that $r_V \to 0$ implies $a \to 0$. In particular, a delta function with positive prefactor has scattering length zero.
- There are contact potentials with negative scattering length and no bound state and such with positive scattering length and one bound state.
- There is no contact potential with negative scattering length and a bound state, nor one with two or more bound states.

In the remainder of this section, we will construct the contact potential explicitly as limit of square-well potentials. Then we discuss its properties, compute the Green functions and finally derive the momentum-space representation for later use in Bogoliubov theory. A more thorough treatment that also explains above conditions can be obtained by considering self-adjoint extensions of a Hamiltonian with reduced domain of definition. For this, we refer to [Alb+88], where also lower dimensions and multiple scattering centres are treated.

2.3.1 Construction as Limit of Square Well Potentials

According to above conditions, it is the vicinity of the rightmost pole in figure 2.1, that can be described as a point interaction. If $r_V \to 0$ is taken in equation (2.7), $\tan(q_0 r_V)/q_0 r_V$ must diverge to yield a non-zero scattering length. Since we are interested in the first divergence, this implies $q_0 r_V = \frac{\pi}{2} + \epsilon$ with an $\epsilon \to 0$. Consequently, $|V_0| = \mathcal{O}(r_V^{-2})$. A delta function with negative prefactor, on the other hand, has a height of $-\mathcal{O}(r_V^{-3})$, and is therefore much too strong to describe a valid contact potential. This is very different from the repulsive case, where a delta function is too *weak* to lead to a non-zero scattering length.

The leading term of q_0 is independent of the scattering length and so we must compute ϵ first order in r_V by expanding the tangent:

$$\tan(q_0 r_V) = \tan\left(\frac{\pi}{2} + \epsilon\right) = -\frac{1}{\epsilon} + \mathcal{O}(\epsilon)\,,$$

and from the scattering length equation (2.7), we get

$$\begin{aligned} a q_0 r_V &= -r_V \tan(q_0 r_V) + \mathcal{O}(r_V) \\ \Rightarrow \quad a\frac{\pi}{2} &= \frac{r_V}{\epsilon} + \mathcal{O}(r_V) \\ \Rightarrow \quad \epsilon &= \frac{2 r_V}{\pi a} + \mathcal{O}(r_V^2)\,, \end{aligned}$$

which leads to the result for the potential height:

$$2 m_{\mathrm{red}} |V_0| = \frac{\pi^2}{4 r_V^2} + \frac{2}{a r_V} + \mathcal{O}(1)\,.$$

As already mentioned, the scattering length appears only in the next-to-leading term. A small relative (but large absolute) change in the potential height thus leads to very different scattering physics.

Scattering States As $r_V \to 0$, the formulae for the region $r > r_V$ become valid everywhere:

$$\begin{aligned} u_0(r) &\sim r - a \\ u_k(r) &\sim \sin(kr + \delta_k)\,. \end{aligned}$$

Equation (2.8) for the scattering phase can be solved (for finite energies $k = \mathcal{O}(1)$): we have $q_k = \sqrt{-V_0 + k^2} = q_0 + \mathcal{O}(r_V)$ and thus

$$\begin{aligned} \frac{\tan(k r_V + \delta_k)}{k} = \frac{\tan(q_k r_V)}{q_k} &= \frac{-1/\epsilon + \mathcal{O}(r_V)}{\pi/2 r_V + \mathcal{O}(1)} = -a + \mathcal{O}(r_V) \\ \Rightarrow \quad \tan\delta_k &= -ak + \mathcal{O}(r_V)\,. \end{aligned}$$

With $\sin(kr + \delta_k) = \cos(\delta_k)(\sin(kr) + \tan(\delta_k)\cos(kr))$, this leads to

$$u_k(r) \sim \sin(kr) - ak\cos(kr)\,.$$

Bound States From the binding energy equations (2.6a), we obtain

$$2m_{\text{red}}|V_0| = q_B^2 + \kappa^2 = q_B^2\left(1 + \frac{1}{\tan^2 q_B r_V}\right) = \frac{1}{r_V^2}\frac{(q_B r_V)^2}{\sin^2(q_B r_V)}$$
$$\Rightarrow \quad \frac{(q_B r_V)^2}{\sin^2(q_B r_V)} = \frac{\pi^2}{4} + \frac{2r_V}{a} + \mathcal{O}(r_V^2)\,.$$

The equation $x^2/\sin^2(x) \approx \pi^2/4$ has $x \approx \pi/2$ as only solution. Therefore, $q_B r_V = \frac{\pi}{2} + \epsilon'$ and ϵ' can be determined to leading order:

$$\frac{\frac{\pi^2}{4} + \pi\epsilon' + \mathcal{O}(\epsilon'^2)}{1 + \mathcal{O}(\epsilon'^2)} = \frac{\pi^2}{4} + 2\frac{r_V}{a} + \mathcal{O}(r_V^2)$$
$$\Rightarrow\ \epsilon' = \frac{2r_V}{\pi a} + \mathcal{O}(r_V^2)\,.$$

From this we get

$$\kappa = -\frac{1}{r_V}\frac{(q_B r_V)}{\tan(q_B r_V)} = \frac{1}{a} + \mathcal{O}(r_V)\,.$$

From the requirement $\kappa > 0$, a bound state exists only for $a > 0$. In the limit $r_V \to 0$, the wave function and energy are then given by

$$u_B(r) \sim \exp(-r/a)$$
$$E_B = \frac{1}{2m_{\text{red}}a^2}\,.$$

Even though we have derived these relations here for a square well potential, they are valid for all potential shapes. It is interesting to note that in general, the scattering length controls only the low-energy scattering states but has nothing to do with the bound states. For the contact potential, however, even the latter are parameterised by the scattering length.

2.3.2 Contact Condition and Fermi Pseudo-Potential

The generalised eigenstates derived above have a peculiarity: they do not fulfil $u(0) = 0$ as for regular potentials. Instead,

$$u(0) = -au'(0)\,, \tag{2.9}$$

a relation known as the contact condition. The eigenvalue equation, on the other hand, is simply

$$-\frac{u''}{2m_{\text{red}}} = Eu\,, \tag{2.10}$$

which looks exactly like the free radial Schrödinger equation. However, it is *not* true that $(-\Delta/2m_{\text{red}})\phi = E\phi$. After all, the boundary condition (2.9) means, that ϕ has a r^{-1}-pole at zero and the Laplacian gets a distributional part in addition to the regular $\frac{1}{r}\frac{\partial^2}{\partial r^2}r$.

It is nonetheless possible to write the Hamiltonian in the familiar form

$$H = -\frac{\Delta}{2m_{\text{red}}} + V\,,$$

if one uses a so-called pseudo-potential, originally due to Fermi [Fer36; Bre47; Bla52; HY57]:

$$V\phi = 4\pi a \delta^{(3)}(r) \frac{\partial}{\partial r}(r\phi)\,. \tag{2.11}$$

Note that V is no longer a multiplication operator. It is designed in such a way, that the distributional part of the Laplacian is cancelled if the contact condition (2.9) is fulfilled by the s-wave part of the wave function.

Due to the different conditions at $r = 0$, the contact Hamiltonian has a different domain of definition than a usual Hamiltonian, even though both are dense subsets of the Hilbert space. This poses a problem when considering the dynamics after a *quench*, that is, after an instantaneous change in the interaction strength: One has to solve the Schrödinger equation with an initial state, which is not in the domain of definition of the Hamiltonian. Fortunately, the Schrödinger equation can be extended to cover this in a well-defined way: after all, the time-evolution operator $\exp(-iHt)$ is unitary, hence bounded, and can be continuously extended to the entire Hilbert space. It is thus sufficient to approximate (in L^2 norm) the initial state by one that has the correct contact condition. Alternatively, one can directly apply the propagator, which we derive in the next section, to arbitrary initial states.

2.3.3 Propagator of the Contact Hamiltonian

The propagator of the contact Hamiltonian can be computed analytically from the generalised eigenstates. In the calculation, we shall make use of some of the integrals in appendix A. Also, we set $2m_{\text{red}} = 1$ for simplicity; the complete result can be obtained by rescaling t appropriately.

Normalisation of eigenstates

We have derived the s-wave eigenstates

$$\begin{aligned} u_0 &= r - a \\ u_B &= \mathcal{N}_B \exp(-r/a) && \text{if } a > 0 \\ u_k &= \mathcal{N}_k(\sin(kr) - ak\cos(kr)) && \text{for } k > 0 \end{aligned}$$

of the contact Hamiltonian in section 2.3.1, but not yet computed the normalisation constants. We choose the normalisation such that $4\pi \int_{\mathbb{R}_+} |u_B|^2 = 1$ and $4\pi \int_{\mathbb{R}_+} \overline{u_q} u_k = \delta(q-k)$. Note that if we had $\mathcal{N}_k \to k^{-1}$ as $k \to 0$, then $u_k \to u_0$ and we could include u_0 as a special case into the definition and normalisation condition of u_k. However, we will see that $\mathcal{N}_k \to const$ and thus $u_k \to 0$ – that is, u_0 cannot be normalised in a meaningful way. This is of little importance for the two-body problem, because a single continuum mode plays no essential role anyway.

However, when turning to BEC physics, this will be different, because the zero-mode can be occupied macroscopically.

The following alternative form of u_k will be convenient in the following:

$$u_k = -\mathcal{N}_k \operatorname{Re} e^{ikr}(ak + i)\,.$$

Bound State This one is easy:

$$\begin{aligned} 4\pi \int_{\mathbb{R}_+} |u_B|^2 &= 4\pi\mathcal{N}_B^2 \int_{\mathbb{R}_+} e^{-2r/a} = 2\pi a\mathcal{N}_B^2 \\ \Rightarrow \qquad \mathcal{N}_B &= \frac{1}{\sqrt{2\pi a}} \end{aligned}$$

Continuum States These are a bit more involved as the integrals exist only in the sense of distributions. The essential integral was pre-computed in (A.1d).

$$\begin{aligned} &4\pi \int_{\mathbb{R}_+} \overline{u_k} u_q \\ &\quad \mid \textit{Insert definition of } u_k, u_q \textit{ and expand the 'Re' in } u_q. \\ &= 4\pi\mathcal{N}_k\mathcal{N}_q \int_{\mathbb{R}_+} \mathrm{d}r \operatorname{Re} e^{ikr}(ak+i)\frac{e^{iqr}(aq+i) + e^{-iqr}(aq-i)}{2} \\ &\quad \mid \textit{Use } (\text{A.1d}). \\ &= 2\pi\mathcal{N}_k\mathcal{N}_q \operatorname{Re}\Bigg[\left(\pi\delta(k+q) + \frac{i}{k+q}\right)(ak+i)(aq+i) \\ &\qquad\qquad + \left(\pi\delta(k-q) + \frac{i}{k-q}\right)(ak+i)(aq-i)\Bigg] \\ &\quad \mid \delta(k+q) = 0 \textit{ since } k, q > 0. \textit{ Evaluate the 'Re'.} \\ &= 2\pi\mathcal{N}_k\mathcal{N}_q\left[\frac{1}{k+q}(-ak-aq) + \pi\delta(k-q)(a^2kq+1) + \frac{1}{k-q}(ak-aq)\right] \\ &\quad \mid \textit{First and third terms cancel.} \\ &= 2\pi^2(1+a^2kq)\mathcal{N}_k\mathcal{N}_q\delta(k-q) \end{aligned}$$

and thus

$$\mathcal{N}_k = \frac{1}{\pi\sqrt{2(1+a^2k^2)}}\,.$$

Derivation of the Propagator

Since the contact potential acts only on the s-wave part of the wave function, it is sufficient to compute the s-wave part of the propagator. The full propagator is then given by

$$g^a(\boldsymbol{x}, \boldsymbol{y}, t) = g^0(\boldsymbol{x} - \boldsymbol{y}, t) + g^{a,\,\text{s-wave}}(x, y, t) - g^{0,\,\text{s-wave}}(x, y, t)$$

where

$$g^0(\boldsymbol{x} - \boldsymbol{y}, t) = \frac{\exp\left(-\frac{(\boldsymbol{x}-\boldsymbol{y})^2}{4it}\right)}{(4\pi it)^{3/2}}\,.$$

We have

$$g^{a,\,\text{s-wave}}(x,y,t) = \mathbb{1}_{a>0}\, e^{iE_B t}\phi_B(x)\phi_B(y) + \lim_{\operatorname{Im} t \nearrow 0} \int_{\mathbb{R}_+} e^{-ik^2 t}\phi_k(x)\phi_k(y)\, \mathrm{d}k\,.$$

The integral over the scattering states can be expressed in terms of Gaussian integrals and integral (A.1b).

$$\begin{aligned}
&\int_{\mathbb{R}_+} e^{-ik^2 t}\phi_k(x)\phi_k(y)\, \mathrm{d}k \\
&\quad\big|\ \textit{ϕ_k is anti-symmetric in k, so $\textstyle\int_{\mathbb{R}_+}$ can be replaced by $\frac{1}{2}\int_{\mathbb{R}}$.} \\
&= \frac{1}{2}\int_{\mathbb{R}} e^{-ik^2 t} \frac{-\operatorname{Re} e^{ikx}(ak+i)}{\pi x\sqrt{2(1+a^2k^2)}} \cdot \frac{-\operatorname{Re} e^{iky}(ak+i)}{\pi y\sqrt{2(1+a^2k^2)}}\, \mathrm{d}k \\
&\quad\big|\ \textit{Expand the right ``Re'' and cancel $(ak+i)$.} \\
&= \frac{1}{8\pi^2 xy}\int_{\mathbb{R}} e^{-ik^2 t} \operatorname{Re}\frac{e^{ikx}}{ak-i}\left[e^{iky}(ak+i) + e^{-iky}(ak-i)\right] \mathrm{d}k \\
&\quad\big|\ \textit{The ``Re'' can be omitted since the imaginary part is anti-symmetric anyway. Write $(ak+i)/(ak-i)$ as $1+2i/(ak-i)$} \\
&= \frac{1}{8\pi^2 xy}\int_{\mathbb{R}} e^{-ik^2 t}\left[e^{ik(x+y)} + e^{ik(x-y)} + 2i\frac{e^{ik(x+y)}}{ak-i}\right] \mathrm{d}k \\
&\quad\big|\ \textit{Compute Gaussian integrals and use (A.1b).} \\
&= \frac{1}{8\pi^2 xy}\left[\sqrt{\frac{\pi}{it}}e^{-\frac{(x+y)^2}{4it}} + \sqrt{\frac{\pi}{it}}e^{-\frac{(x-y)^2}{4it}}\right. \\
&\qquad\left. -\frac{2\pi}{a}e^{\frac{it}{a^2}-\frac{x+y}{a}}\left(\operatorname{sgn}(a) - \operatorname{erf}\left(\frac{\sqrt{it}}{a} - \frac{x+y}{2\sqrt{it}}\right)\right)\right]
\end{aligned}$$

Together with the part of the bound state,

$$\mathbb{1}_{a>0} e^{iE_B t}\phi_B(x)\phi_B(y) = \mathbb{1}_{a>0}\frac{e^{\frac{it}{a^2}-\frac{x+y}{a}}}{2\pi a x y}\,,$$

this yields

$$\begin{aligned}
&g^{a,\,\text{s-wave}}(x,y,t) \\
&= \frac{1}{8\pi^2 xy}\left[\sqrt{\frac{\pi}{it}}\exp\left(-\frac{(x+y)^2}{4it}\right) + \sqrt{\frac{\pi}{it}}\exp\left(-\frac{(x-y)^2}{4it}\right)\right. \\
&\qquad\left. + \frac{2\pi}{a}\exp\left(\frac{it}{a^2} - \frac{x+y}{a}\right)\left(1 - \operatorname{erf}\left(\frac{x+y}{2\sqrt{it}} - \frac{\sqrt{it}}{a}\right)\right)\right] \\
&= \frac{1}{8\pi xy}\left[\frac{1}{\sqrt{i\pi t}}\exp\left(-\frac{(x-y)^2}{4it}\right)\right. \\
&\qquad\left. + \exp\left(-\frac{(x+y)^2}{4it}\right)\left(\frac{1}{\sqrt{i\pi t}} + \frac{2}{a}\operatorname{erfcx}\left(\frac{x+y}{2\sqrt{it}} - \frac{\sqrt{it}}{a}\right)\right)\right]
\end{aligned}$$

in terms of the scaled complementary error function $\operatorname{erfcx} z = e^{z^2}(1-\operatorname{erf} z)$. For the s-wave part of the free propagator, we can set $a = 0$ and get

$$g^{0,\,\text{s-wave}}(x,y,t) = \frac{1}{8\pi xy\sqrt{i\pi t}}\left[e^{-\frac{(x-y)^2}{4it}} - e^{-\frac{(x+y)^2}{4it}}\right]$$

such that, in total,

$$g^a(\boldsymbol{x},\boldsymbol{y},t) = g^0(\boldsymbol{x}-\boldsymbol{y},t) + \frac{e^{-\frac{(x+y)^2}{4it}}}{4\pi xy}\left[\frac{1}{\sqrt{i\pi t}} + \frac{1}{a}\operatorname{erfcx}\left(\frac{x+y}{2\sqrt{it}} - \frac{\sqrt{it}}{a}\right)\right]. \tag{2.12}$$

2.3.4 The Contact Interaction in Momentum Space

When discussing Bogoliubov theory, we will need a representation of the contact interaction in momentum space.

Rescaling a potential in position space to a single point with growing prefactor as $V(r) = \alpha_{r_V}\tilde{V}(r/r_V)$ corresponds in momentum space to expanding it according to

$$v(k) = r_V^3\alpha_{r_V}\tilde{v}(kr_V)\,.$$

Since $\alpha \sim r_V^{-2}$, the prefactor tends to zero as r_V. The potential operator acts in momentum space by folding v with the wave function. However, v varies on momentum scales $\Lambda := r_V^{-1}$ and one may approximate

$$(2\pi)^{-3}(v*\psi)(\boldsymbol{k}) = \int \mathrm{d}^3\boldsymbol{q}\, v(\boldsymbol{k}-\boldsymbol{q})\psi(\boldsymbol{q}) \approx \int \mathrm{d}^3\boldsymbol{q}\, v(\boldsymbol{q})\psi(\boldsymbol{q})$$

for $k = \mathcal{O}(1)$, thereby simplifying $\hat{V}$ to a rank-1 operator. The right-hand side has, however, two inconveniences: *(i)* The operator defined by it is not hermitian, since $\langle\phi|V\psi\rangle = \int\bar{\phi}\cdot\int v\psi$ while $\langle V\phi|\psi\rangle = \int v\bar{\phi}\cdot\int\psi$. *(ii)* It is constant and therefore not normalisable despite the small prefactor of v. Both can be fixed by also making a small adjustment to the scalar product in terms of a cutoff function:

$$\begin{aligned} f(k/\Lambda) &:= v(k)/v(0) \\ (\phi|\psi) &:= \int \overline{\phi(\boldsymbol{k})}\psi(\boldsymbol{k})f(k/\Lambda)\,\mathrm{d}^3\boldsymbol{k}\,. \end{aligned}$$

This has vanishing impact on the scalar product of normalisable wave functions because $f(k/\Lambda) \approx 1$ for $k = \mathcal{O}(1)$. For practical purposes, using the modified scalar product means that the cutoff function f must be used in essentially every momentum integral. In the following, we will make use of the shorthand notation

$$\int^{\Lambda} \cdot\ \mathrm{d}^3\boldsymbol{k} := \int \cdot\, f(k/\Lambda)\,\mathrm{d}^3\boldsymbol{k}\,.$$

Depending on whether or not the limit $\Lambda\to\infty$ exists for an expression, it is called *UV-convergent* or *UV-divergent*. If an integral is UV convergent,

we may usually directly take the limit and therefore omit the Λ. The potential operator is commonly written as

$$\hat{V}\psi = g_\Lambda \fint^\Lambda \psi(\boldsymbol{k})\,\mathrm{d}^3\boldsymbol{k}$$

and $g_\Lambda = v(0)$ is known as the coupling parameter.

Since the shape of the potential becomes unimportant in the limit of the contact interaction, it is not necessary to choose a shape in position space and Fourier transform it. Instead, one may directly choose the momentum space shape f and compute the prefactor g_Λ accordingly to match the scattering length. From the zero-energy scattering equation

$$\frac{k^2}{2m_\mathrm{red}}\psi_0(k) + g_\Lambda \fint^\Lambda \psi_0(k)\,\mathrm{d}^3\boldsymbol{k} = 0\,,$$

one can see that $k^2\psi_0$ must be constant, which is the case for $\psi_0 \sim k^{-2}$ and for $\psi_0 \sim \delta^3(\boldsymbol{k})$. Thus, with convenient choice of normalisation,

$$\psi_0(\boldsymbol{k}) = (2\pi)^3\delta^3(\boldsymbol{k}) - \frac{\alpha}{k^2} \tag{2.13}$$

where

$$\begin{aligned} &-\frac{\alpha}{2m_\mathrm{red}} + g_\Lambda - \alpha g_\Lambda \fint^\Lambda \frac{1}{k^2}\,\mathrm{d}^3\boldsymbol{k} = 0 \\ \Rightarrow\quad & g_\Lambda^{-1} = \frac{2m_\mathrm{red}}{\alpha}\left(1 - \alpha \fint^\Lambda \frac{1}{k^2}\,\mathrm{d}^3\boldsymbol{k}\right). \end{aligned}$$

From the Fourier transform $\psi_0(\boldsymbol{r}) = 1 - \alpha/4\pi r$ one can see that $\alpha = 4\pi a$ and thus

$$g_\Lambda^{-1} = 2m_\mathrm{red}\left(\frac{1}{4\pi a} - \fint^\Lambda \frac{1}{k^2}\,\mathrm{d}^3\boldsymbol{k}\right). \tag{2.14}$$

Chapter 3

The Bose Gas

In this chapter, we review two of the most widely used descriptions of the Bose gas: Bogoliubov theory (BT) and Gross-Pitaevskii theory (GPT). Both will appear again in part II on the Bose polaron. More information on the Bose gas can be found in [PS03; Lie+05; Yng14].

3.1 Bogoliubov Theory

The problem of a weakly interacting Bose gas is not an easy one because a perturbative treatment fails. In 1947, Bogoliubov [Bog47] was able to provide a consistent description by assuming the majority of atoms to be condensed in the zero-mode and treating the remaining ones as fluctuations. He showed that a linear dispersion emerges and was able to explain the phenomenon of superfluidity in Bose gases. His theory has since become a standard description of condensates with no spatial density variation.

In this section, we derive the basic theory. It serves as a prelude to chapter 6, which treats the Bose polaron in BT, and introduces some of the notations and symbols used therein.

3.1.1 Derivation

BT works in momentum space in order to be able to single out the zero-momentum mode. We will assume that the volume is finite and interpret integrals as scaled sums. The Hamiltonian of the Bose gas thus reads

$$H = \fint_{\boldsymbol{k}} \frac{k^2}{2m_{\mathrm{B}}} \hat{a}_{\boldsymbol{k}}^\dagger \hat{a}_{\boldsymbol{k}} + \frac{1}{2} \fint_{\boldsymbol{p},\boldsymbol{k},\boldsymbol{q}} v_{\boldsymbol{p}}^{\mathrm{BB}} \hat{a}_{\boldsymbol{k}+\boldsymbol{p}}^\dagger \hat{a}_{\boldsymbol{q}-\boldsymbol{p}}^\dagger \hat{a}_{\boldsymbol{q}} \hat{a}_{\boldsymbol{k}}.$$

The central assumption is that most particle are condensed in the zero-mode. Therefore, terms involving three or more operators $\hat{a}_{\boldsymbol{k}}^{(\dagger)}$ with $\boldsymbol{k} \neq 0$ are considered small in comparison to those involving zero-mode operators and are neglected. We follow Girardeau [Gir61] and first isolate terms depending only on the total particle number $N = \fint_{\boldsymbol{k}} \hat{a}_{\boldsymbol{k}}^\dagger \hat{a}_{\boldsymbol{k}}$

from the interaction part H_{int} of the Hamiltonian.

$$\begin{aligned} H_{\text{int}} &= \frac{v^{\text{BB}}(0)}{2\mathscr{V}} \fint_{\boldsymbol{k},\boldsymbol{q}} \hat{a}^\dagger_{\boldsymbol{k}} \hat{a}^\dagger_{\boldsymbol{q}} \hat{a}_{\boldsymbol{q}} \hat{a}_{\boldsymbol{k}} + \fint_{\boldsymbol{p}\neq 0} \frac{v^{\text{BB}}_p}{2} \fint_{\boldsymbol{k},\boldsymbol{q}} \hat{a}^\dagger_{\boldsymbol{k}+\boldsymbol{p}} \hat{a}^\dagger_{\boldsymbol{q}-\boldsymbol{p}} \hat{a}_{\boldsymbol{q}} \hat{a}_{\boldsymbol{k}} \\ &= v^{\text{BB}}(0) \frac{N(N-1)}{2\mathscr{V}} + \fint_{\boldsymbol{p}\neq 0} \frac{v^{\text{BB}}_p}{2} \fint_{\boldsymbol{k},\boldsymbol{q}} \hat{a}^\dagger_{\boldsymbol{k}+\boldsymbol{p}} \hat{a}^\dagger_{\boldsymbol{q}-\boldsymbol{p}} \hat{a}_{\boldsymbol{q}} \hat{a}_{\boldsymbol{k}}. \end{aligned}$$

To the remaining term, the approximation is applied.

$$\begin{aligned} \approx \frac{nNv^{\text{BB}}(0)}{2} + \frac{1}{2\mathscr{V}^2} \fint_{\boldsymbol{p}\neq 0} v^{\text{BB}}_p \big(& \hat{a}^\dagger_{\boldsymbol{p}} \hat{a}^\dagger_{-\boldsymbol{p}} \hat{a}_0 \hat{a}_0 + \hat{a}^\dagger_0 \hat{a}^\dagger_0 \hat{a}_{-\boldsymbol{p}} \hat{a}_{\boldsymbol{p}} \\ & + \hat{a}^\dagger_{\boldsymbol{p}} \hat{a}^\dagger_0 \hat{a}_{\boldsymbol{p}} \hat{a}_0 + \hat{a}^\dagger_0 \hat{a}^\dagger_{-\boldsymbol{p}} \hat{a}_0 \hat{a}_{-\boldsymbol{p}} \big). \end{aligned}$$

The second step consists in replacing the zero-momentum operators $\hat{a}^\dagger_0$ and $\hat{a}_0$ by c-numbers. The motivation for this is that when the zero-mode is occupied by a macroscopic number of particles N_0 of order N – this amounts to $\hat{a}^{(\dagger)}_0 \approx \sqrt{N_0 \mathscr{V}}$, such that $\fint \hat{a}^\dagger_0 \hat{a}_0 \sim N$ – then the commutator $[\hat{a}_0, \hat{a}^\dagger_0] = \mathscr{V}$ is negligible in comparison to $\hat{a}^\dagger_0 \hat{a}_0 \approx N_0 \mathscr{V}$ ([1]). The resulting Hamiltonian reads

$$H = \frac{nNv^{\text{BB}}(0)}{2} + \text{He} \fint_{\boldsymbol{k}\neq 0} \left[\left(\frac{k^2}{2m_{\text{B}}} + n_0 v^{\text{BB}}_k \right) \hat{a}^\dagger_{\boldsymbol{k}} a_{\boldsymbol{k}} + n_0 v^{\text{BB}}_k \hat{a}_{\boldsymbol{k}} \hat{a}_{-\boldsymbol{k}} \right].$$

where $n_0 = N_0/\mathscr{V}$ is the condensate density.

Finally, this Hamiltonian is diagonalised by the Bogoliubov transformation

$$S = \exp\left(\frac{1}{2} \fint_{\boldsymbol{k}} \phi_k \big(\hat{a}^\dagger_{\boldsymbol{k}} \hat{a}^\dagger_{-\boldsymbol{k}} - \hat{a}_{\boldsymbol{k}} \hat{a}_{-\boldsymbol{k}} \big) \right)$$

for a spherically symmetric real function ϕ. It defines new operators $\hat{b}_{\boldsymbol{k}} = S \hat{a}_{\boldsymbol{k}} S^{-1}$, which can be computed from the Hadamard lemma $e^X \hat{a} e^{-X} = \sum_n [X, \hat{a}]_n \,/\, n!$. We have

$$\begin{aligned} [\ln S, \hat{a}_{\boldsymbol{k}}] &= -\phi_k \hat{a}^\dagger_{-\boldsymbol{k}} \\ [\ln S, \hat{a}^\dagger_{\boldsymbol{k}}] &= -\phi_k \hat{a}_{-\boldsymbol{k}} \\ \Rightarrow [\ln S, \hat{a}_{\boldsymbol{k}}]_n &= \begin{cases} \phi^n_k \hat{a}_{\boldsymbol{k}} & \text{if } n \text{ even} \\ -\phi^n_k \hat{a}^\dagger_{-\boldsymbol{k}} & \text{if } n \text{ odd.} \end{cases} \end{aligned}$$

Thus

$$\begin{aligned} \hat{b}_{\boldsymbol{k}} &= \cosh(\phi_k)\, \hat{a}_{\boldsymbol{k}} - \sinh(\phi_k) \hat{a}^\dagger_{-\boldsymbol{k}} \\ \hat{b}^\dagger_{\boldsymbol{k}} &= \cosh(\phi_k)\, \hat{a}^\dagger_{\boldsymbol{k}} - \sinh(\phi_k) \hat{a}_{-\boldsymbol{k}} \end{aligned}$$

and inversely

$$\begin{aligned} \hat{a}_{\boldsymbol{k}} &= \cosh(\phi_k)\, \hat{b}_{\boldsymbol{k}} + \sinh(\phi_k) \hat{b}^\dagger_{-\boldsymbol{k}} \\ \hat{a}^\dagger_{\boldsymbol{k}} &= \cosh(\phi_k)\, \hat{b}^\dagger_{\boldsymbol{k}} + \sinh(\phi_k) \hat{b}_{-\boldsymbol{k}}. \end{aligned}$$

[1] In fact, it is not necessary that the zero-mode is occupied macroscopically, as was shown by Ginibre [Gin68]: if it is not, we have just eliminated a single continuum mode, which plays no role. But in this case, the replacement has no practical interest.

The requirement that terms of the form $\hat{b}_{\boldsymbol{k}}\hat{b}^{\dagger}_{-\boldsymbol{k}}$ vanish leads to

$$\begin{aligned}\tanh 2\phi_k &= -\frac{1}{1+\frac{k^2}{2m_{\mathrm{B}}n_0 v_k^{\mathrm{BB}}}}\\ \Leftrightarrow \quad e^{4\phi_k} &= \frac{k^2}{k^2+4m_{\mathrm{B}}n_0 v_k^{\mathrm{BB}}}.\end{aligned}$$

The diagonalised Hamiltonian then reads

$$H = E_0 + \fint_{\boldsymbol{k}} \omega_k \hat{b}^{\dagger}_{\boldsymbol{k}}\hat{b}_{\boldsymbol{k}}$$

where

$$\begin{aligned}\omega_k &= \frac{k^2}{2m_{\mathrm{B}}}e^{-2\phi_k} = \frac{k}{2m_{\mathrm{B}}}\sqrt{k^2+4m_{\mathrm{B}}n_0 v_k^{\mathrm{BB}}}\\ E_0 &= \frac{nNv_0^{\mathrm{BB}}}{2} + \mathscr{V}\fint_{\boldsymbol{k}}\left(\frac{k^2}{m_{\mathrm{B}}}\Big(\sqrt{1+\frac{4m_{\mathrm{B}}n_0 v_k^{\mathrm{BB}}}{k^2}}-1\Big) - \frac{n_0 v_k^{\mathrm{BB}}}{2}\right).\end{aligned}$$

An important point is that the dispersion ω_k is linear for small k with a proportionality constant c. According to Landau's theory [Lan41], this explains the phenomenon of superfluidity. One can show that the critical velocity c is equivalent to the speed of sound in the Bose gas and that the Bogoliubov modes can be interpreted as phonons.

The ground state of the system is given by the *phonon vacuum*

$$|0_{\hat{b}}\rangle = S\,|0\rangle\,.$$

(Note that $|0\rangle$ does not correspond to vacuum but to an ideal BEC because the zero-mode was removed by the c-number substitution.) Even in the ground state, particles are removed from the condensate. This *condensate depletion* is given by

$$n - n_0 = \frac{1}{\mathscr{V}}\,\langle 0_{\hat{b}}|\fint_{\boldsymbol{k}\neq 0}\hat{a}^{\dagger}_{\boldsymbol{k}}\hat{a}_{\boldsymbol{k}}|0_{\hat{b}}\rangle = \fint_{\boldsymbol{k}}\sinh(\phi_k)^2.$$

It was an initial requirement of the theory that this number be small compared to n. For this to be true, ϕ – and in turn $n_0 v_k^{\mathrm{BB}}$ – must be small.

3.1.2 Local Potential

Bogoliubov theory is most successful in combination with a Lee-Huang-Yang pseudo-potential $V^{\mathrm{BB}}(r) = \frac{4\pi a_{\mathrm{BB}}}{m_{\mathrm{B}}}\delta^3(r)$, leading to $v^{\mathrm{BB}}(k) = \frac{4\pi a_{\mathrm{BB}}}{m_{\mathrm{B}}}$. This yields universal results that depend only on the scattering length a_{BB}. Most quantities can be conveniently expressed by another important length scale, the *healing length*

$$\xi = \frac{1}{\sqrt{8\pi a_{\mathrm{BB}} n_0}}.$$

It defines the scale on which local perturbations of the condensate decay (are *healed*). This leads to

$$\begin{aligned} e^{4\phi_k} &= \frac{\xi^2 k^2}{\xi^2 k^2 + 2} \\ \omega_k &= ck\sqrt{1 + \frac{\xi^2 k^2}{2}} \\ c &= \frac{1}{\sqrt{2} m_\mathrm{B} \xi} \\ n - n_0 &= \frac{\sqrt{2}}{12\pi^2 \xi^3}. \end{aligned}$$

The relative condensate depletion depends only on the dimensionless *gas parameter* $n_0 a_{\mathrm{BB}}^3$:

$$\frac{n - n_0}{n} = \frac{8}{3\sqrt{\pi}} \sqrt{n_0 a_{\mathrm{BB}}^3}.$$

The applicability of BT is thus directly related to the smallness of the gas parameter. A typical value for experiments is $n_0 a_{\mathrm{BB}}^3 = 10^{-5}$.

3.2 Gross-Pitaevskii Theory

BT assumes condensation in the zero-momentum mode and thus homogeneity in space. It may thus be inapplicable for a trapped gas or one with a local perturbation, which require spatial variation of the condensed mode. A theory to treat such situations was developed independently by Gross [Gro61] and Pitaevskii [Pit61] (GP) to describe vortices in condensates.

3.2.1 Derivation

A heuristic derivation starts from the Hamiltonian with a Lee-Huang-Yang potential term (V^{ext} is an external trapping potential)

$$H = \int_{\boldsymbol{x}} \Big(\hat{a}_{\boldsymbol{x}}^\dagger \frac{-\Delta}{2m_\mathrm{B}} \hat{a}_{\boldsymbol{x}} + \frac{2\pi a_{\mathrm{BB}}}{m_\mathrm{B}} \hat{a}_{\boldsymbol{x}}^\dagger \hat{a}_{\boldsymbol{x}}^\dagger \hat{a}_{\boldsymbol{x}} \hat{a}_{\boldsymbol{x}} + V_{\boldsymbol{x}}^{\mathrm{ext}} \hat{a}_{\boldsymbol{x}}^\dagger \hat{a}_{\boldsymbol{x}} \Big). \tag{3.1}$$

It is now assumed that the particles are condensed in a single mode $\phi_{\boldsymbol{x}}$, such that the wave function is a product state $\Psi(\boldsymbol{x}_1, ..., \boldsymbol{x}_N) = \phi(\boldsymbol{x}_1) \cdots \phi(\boldsymbol{x}_N)$ or, simpler, a coherent state

$$|\Psi\rangle = \exp\left(\int_{\boldsymbol{x}} \left(\phi_{\boldsymbol{x}} \hat{a}_{\boldsymbol{x}}^\dagger - \overline{\phi_{\boldsymbol{x}}} \hat{a}_{\boldsymbol{x}} \right) \right) |0\rangle .$$

The normalisation is $\int_{\boldsymbol{x}} |\phi_{\boldsymbol{x}}|^2 = N$ to yield an average particle number of N. Computing the energy expectation value $\langle \Psi | H | \Psi \rangle$ and the equations of motion yields the GP energy functional and the GP equations (GPE)

$$\begin{aligned} E[\phi] &= \int \left(\frac{|\nabla \phi|^2}{2m_\mathrm{B}} + \frac{2\pi a_{\mathrm{BB}}}{m_\mathrm{B}} |\phi|^4 + V^{\mathrm{ext}} |\phi|^2 \right) \\ i\dot{\phi} &= \left(-\frac{\Delta}{2m_\mathrm{B}} + \frac{4\pi a_{\mathrm{BB}}}{m_\mathrm{B}} |\phi|^2 + V^{\mathrm{ext}} \right) \phi. \end{aligned}$$

Meanwhile these equations have become the standard tools to find the ground state or time evolution of inhomogeneous condensates.

3.2.2 Applicability

The above derivation is simple but also misleading in some aspects. It may appear, for example, that GPT is of limited scope because it relies on a pure product state without any correlations between the particles. Also one might think that the use of the local potential is a limitation and that one would enhance the scope by using a product state with arbitrary potential shapes[2]. Finally, it appears that the first term of the energy functional constitutes the entire kinetic energy of the system while the second captures only the BB repulsion.

These points are, in general, not true. In reality, the two approximations involved – the local potential and the product state – act in favour of each other and removing one would put into question the validity of the other.

The use of a local potential is motivated by a separation of scales, namely that the scattering length is much shorter than the mean-particle distance and than the scale, on which the condensate wave function varies. But the Lee-Huang-Yang term is a peculiar one: even though the Born approximation suggests that the potential $4\pi a_{\mathrm{BB}}/m_{\mathrm{B}} \cdot \delta^3$ has indeed a scattering length of a_{BB}, it really has one of zero. After all, for a repulsive potential, the scattering length may not exceed the potential radius. The result is that by a clever choice of wave functions, the energy of (3.1) with $V^{\mathrm{ext}} = 0$ can be brought arbitrarily close to zero[3], even though the real ground state energy of the free Bose gas is known to be $4\pi a_{\mathrm{BB}} nN/m_{\mathrm{B}}$. We are led to say that (3.1) produces correct results for wave functions that are not able to resolve short-range two-particle correlations. The product state fulfils this requirement.

Conversely, a product state produces correct results with the local potential, but not for arbitrary ones: for a hard-sphere potential, the energy would even diverge.

GPT produces correct results for a large class of potentials. This was proven in [LSY00] for the ground state and in [ESY07; ESY09] for the dynamics. But in general, the real wave function is not of a pure product type but it contains two-body correlations. They do not appear in the final equations because the separation of scales allows to integrate them out, resulting in the universal "potential" term of GPT – which, in reality, also contains the kinetic energy arising from two-body correlations [CS02]. How much of the BB energy is kinetic or potential depends on the potential shape, just as in the two-body problem: For a hard-sphere potential, the energy is entirely kinetic while for a soft one, it is entirely potential.

[2] This is sometimes referred to as non-local GPT but different from the approach in chapter 7.

[3] Take $\Psi = \prod_{i<j} f(\boldsymbol{x}_i - \boldsymbol{x}_j)$ with $f(r) = \max(0, 1 - \epsilon/r)$ the zero-energy scattering solution of a hard-sphere potential with radius ϵ. This vanishes when $\boldsymbol{x}_i = \boldsymbol{x}_j$ for any i, j and thus has a potential energy of zero. The kinetic energy is proportional to ϵ and vanishes as $\epsilon \to 0$.

In the impurity-BEC problem, we will find that the separation of scales upon which GPT relies is no longer present at strong coupling (chapter 7). We will therefore find that the two-body correlations can no longer be integrated out and include them explicitly.

Chapter 4

Impurity-BEC System

We now describe the general situation and present the Hamiltonian of an impurity in a condensate that is investigated in part II.

Since only a single impurity is considered, it is convenient to describe it in first quantised form in terms of its position and momentum operators $\hat{\boldsymbol{x}}_{\mathrm{I}}$ and $\hat{\boldsymbol{p}}_{\mathrm{I}}$. The Hamiltonian thus reads

$$H = H_{\mathrm{I}} + H_{\mathrm{B}} + H_{\mathrm{IB}}$$

where

$$\begin{aligned} H_{\mathrm{I}} &= \frac{\hat{\boldsymbol{p}}_{\mathrm{I}}^2}{2m_{\mathrm{I}}} \\ H_{\mathrm{B}} &= \int_{\boldsymbol{x}} \hat{a}^\dagger_{\boldsymbol{x}} \frac{-\Delta}{2m_{\mathrm{B}}} \hat{a}_{\boldsymbol{x}} + \frac{1}{2} \int_{\boldsymbol{x},\boldsymbol{y}} V^{\mathrm{BB}}(\boldsymbol{x}-\boldsymbol{y}) \hat{a}^\dagger_{\boldsymbol{x}} \hat{a}^\dagger_{\boldsymbol{y}} \hat{a}_{\boldsymbol{y}} \hat{a}_{\boldsymbol{x}} \\ H_{\mathrm{IB}} &= \int_{\boldsymbol{x}} V^{\mathrm{IB}}(\boldsymbol{x}-\hat{\boldsymbol{x}}_{\mathrm{I}}) \hat{a}^\dagger_{\boldsymbol{x}} \hat{a}_{\boldsymbol{x}}. \end{aligned}$$

Wave functions are linear combinations of objects of the form $\psi_{\mathrm{I}}(\boldsymbol{x}_I) \otimes |\Psi_{\mathrm{BB}}\rangle$, i.e. elements of the Hilbert space $\mathscr{H}_{\mathrm{IB}} = L^2(\mathscr{V}) \otimes \mathscr{H}_{\mathrm{B}}$ where $\mathscr{H}_{\mathrm{B}}$ is the Fock space of bosons.

4.1 LLP Transformation

There is canonical transformation introduced by Lee, Low and Pines (LLP) [LLP53] that allows to eliminate the impurity degrees of freedom (a slightly more detailed account was given by Girardeau [Gir61]). It makes use of conservation of total momentum and is applicable to all translation-invariant impurity-in-medium problems.

The transformation operator is

$$S = \exp(i\, \hat{\boldsymbol{x}}_{\mathrm{I}} \cdot \hat{\boldsymbol{P}}_{\mathrm{B}})$$

where $\hat{\boldsymbol{P}}_{\mathrm{B}} = \int_{\boldsymbol{x}} \hat{a}^\dagger_{\boldsymbol{x}} \hat{\boldsymbol{p}}_{\mathrm{B}} \hat{a}_{\boldsymbol{x}}$ is the total boson momentum operator. (Or total momentum of medium excitations in different polaron contexts. Note that the total momentum of Bogoliubov modes equals the total Boson momentum, such that the LLP transformation commutes with the

Bogoliubov transformation.) We will, this time, not define new mode operators as result of the transformation but instead apply it directly to the Hamiltonian:

$$H_{\mathrm{LLP}} = SHS^{-1}.$$

The price for this is that the same quantities have different physical meaning in the context of the LLP Hamiltonian than for the original one.

The application of S to the involved operators yields

$$\begin{aligned} S\hat{a}_{\boldsymbol{x}}^{(\dagger)}S^{-1} &= \hat{a}_{\boldsymbol{x}-\hat{\boldsymbol{x}}_{\mathrm{I}}}^{(\dagger)} \\ S\hat{\boldsymbol{x}}_{\mathrm{I}}S^{-1} &= \hat{\boldsymbol{x}}_{\mathrm{I}} \\ S\hat{\boldsymbol{p}}_{\mathrm{I}}S^{-1} &= \hat{\boldsymbol{p}}_{\mathrm{I}} - \hat{\boldsymbol{P}}_{\mathrm{B}}. \end{aligned}$$

Note that in the first line, $\boldsymbol{x}$ changed its meaning from an absolute boson coordinate to one relative to the impurity. In the last line, $\hat{\boldsymbol{p}}_{\mathrm{I}}$ changed its meaning to the total momentum, and will be denoted $\hat{\boldsymbol{p}}_0$ in the following.

The transformed parts of the Hamiltonian read

$$\begin{aligned} SH_{\mathrm{I}}S^{-1} &= \frac{\left(\hat{\boldsymbol{p}}_0 - \int_{\boldsymbol{x}} \hat{a}_{\boldsymbol{x}}^\dagger \hat{\boldsymbol{p}} \hat{a}_{\boldsymbol{x}}\right)^2}{2m_{\mathrm{I}}} \\ SH_{\mathrm{B}}S^{-1} &= H_{\mathrm{B}} \\ SH_{\mathrm{IB}}S^{-1} &= \int_{\boldsymbol{x}} V^{\mathrm{IB}}(\boldsymbol{x}) \hat{a}_{\boldsymbol{x}}^\dagger \hat{a}_{\boldsymbol{x}}. \end{aligned}$$

The last line has simplified considerably: In relative coordinates, the IB potential plays the role of an external one. However, in H_{I}, the impurity momentum is now expressed as difference between total and boson momentum. This leads to fourth order terms in boson operators, which can be interpreted as an effective interaction induced by the mobile impurity. Wave functions of the form $\psi \otimes |\Psi\rangle$ are now more difficult to interpret: Since $\hat{\boldsymbol{x}}_{\mathrm{I}}$ commutes with S, $|\psi(\boldsymbol{x})|^2$ still represents the probability of finding the impurity at $\boldsymbol{x}$. However, $\int_{\boldsymbol{x}} \overline{\psi_{\boldsymbol{x}}} \hat{\boldsymbol{p}} \psi_{\boldsymbol{x}}$ is now the expectation value of the *total* momentum.

The total momentum operator $\hat{\boldsymbol{p}}_0$ commutes with the Hamiltonian and may be replaced with its expectation value $\boldsymbol{p}_0$. This assumes that the total wave function is in a momentum eigenstate. If it is not, it can be written as linear combination of such states and each constituent may be treated separately by using the Hamiltonian with the corresponding momentum. Taking all terms together, the total Hamiltonian with fixed momentum reads

$$\begin{aligned} H_{\mathrm{LLP}} = \frac{\left(\boldsymbol{p}_0 - \int_{\boldsymbol{x}} \hat{a}_{\boldsymbol{x}}^\dagger \hat{\boldsymbol{p}} \hat{a}_{\boldsymbol{x}}\right)^2}{2m_{\mathrm{I}}} + \int_{\boldsymbol{x}} \hat{a}_{\boldsymbol{x}}^\dagger \frac{\hat{\boldsymbol{p}}^2}{2m_{\mathrm{B}}} \hat{a}_{\boldsymbol{x}} \\ + \frac{1}{2}\int_{\boldsymbol{x},\boldsymbol{y}} V^{\mathrm{BB}}(\boldsymbol{x}-\boldsymbol{y}) \hat{a}_{\boldsymbol{x}}^\dagger \hat{a}_{\boldsymbol{y}}^\dagger \hat{a}_{\boldsymbol{y}} \hat{a}_{\boldsymbol{x}} + \int_{\boldsymbol{x}} V^{\mathrm{IB}}(\boldsymbol{x}) \hat{a}_{\boldsymbol{x}}^\dagger \hat{a}_{\boldsymbol{x}}. \end{aligned} \tag{4.1}$$

This is the Hamiltonian that will be employed in part II.

4.2 Quench Dynamics

To probe the dynamical properties of the impurity-BEC system, a common approach is to start from a Bose gas in its ground state without impurity and then add the impurity interactions at $t = 0$. This situation can be realised in experiments by transferring the impurity from a non-interacting to an interacting state by, for example, a hyperfine flip in a situation where one hyperfine state is strongly interacting close to a Feshbach resonance while the other state has negligible coupling. The sudden switching on of interactions is called a *quench*. We will adopt this scheme for the dynamical situations discussed in part II.

Part II

Methods and Results

Chapter 5

Heavy Impurity in an Ideal BEC

The simplest case is that of a localised impurity in a non-interacting BEC. Despite – or perhaps rather because of – its simplicity, this problem has not received much attention in the literature. Exceptions are a short discussion in the context of RF spectra [Shc+16b], the investigation of Efimov physics near unitarity in a two-channel model [Shi+18] and our analysis in [DSE19], where we discuss qualitative features of the dynamics. Nonetheless, this simple case does already present some surprisingly interesting features, in particular when V^{IB} allows for a bound state between the impurity and one boson. In this case, the many-body energy is not bounded below as $N, V \to \infty$: in absence of any repulsion between them, all bosons could collectively enter the bound state. One might therefore suspect that the dynamics would be unstable as well with an ever growing number of particles getting bound to the impurity. This turns out not to be the case: In absence of inter-boson interactions, there is no decay channel that allows the system to loose a sufficient amount of energy such that it cannot approach the ground state. Instead, the system keeps oscillating between the BEC and the bound state.

For $m_{\mathrm{I}} \to \infty$ and $V^{\mathrm{BB}} \to 0$, the Hamiltonian reduces to a quadratic one,

$$H = \int_{\boldsymbol{x}} \hat{a}^\dagger_{\boldsymbol{x}} \left[\frac{\hat{\boldsymbol{p}}^2}{2m_{\mathrm{B}}} + V^{\mathrm{IB}}(\boldsymbol{x}) \right] \hat{a}_{\boldsymbol{x}} \,,$$

which can be solved by a product state ansatz $|\Psi\rangle = \left(\int_{\boldsymbol{x}} \phi_{\boldsymbol{x}} \hat{a}^\dagger_{\boldsymbol{x}}\right)^N |0\rangle$. ϕ, the condensate wave function, obeys the Schrödinger equation of the two-body problem of the impurity and one boson in relative coordinates:

$$i\partial_t \phi = \left[\frac{\hat{\boldsymbol{p}}^2}{2m_{\mathrm{B}}} + V^{\mathrm{IB}} \right] \phi \,. \tag{5.1}$$

Since the condensate wave function evolves according to the same equation (5.1) as the wave function of the two-body problem, it may seem that the two problems are equivalent. There is, however, one important difference, that concerns the domain of the functions ϕ, to

which the equation is applied. In the two-body case, they are square-integrable. While the continuum states serve well as a calculational tool, they are only relevant in normalisable superpositions, for otherwise, the probability of finding the two particles at a finite distance is zero. For the BEC, on the other hand, the relevant wave functions are those that correspond to a finite number of particles in each unit volume, such as the constant function. It is convenient to choose the normalisation of the ϕ as $\int|\phi|^2 = N$, in order to allow for convergence in the thermodynamic limit.

5.1 Decomposition in Terms of Two-Body Eigenstates

The difference between the two types of wave functions becomes clear when decomposing ϕ with respect to the eigenstates of the two-body Hamiltonian. Let us denote by $\psi_{\mathrm{b},i}$ the bound states with energy $-E_{\mathrm{b},i}$ and by ψ_k the continuum states with energy $E_k = k^2$, setting $2m_{\mathrm{B}} = 1$ for convenience. We consider only s-wave states, such that $k \in \mathbb{R}_+$ is scalar. A normalisable, spherically symmetric state $\phi_{\text{2-body}}$ can therefore be decomposed as

$$\phi_{\text{2-body}} = \sum_i \alpha_{\mathrm{b},i}\psi_{\mathrm{b},i} + \int_{\mathbb{R}_+} \alpha_k\psi_k \,\mathrm{d}k$$

and has the time-evolution (we set $2m_{\mathrm{B}} = 1$ for this chapter)

$$\phi_{\text{2-body}}(t) = \sum_i \alpha_{\mathrm{b},i}\psi_{\mathrm{b},i}e^{iE_{\mathrm{b},i}t} + \int_{\mathbb{R}_+} \alpha_k\psi_k e^{-ik^2t} \,\mathrm{d}k\,. \tag{5.2}$$

For a BEC, however, the overlap with the $k = 0$-mode is infinite such that, replacing $\alpha_k \to \alpha_0\delta(k) + \alpha_k$, one obtains

$$\begin{aligned}\phi_{\mathrm{BEC}} &= \alpha_0\psi_0 + \sum_i \alpha_{\mathrm{b},i}\psi_{\mathrm{b},i} + \int_{\mathbb{R}_+} \alpha_k\psi_k \,\mathrm{d}k \\ \phi_{\mathrm{BEC}}(t) &= \alpha_0\psi_0 + \sum_i \alpha_{\mathrm{b},i}\psi_{\mathrm{b},i}e^{iE_{\mathrm{b},i}t} + \int_{\mathbb{R}_+} \alpha_k\psi_k e^{-ik^2t} \,\mathrm{d}k\,. \end{aligned} \tag{5.3}$$

One can see two things from this decomposition.

(*i*) Even though the state is not normalisable the coefficients of the bound states, $\alpha_{\mathrm{b},i}$, are finite: they are obtained from $\alpha_{\mathrm{b},i} = \int_{\mathscr{V}} \overline{\psi_{\mathrm{b},i}}\phi_{\mathrm{BEC}}$ and $\psi_{\mathrm{b},i}$ decays exponentially. This means that the system does not approach its ground state with an infinite number of particles in the lowest bound state, but it remains dynamically stable.

(*ii*) In quantum mechanical systems, multiple energy levels can lead to oscillations with a frequency corresponding to the energy difference. In (5.2), this requires at least two bound states – oscillations between

a single bound state and the continuum will always dephase. In (5.3), however, the BEC state ψ_0 plays the role of an additional bound state with energy zero, such that oscillations are possible even when just one bound state exists.

This behaviour is visualised in fig. 5.1, where the density expectation value $|\phi(r,t)|^2$ is shown for an initial normalisable (gaussian) state and a BEC state in the case where one bound state exists. While the gaussian state converges to the profile of the bound state, the BEC profile keeps oscillating. Remarkably, it features a halo of depletion around the impurity which reaches zero density at certain times. A more detailed discussion of density profiles will be given in chapter 6 for an interacting Bose gas, including attractive coupling and mobile impurities.

Energy of the Zero-Energy Mode Equation (5.3) is, in fact, not quite correct. Namely, we have assumed infinite volume to obtain a mode with $k = 0$ and a continuum, and only afterwards chosen the wave function such that it corresponds to a density of n. In reality, volume and particle number are large but finite and what we should really do is take the thermodynamic limit and therefore start with a finite volume and suitable boundary conditions (zero boundary conditions being the most realistic). This causes essentially two differences:

- The continuum becomes discrete with the allowed values determined by the boundary conditions. Approximating the resulting sums by integrals as above causes an error $\mathcal{O}(\mathscr{V}^{-1})$.
- $k = 0$ is not included in the allowed discrete values. The zero-mode is therefore to be replaced with lowest-lying positive-energy mode, which has an energy of $\mathcal{O}(\mathscr{V}^{-1})$.

The first point is not important because the continuum is occupied by less than $\mathcal{O}(\mathscr{V})$ particles (precisely, by $\mathcal{O}(n\mathscr{V}^{1/3})$, as we will see below). The second point, however, is important because the zero-mode is occupied by $\mathcal{O}(N)$ particles, leading to a non-zero error $\mathcal{O}(n)$. Therefore, this energy $E_0 = \mathcal{O}(\mathscr{V}^{-1})$ should be included in equation (5.3) by means of a time-evolution factor $\exp(-iE_0t)$ for the zero-mode.

The value of E_0 can be estimated from using the formula for $k = 0$, but not using the energy *eigenvalue* but the value of the energy *functional* $E[\psi_0] = \int(|\nabla\psi_0|^2 + V^{\mathrm{IB}}|\psi_0|^2) \,/\, \int|\psi_0|^2$. The two are different because the boundary conditions are violated by ψ_0: In a ball B_R of radius R, we have

$$\begin{aligned}
E_0 &= \int_{B_R} (|\nabla\psi_0|^2 + V^{\mathrm{IB}}|\psi_0|^2) \Big/ \int_{B_R} |\psi_0|^2 \\
&= \left(\int_{\partial B_R} \overline{\psi_0}\nabla\psi_0 \cdot \mathrm{d}\boldsymbol{r} + \int_{B_R} \overline{\psi_0}(-\Delta + V^{\mathrm{IB}})\psi_0\right) \Big/ \int_{B_R} |\psi_0|^2 \\
&\quad \Big| \textit{ By definition of the scattering length, } \psi_0 \to 1 - a_{IB}/r \textit{ for large } r. \\
&= 4\pi R^2 \left(1 - \frac{a_{\mathrm{IB}}}{R}\right) \frac{a_{\mathrm{IB}}}{R^2} \Big/ (\mathscr{V} + \mathcal{O}(\mathscr{V} a_{\mathrm{IB}}/R)) \\
&= 4\pi a_{\mathrm{IB}} \,/\, \mathscr{V} + \mathcal{O}(\mathscr{V}^{-4/3}).
\end{aligned}$$

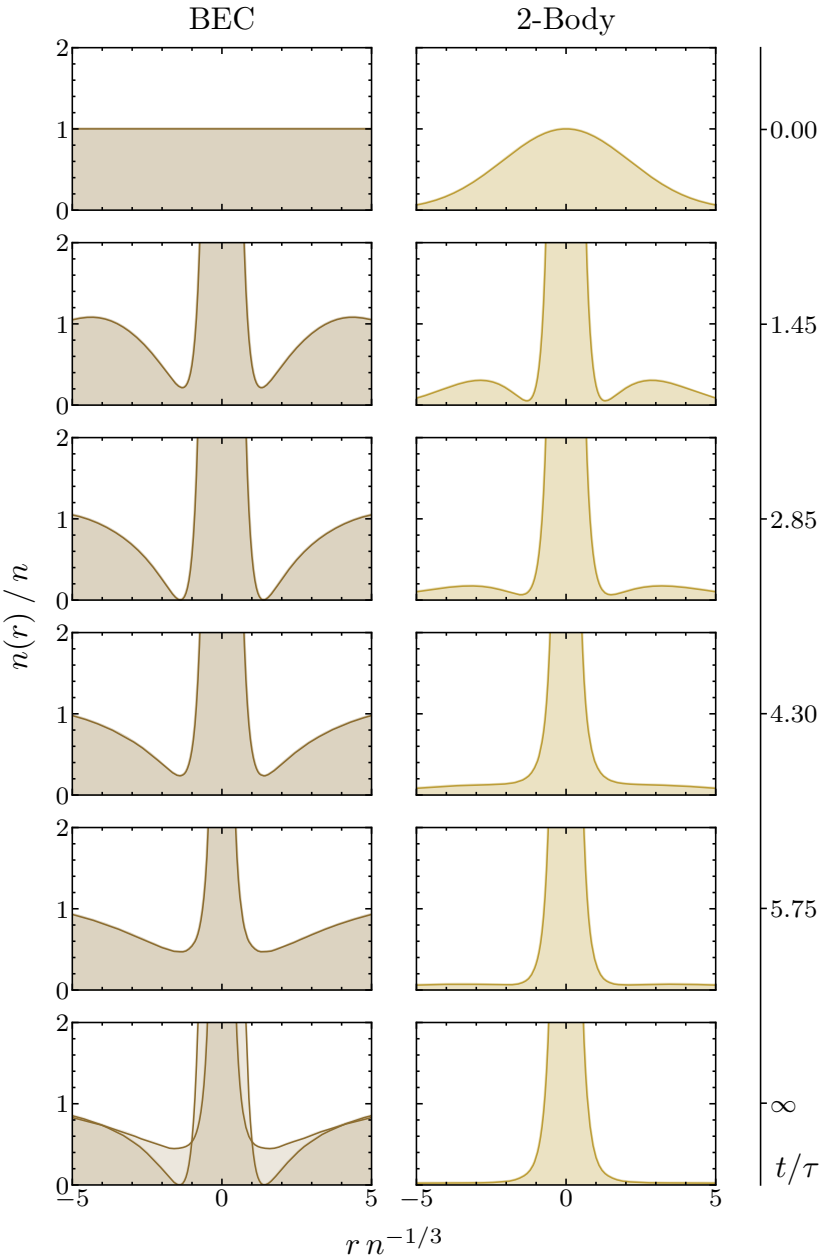

Figure 5.1: Comparison of the time evolution of a normalisable and a non-normalisable initial state obeying the two-body Schrödinger equation. The potential V^{IB} is a contact interaction with positive scattering length and thus has a single bound state. The last row shows the asymptotic behaviour for long times, where the BEC state keeps oscillating between the two limit curves shown, while the normalisable state has converged to the bound state. The scattering length is $a_{\mathrm{IB}} = 1.0n^{-1/3}$, the time unit is the BEC time scale $\tau = m_{\mathrm{B}} n_0^{-2/3}/\hbar$.

In fact, it does not matter if the time evolution factor $\exp(-iE_0t)$ is attributed only to the first term in (5.3) or to all terms, because only the first one is of order N. Therefore, we may as well use a global phase factor for the many-body wave function and retain expression (5.3):

$$|\Psi(t)\rangle = e^{-i4\pi a_{\mathrm{IB}} nt} \left(\hat{\phi}^\dagger_{\mathrm{BEC}}(t)\right)^N |0\rangle \tag{5.4}$$

$$\text{where} \quad \hat{\phi}^\dagger_{\mathrm{BEC}}(t) = \int_{\boldsymbol{x}} \phi_{\mathrm{BEC}}(\boldsymbol{x}, t)\hat{a}^\dagger_{\boldsymbol{x}}.$$

For time-local observables, this plays no role but when computing, for example, the RF spectrum from the time-dependent overlap, the phase factor is essential.

5.2 Exact Time Evolution of a BEC in Presence of a Stationary Contact Potential

For the case where V^{IB} is a contact potential, the coefficients and time evolution in (5.3) can be computed explicitly for an initially flat BEC, $\phi_{\mathrm{BEC}}(t=0) = \sqrt{n}$. This is not just an academic exercise but will serve as a useful ingredient in our numerical computations for the interacting case.

5.2.1 Projection of Condensate State onto Eigenstates of the Contact Hamiltonian

In section 2.3 we have derived the eigenstates of the contact Hamiltonian

$$\begin{aligned} u_0 &= r - a_{\mathrm{IB}} \\ u_{\mathrm{b}} &= \frac{\exp(-r/a_{\mathrm{IB}})}{\sqrt{\pi a_{\mathrm{IB}}}} && \text{if } a_{\mathrm{IB}} > 0 \\ u_k &= \frac{\sin(kr) - a_{\mathrm{IB}} k \cos(kr)}{\pi\sqrt{2(1 + a^2_{\mathrm{IB}} k^2)}} && \text{for } k > 0 \end{aligned}$$

and the coefficients α in equation (5.3) are computed from projecting the BEC state $u_{\mathrm{BEC}} = \sqrt{n}r$ onto them. For the zero mode, we clearly get $\alpha_0 = \sqrt{n}$. Thus,

$$u_{\mathrm{BEC}} = \sqrt{n}u_0 + a_{\mathrm{IB}}\sqrt{n}\,,$$

and we must project the remaining term $a_{\mathrm{IB}}\sqrt{n}$ onto u_{b} and u_k. While it is clear that the 0-mode part is not normalisable, it is interesting to note that the remainder still is not. This basically means that there are infinitely many particles in the continuum, even though this is only a vanishing fraction of all particles: $\int_{\boldsymbol{r}} |\sqrt{n}\frac{a_{\mathrm{IB}}}{r}|^2 \sim n\mathscr{V}^{1/3}$ in comparison to $\int_{\boldsymbol{r}} |\sqrt{n}\psi_0|^2 \sim n\mathscr{V} = N$.

Projection onto Bound State This is just an integral over an exponential.

$$\begin{aligned}\alpha_\mathrm{b} &= 4\pi \int_{\mathbb{R}_+} a_\mathrm{IB}\sqrt{n} u_\mathrm{b}(r)\,\mathrm{d}r \\ &= 2\sqrt{2\pi a_\mathrm{IB} n}\int_{\mathbb{R}_+} e^{-r/a_\mathrm{IB}}\,\mathrm{d}r \\ &= 2a_\mathrm{IB}\sqrt{2\pi a_\mathrm{IB} n}\,.\end{aligned}$$

Projection onto Continuum Here, the integral is in the sense of distributions and we need, once again, equation (A.1d).

$$\begin{aligned}\alpha_k &= 4\pi \int_{\mathbb{R}_+} a_\mathrm{IB}\sqrt{n} u_k(r)\,\mathrm{d}r \\ &= \frac{-2a_\mathrm{IB}\sqrt{2n}}{\sqrt{1+a_\mathrm{IB}^2k^2}}\,\mathrm{Re}\int_{\mathbb{R}_+} e^{ikr}(a_\mathrm{IB}k+i)\,\mathrm{d}r \\ &\quad \Big| \text{ (A.1d)} \\ &= \frac{-2a\sqrt{2n}}{\sqrt{1+a_\mathrm{IB}^2k^2}}\,\mathrm{Re}\left(\pi\delta(k)+\frac{i}{k}\right)(a_\mathrm{IB}k+i) \\ &= \frac{2a_\mathrm{IB}\sqrt{2n}}{k\sqrt{1+a_\mathrm{IB}^2k^2}}\,.\end{aligned}$$

5.2.2 Time Evolution

We can now insert the coefficients α into

$$u_\mathrm{BEC}(r,t) = \sqrt{n}u_0(r) + \mathbb{1}_{a_\mathrm{IB}>0}\alpha_\mathrm{b}u_\mathrm{b}(r)e^{iE_\mathrm{b}t} + \int_{\mathbb{R}_+}\alpha_k u_k(r)e^{-ik^2t}\,\mathrm{d}k$$

and compute the k-integral. This is done by similar means as for the propagator in section 2.3.3[1].

[1] We could have used the result for the propagator instead of computing the coefficients α_k, but it is more convenient to perform the integrals in reverse order.

$$
\begin{aligned}
&\int_{\mathbb{R}_+} \alpha_k u_k(r) e^{-ik^2 t}\,\mathrm{d}k \\
&= \int_{\mathbb{R}_+} e^{-ik^2 t} \frac{-\operatorname{Re} e^{ikr}(a_{\mathrm{IB}}k + i)}{\pi\sqrt{2(1+a_{\mathrm{IB}}^2 k^2)}} \frac{2a_{\mathrm{IB}}\sqrt{2n}}{k\sqrt{1+a_{\mathrm{IB}}^2 k^2}}\,\mathrm{d}k \\
&= \frac{-2a_{\mathrm{IB}}\sqrt{n}}{\pi} \int_{\mathbb{R}_+} e^{-ik^2 t} \operatorname{Re} \frac{e^{ikr}}{k(a_{\mathrm{IB}}k - i)}\,\mathrm{d}k \\
&\quad \Big| \textit{ The integrand is symmetric in } k\textit{, so we can replace } \textstyle\int_{\mathbb{R}_+} \to \frac{1}{2}\int_{\mathbb{R}}\textit{. For later use, introduce an } \operatorname{Im} t < 0\textit{.} \\
&= \frac{-a_{\mathrm{IB}}\sqrt{n}}{\pi} \lim_{\operatorname{Im} t \nearrow 0} \int_{\mathbb{R}} e^{-ik^2 t} \operatorname{Re} \frac{e^{ikr}}{k(a_{\mathrm{IB}}k - i)}\,\mathrm{d}k \\
&\quad \Big| \textit{ The imaginary part of the fraction is anti-symmetric in } k\textit{, so the "Re" can be omitted. This requires using a principal value integral since the imaginary part has a pole at 0. Then use a partial fraction decomposition.} \\
&= \frac{-a_{\mathrm{IB}}\sqrt{n}}{\pi} \lim_{\operatorname{Im} t \nearrow 0} \mathcal{P}\int_{\mathbb{R}} e^{-ik^2 t + ikr} \left(\frac{i}{k} - \frac{a_{\mathrm{IB}} i}{a_{\mathrm{IB}}k - i}\right)\mathrm{d}k \\
&\quad \Big| \text{ (A.1c), (A.1b)} \\
&= a_{\mathrm{IB}}\sqrt{n}\Bigg(\operatorname{erf}\left(\frac{r}{2\sqrt{it}}\right) \\
&\qquad\qquad - e^{it/a_{\mathrm{IB}}^2 - r/a_{\mathrm{IB}}}\left(\operatorname{sgn} a_{\mathrm{IB}} - \operatorname{erf}\left(\frac{\sqrt{it}}{a_{\mathrm{IB}}} - \frac{r}{2\sqrt{it}}\right)\right)\Bigg)
\end{aligned}
$$

Together with the parts of the bound state and the zero mode,

$$
\begin{aligned}
\mathbb{1}_{a_{\mathrm{IB}}>0}\alpha_{\mathrm{b}} u_{\mathrm{b}}(r) e^{iE_{\mathrm{b}}t} &= \mathbb{1}_{a_{\mathrm{IB}}>0} 2a_{\mathrm{IB}}\sqrt{n} e^{it/a_{\mathrm{IB}}^2 - r/a_{\mathrm{IB}}} \\
\alpha_0 u_0(r) &= \sqrt{n}r - \sqrt{n}a_{\mathrm{IB}}\,,
\end{aligned}
$$

this yields

$$
\begin{aligned}
\phi_{\mathrm{BEC}}(\boldsymbol{r}, t) = \sqrt{n} - \sqrt{n}\frac{a_{\mathrm{IB}}}{r} e^{-r^2/4it}\Bigg(&\operatorname{erfcx}\left(\frac{r}{2\sqrt{it}}\right) \\
&- \operatorname{erfcx}\left(\frac{r}{2\sqrt{it}} - \frac{\sqrt{it}}{a_{\mathrm{IB}}}\right)\Bigg) \qquad (5.5)
\end{aligned}
$$

in terms of the scaled complementary error function $\operatorname{erfcx} z = e^{z^2}(1 - \operatorname{erf} z)$, shown in fig. 5.2.

Asymptotics For long times, (5.5) has the asymptotics

$$
\phi_{\mathrm{BEC}} \to \sqrt{n} - \sqrt{n}\frac{a_{\mathrm{IB}}}{r}\left(1 - e^{-r/a_{\mathrm{IB}}} \operatorname{erfcx}\left(-\frac{\sqrt{it}}{a_{\mathrm{IB}}}\right)\right).
$$

From fig. 5.2 one can see that $\operatorname{erfcx}(-\sqrt{it}/a_{\mathrm{IB}})$ converges to zero for $a_{\mathrm{IB}} < 0$. Here, the wave function converges to the scattering solution $\sqrt{n}(1 - a_{\mathrm{IB}}/r)$. For $a_{\mathrm{IB}} > 0$ however, $\operatorname{erfcx}(-\sqrt{it}/a_{\mathrm{IB}})$ oscillates. But

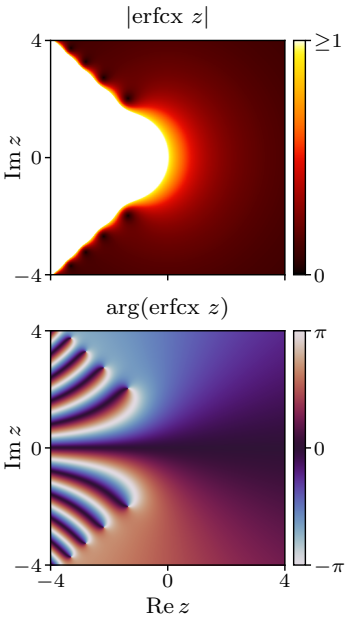

Figure 5.2: Absolute value and phase of the scaled complementary error function.

the zeros of erfcx z are not precisely on the line $z = -\sqrt{it}$ but shifted further away from the real axis. Therefore, the wave function does not periodically reach the zero-mode. Instead, we find that |erfcx| slowly converges to 2 with oscillating phase factor. The real values of ± 2 can be considered the extremal cases and lead to the limiting curves in fig. 5.1. Here, the wave function is $\phi_{\text{BEC}} = \sqrt{n}\left(1 - \frac{a_{\text{IB}}}{r}\left(1 \mp 2e^{-r/a_{\text{IB}}}\right)\right)$. In particular, it periodically has a zero. This explains the fact that the density reaches zero in fig. 5.1 but that these zeros are not located at $r = a_{\text{IB}}$ as in the scattering solution. Instead, they are determined by $1 = \frac{a_{\text{IB}}}{r_0}\left(1 + 2e^{-r_0/a_{\text{IB}}}\right)$, which yields $r_0/a_{\text{IB}} \approx 1.45$. This value is independent of parameters.

5.3 RF Spectrum

The knowledge of the wave function after a quench in an ideal BEC gives us access to a large number of physical observables in this limiting case. The results are already interesting on their own and are also useful as a basis for discussing results of approximating methods for the more complicated cases of finite mass and an interacting BEC.

In this section, we compute the time-dependent overlap and the RF spectrum:

$$\begin{aligned}
\text{Time-dependent overlap:} \quad S(t) &= \langle\Psi(0)|\Psi(t)\rangle \\
&= \langle\Psi(0)|e^{-iHt}|\Psi(0)\rangle \\
\text{RF spectrum:} \quad A(\omega) &= \frac{1}{\pi}\,\text{Re}\int_0^\infty e^{i\omega t}S(t) \\
&= \langle\Psi(0)|\delta(\omega - H)|\Psi(0)\rangle\,.
\end{aligned}$$

The RF spectrum is an interesting quantity because it allows to directly measure spectral properties of the many-body Hamiltonian H. More precisely, it corresponds to the weights of the spectral decomposition of the initial state with respect to H. Such spectra have already been measured with different atom species [Hu+16; Jør+16; Yan+20]. Theoretically, they have been computed for an interacting gas in Bogoliubov theory in [Sha+14] within the Fröhlich model (attractive side only) and in [RS13; Shc+16b] beyond the Fröhlich model. The supplemental material of [Shc+16b] contains a comparison with experiments, showing excellent agreement. The interest in computing the spectrum here for the simpler case lies in the fact that the result is numerically exact and can be well understood due to the simple structure of the wave function. In fact, we will find no qualitative difference to the situation in [Shc+16b].

5.3.1 Time-Dependent Overlap

It is convenient to use a coherent state instead of a product state, thereby allowing for a relatively small variance in the number of particles, and to normalise the wave function:

$$|\psi(t)\rangle = \exp\left(-i4\pi a_{\text{IB}} n t + \hat{\phi}^\dagger_{\text{BEC}}(t) - \frac{\int|\phi_{\text{BEC}}|^2}{2}\right)|0\rangle\,.$$

Then, with the Baker-Campbell-Hausdorff formula,

$$\begin{aligned} S(t) &= \exp\Big(-i4\pi a_{\mathrm{IB}} nt + [\hat{\phi}_{\mathrm{BEC}}(0), \hat{\phi}^\dagger_{\mathrm{BEC}}(t)] - \int |\phi_{\mathrm{BEC}}|^2\Big) \\ &= \exp\Big(-i4\pi a_{\mathrm{IB}} nt + \mathbb{1}_{a_{\mathrm{IB}}>0}|\alpha_{\mathrm{b}}|^2\big(e^{iE_{\mathrm{b}}t}-1\big) \\ &\qquad + \int_0^\infty \mathrm{d}k\, |\alpha_k|^2\big(e^{-ik^2t}-1\big)\Big). \end{aligned}$$

Once again, the integral can be computed analytically.

$$\begin{aligned} &\int_0^\infty \big(e^{-ik^2t}-1\big)|\alpha_k|^2\ \mathrm{d}k \\ &\quad \Big|\ \textit{Again, } \textstyle\int_0^\infty \to \frac{1}{2}\int_{\mathbb{R}} \\ &= 4a_{\mathrm{IB}}^2 n \int_{\mathbb{R}} \frac{e^{-ik^2t}-1}{k^2(1+a_{\mathrm{IB}}^2k^2)}\ \mathrm{d}k \\ &= 4a_{\mathrm{IB}}^2 n\left(\int_{\mathbb{R}} \frac{e^{-ik^2t}-1}{k^2}\ \mathrm{d}k - a_{\mathrm{IB}}^2\int_{\mathbb{R}} \frac{e^{-ik^2t}-1}{1+a_{\mathrm{IB}}^2k^2}\ \mathrm{d}k\right) \\ &\quad \Big|\ \textit{First integral } I(t)\textit{: } \tfrac{\partial}{\partial t}I(t) = -i\textstyle\int_{\mathbb{R}} e^{-ik^2t} = -i\sqrt{\frac{\pi}{it}}\textit{, thus } I(t) = -2\sqrt{i\pi t}. \\ &\quad \Big|\ \textit{Second integral: Equation } (\mathrm{A.1a}). \\ &= 4a_{\mathrm{IB}}^2 n\left(-2\sqrt{i\pi t} - a_{\mathrm{IB}}\pi e^{it/a_{\mathrm{IB}}^2}\left(\operatorname{sgn} a_{\mathrm{IB}} - \operatorname{erf}\frac{\sqrt{it}}{a_{\mathrm{IB}}}\right) + a_{\mathrm{IB}}\pi \operatorname{sgn} a_{\mathrm{IB}}\right) \end{aligned}$$

Together with $|\alpha_{\mathrm{b}}|^2\big(e^{iE_{\mathrm{b}}t}-1\big) = 8\pi a_{\mathrm{IB}}^3 n\big(e^{it/a_{\mathrm{IB}}^2}-1\big)$, we arrive at

$$S(t) = \exp\left(-i4\pi a_{\mathrm{IB}} nt + 4\pi a_{\mathrm{IB}}^3 n\left(\operatorname{erfcx}\left(-\frac{\sqrt{it}}{a_{\mathrm{IB}}}\right) - 1 - \frac{2}{a_{\mathrm{IB}}}\sqrt{\frac{it}{\pi}}\right)\right). \tag{5.6}$$

5.3.2 RF Spectrum

Fourier-transforming (5.6) numerically for a range of scattering lengths, we arrive at the RF spectrum, fig. 5.3. We can understand in detail how it emerges from the two-body spectrum. For this, a different formulation of $A(\omega)$ is useful, which allows to view it as a delta peak at $\omega = 0$, which is subsequently shifted and broadened by three operators corresponding to the three parts of the two-body spectrum (zero-mode, bound state and continuum).

$$\begin{aligned} A(\omega) &= (\mathscr{F}^{-1}S)(\omega) \\ &= (\mathscr{F}^{-1}S\mathscr{F}\mathscr{F}^{-1}1)(\omega) \\ &= A_0A_{\mathrm{b}}A_{\mathrm{c}}\delta(\omega) \end{aligned}$$

Interpret S as multiplication operator acting on the constant function 1.

where

$$\begin{aligned} A_0 &= \mathscr{F}^{-1}\exp(-i4\pi a_{\mathrm{IB}} nt)\mathscr{F} \\ A_{\mathrm{b}} &= \mathscr{F}^{-1}\exp\left(|\alpha_{\mathrm{b}}|^2\big(e^{iE_{\mathrm{b}}t}-1\big)\right)\mathscr{F} \\ A_{\mathrm{c}} &= \mathscr{F}^{-1}\exp\left(\int_0^\infty \mathrm{d}k\, |\alpha_k|^2\big(e^{-ik^2t}-1\big)\right)\mathscr{F}. \end{aligned}$$

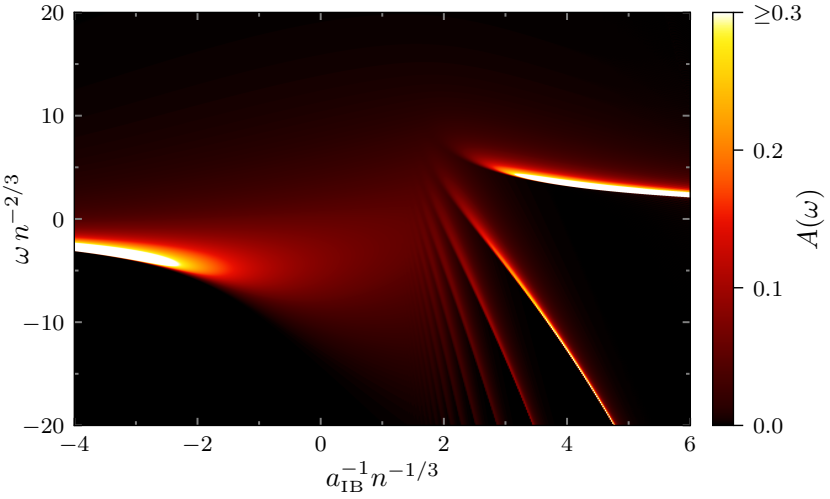

Figure 5.3: Numerically exact RF spectrum of a localised impurity in an ideal BEC. For weak coupling, the spectrum is dominated by the zero-energy mode ϕ_0 with energy $4\pi a_{\mathrm{IB}} n$. On the repulsive side, the singly and multiply occupied bound state leads to additional peaks at distances, which are multiples of $1/2m_{\mathrm{red}}a_{\mathrm{IB}}^2$. At strong coupling, the ψ_0-peak gets weaker and is replaced by a smeared-out contribution of the continuum.

Note that these operators commute. Introducing the shift operator

$$\sigma_E f(\omega) = f(\omega - E)$$
$$\sigma_E = e^{-E\partial_\omega} = \mathscr{F}^{-1} e^{-iEt} \mathscr{F},$$

we can write

$$A_0 = \sigma_{4\pi a_{\mathrm{IB}} n}$$
$$A_{\mathrm{b}} = \exp\left(|\alpha_{\mathrm{b}}|^2(\sigma_{-E_{\mathrm{b}}} - 1)\right)$$
$$A_{\mathrm{c}} = \exp\left(\int_0^\infty \mathrm{d}k\, |\alpha_k|^2(\sigma_{k^2} - 1)\right).$$

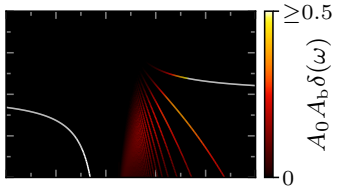

Figure 5.4: The spectrum without the continuum part, consisting of the lines $4\pi a_{\mathrm{IB}} n - jE_{\mathrm{b}}$ with poissonian weights. The axes are the same as in fig. 5.3.

The effect of the three parts of the two-body spectrum can thus be discussed independently.

- The zero-mode simply shifts the many-body spectrum by $4\pi a_{\mathrm{IB}} n$. In fig. 5.3, this corresponds to the strongest peaks that may be seen at weak coupling, but not at strong coupling due to the broadening and shifting by the continuum.

- For the effect of the bound state, we may expand

$$A_{\mathrm{b}} = \sum_{j=0}^{\infty} \frac{|\alpha_{\mathrm{b}}|^{2j}}{j!} e^{-|\alpha_{\mathrm{b}}|^2} \sigma_{-jE_{\mathrm{b}}}. \tag{5.7}$$

  The bound state thus causes shifts by multiples of the binding energy, leading to the additional lines on the repulsive side in the figure. They correspond to many-body eigenstates of the form $\hat{\psi}_{\mathrm{b}}^{\dagger j} \hat{\psi}_0^{\dagger N-j} |0\rangle$. According to (5.7), their weights are given by a Poisson distribution with mean value $|\alpha_{\mathrm{b}}|^2 = 8\pi a_{\mathrm{IB}}^3 n$. For weak coupling, this value is small, meaning that the bound state is occupied at most once and that only one additional peak may be

seen. For stronger coupling, multiply bound states gain weight and additional lines appear in the spectrum. As the lines get denser and the broadening by then continuum stronger, a smooth crossover to the attractive side takes place. A sketch of the purely discrete part of the spectrum is shown in fig. 5.4.

- The continuum, finally, broadens the peaks. Since the energies are positive, the broadening happens only in one direction, such that the lines in fig. 5.4 constitute the lower bounds of the broadened lines in fig. 5.3. At stronger coupling, the continuum contributes also a shift that cancels the zero-energy shift on the attractive side and the mean effect of the bound states on the repulsive side. This is necessary because the initial state has energy zero and there are no decay mechanisms that would allow for a convergence towards the ground state.

  The shape of the peaks is determined by $A_c\delta(\omega)$, which depends only on $|a_{IB}|$. It is shown for three values in fig. 5.5. For weak coupling, we may estimate it by approximating $|\alpha_k|^2 \approx 4a_{IB}^2 n \,/\, k^2$, leading to $\int_0^\infty \mathrm{d}k\, |\alpha_k|^2 \left(e^{-ik^2 t} - 1\right) \approx -8a_{IB}^2 n \sqrt{i\pi t}$. The exponential of this has the Fourier transform

$$A_c\delta(\omega) \approx \mathbb{1}_{\omega>0} \frac{4\pi a_{IB}^3 n}{\omega^{3/2}} \exp\left(-\frac{16\pi a_{IB}^4 n^2}{\omega}\right).$$

  In fig. 5.5, the narrowest peak is of this form. One can see the $\omega^{-3/2}$-shape, which is regularised by the exponential near zero. For stronger couplings, the shape becomes more complicated as the erfcx -1 in equation (5.6) becomes important.

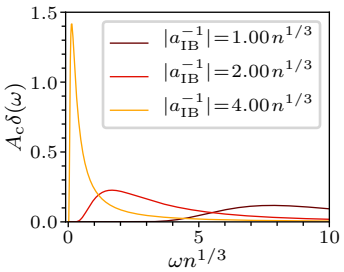

Figure 5.5: Shape of the peaks in the RF spectrum for different coupling strengths.

5.4 Original Contribution and Relation to Other Works

This section contains a summary of which findings of this chapter are new and how they relate to previous works.

- Concerning the discussion that a single bound state can give rise to oscillations, we have given an analytical argument similar to the one in this chapter in [DSE19]. Therein, we worked in momentum space and made use of a c-number substitution as in Bogoliubov theory; c.f. the analysis in section 6.6.
- Dynamical density profiles were also computed in [DSE19]. The more detailed discussion therein will be presented in the next chapter for an interacting Bose gas.
- The analytical computation of the wave function and time-dependent overlap are new and so far unpublished.
- An RF spectrum similar to fig. 5.3 has been computed by Shchadilova *et al.* [Shc+16b] for a finite-mass impurity and an interacting BEC, using Bogoliubov approximation and a coherent state

ansatz. Results for limited excitation number had been obtained earlier by Rath and Schmidt [RS13] and a treatment of attractive coupling within the Fröhlich model had been given by Shashi *et al.* [Sha+14]. The computation here complements [Shc+16b] by showing that the qualitative features remain correct in a numerically exact treatment. This is important because the Bogoliubov treatment has a dynamical instability at strong coupling. That the results agree nonetheless shows that this instability does not enter in the RF spectrum even though it may lead to unphysical results in other observables, as we will see in the next chapter.

- The discussion of the RF spectrum in [Shc+16b] covered the basic relations to the two-body spectrum and how it is modified by the BB interaction. For the non-interacting case, we went further in this chapter by deriving the weights of the multiply bound states and by discussing the shape of the peaks.

5.5 Summary and Outlook

We have treated the problem of an infinitely heavy impurity in an ideal BEC analytically and seen that qualitative differences to the two-body problem emerge and originate in the macroscopic occupation of the zero-mode. In presence of a bound state, oscillations between the zero-mode and multiply bound states result. These do not decay within the ideal gas and it will be an important question for the next chapters if this remains true in an interacting gas.

The time evolution for the case of a contact potential has been solved exactly. The result provides insights into the structure of the wave function, in particular at long times. This explains halos of complete depletion in the condensate density in the time evolution at a universal distance $r_0/a_{\mathrm{IB}} \approx 1.45$. In contrast, the zero mode has a zero at $r = a_{\mathrm{IB}}$. These depletion maxima are as well of particular interest for the analysis of the interacting BEC in the next chapters because a BB repulsion acts in favour of a more homogeneous condensate.

We have computed an analytical formula for the time-dependent overlap and used it to numerically compute the RF spectrum. Its features can be well-understood in terms of the zero-mode, which causes a peak at $4\pi a_{\mathrm{IB}} n$, the bound state (if existent), which leads to additional peaks at distances of the binding energy, and the continuum, which broadens and shifts the peaks near the resonance and leads to a smooth crossover. Remarkably, the results are very similar to those previously obtained [Shc+16b] for the more complicated case of an interacting BEC and a mobile impurity.

Chapter 6

The Bose Polaron in Bogoliubov Approximation

The most widely adopted method for theoretical investigations of the Bose polaron is Bogoliubov theory. This is, for one thing, due to the fact that Bogoliubov theory is a successful theory for the weakly interacting Bose gas, that naturally includes quantum fluctuations and non-zero temperature and can easily be extended to include an impurity. For the other thing, a Fröhlich-type Hamiltonian can be derived from it with one further approximation is made, thereby making direct connection to the classical solid-state polaron and allowing techniques for it to be applied.

In this chapter, we first derive the general Hamiltonian and discuss a number of further approximations that are commonly applied to it. An overview of previous literature on the resulting models and techniques for solving it follows. Afterwards, we go in more detail through the methods, that were applied by the author in his own research and the results obtained from it. These are, in large parts, published in [DSE19].

The material is presented in a self-contained way; a differentiation on which findings are new and how they relate to previous works is given at the end of the chapter.

6.1 The Bogoliubov Hamiltonian with Impurity

Starting point is, once again, the LLP Hamiltonian, but this time in momentum space:

$$H_{\mathrm{LLP}} = \frac{\left(\boldsymbol{p}_0 - \fint_{\boldsymbol{k}} \boldsymbol{k}\hat{a}^\dagger_{\boldsymbol{k}}\hat{a}_{\boldsymbol{k}}\right)^2}{2m_{\mathrm{I}}} + \fint_{\boldsymbol{k}} \frac{\boldsymbol{k}^2}{2m_{\mathrm{B}}}\hat{a}^\dagger_{\boldsymbol{k}}\hat{a}_{\boldsymbol{k}} + \frac{1}{2}\fint_{\boldsymbol{k},\boldsymbol{q},\boldsymbol{p}} v^{\mathrm{BB}}(\boldsymbol{p})\hat{a}^\dagger_{\boldsymbol{k}+\boldsymbol{p}}\hat{a}^\dagger_{\boldsymbol{q}-\boldsymbol{p}}\hat{a}_{\boldsymbol{q}}\hat{a}_{\boldsymbol{k}} + \fint_{\boldsymbol{k},\boldsymbol{q}} v^{\mathrm{IB}}(\boldsymbol{k}-\boldsymbol{q})\hat{a}^\dagger_{\boldsymbol{k}}\hat{a}_{\boldsymbol{q}}\,.$$

The derivation is relatively straight-forward: The Bogoliubov approximation and rotation are applied to the bosonic part of the Hamiltonian in the same way as without impurity and all that is left to do is to apply the c-number substitution and Bogoliubov rotation to the impurity-related terms as well. For the kinetic term, note that $\hat{a}^\dagger_{\boldsymbol{k}}\hat{a}_{\boldsymbol{k}} - \hat{a}^\dagger_{-\boldsymbol{k}}\hat{a}_{-\boldsymbol{k}} = \hat{b}^\dagger_{\boldsymbol{k}}\hat{b}_{\boldsymbol{k}} - \hat{b}^\dagger_{-\boldsymbol{k}}\hat{b}_{-\boldsymbol{k}}$ and that the zero-mode does not enter, such that

$$\frac{\left(\boldsymbol{p}_0 - ⨍_{\boldsymbol{k}}\, \boldsymbol{k}\hat{a}^\dagger_{\boldsymbol{k}}\hat{a}_{\boldsymbol{k}}\right)^2}{2m_{\mathrm{I}}} = \frac{\left(\boldsymbol{p}_0 - ⨍_{\boldsymbol{k}}\, \boldsymbol{k}\hat{b}^\dagger_{\boldsymbol{k}}\hat{b}_{\boldsymbol{k}}\right)^2}{2m_{\mathrm{I}}}\,.$$

For the interaction term (we write $c_k = \cosh(\phi_k)$ and $s_k = \sinh(\phi_k)$),

$$\begin{aligned}
&⨍_{\boldsymbol{k},\boldsymbol{q}} v^{\mathrm{IB}}(\boldsymbol{k}-\boldsymbol{q})\hat{a}^\dagger_{\boldsymbol{k}}\hat{a}_{\boldsymbol{q}} \\
&\quad\Big|\ \textit{Split integral into } \boldsymbol{k}=\boldsymbol{q}\textit{, yielding } v^{IB}(0)n\textit{, and } \boldsymbol{k}\neq\boldsymbol{q}. \\
&\quad\Big|\ \textit{Insert } \hat{a}_{\boldsymbol{k}} = \sqrt{n_0}(2\pi)^3\delta^3(\boldsymbol{k}) + c_k\hat{b}_{\boldsymbol{k}} + s_k\hat{b}^\dagger_{-\boldsymbol{k}}. \\
&= v^{\mathrm{IB}}(0)n + \sqrt{n_0}⨍_{\boldsymbol{k}} v^{\mathrm{IB}}(k)\Big(c_k\hat{b}^\dagger_{\boldsymbol{k}} + s_k\hat{b}_{-\boldsymbol{k}} + c_k\hat{b}_{-\boldsymbol{k}} + s_k\hat{b}^\dagger_{\boldsymbol{k}}\Big) \\
&\qquad\qquad + ⨍_{\boldsymbol{k}\neq\boldsymbol{q}} v^{\mathrm{IB}}(\boldsymbol{k}-\boldsymbol{q})\Big(c_k\hat{b}^\dagger_{\boldsymbol{k}} + s_k\hat{b}_{-\boldsymbol{k}}\Big)\Big(c_q\hat{b}_{\boldsymbol{q}} + s_q\hat{b}^\dagger_{-\boldsymbol{q}}\Big) \\
&= v^{\mathrm{IB}}(0)n + \sqrt{n_0}⨍_{\boldsymbol{k}} v^{\mathrm{IB}}(k)(c_k+s_k)\big(\hat{b}^\dagger_{\boldsymbol{k}} + \hat{b}_{-\boldsymbol{k}}\big) \\
&\qquad + ⨍_{\boldsymbol{k},\boldsymbol{q}} v^{\mathrm{IB}}(\boldsymbol{k}-\boldsymbol{q})\Big((c_kc_q + s_ks_q)\hat{b}^\dagger_{\boldsymbol{k}}\hat{b}_{\boldsymbol{q}} + c_ks_q\big(\hat{b}^\dagger_{\boldsymbol{k}}\hat{b}^\dagger_{-\boldsymbol{q}} + \hat{b}_{\boldsymbol{k}}\hat{b}_{-\boldsymbol{q}}\big)\Big) \\
&= v^{\mathrm{IB}}(0)n + 2\,\mathrm{He}\,\sqrt{n_0}⨍_{\boldsymbol{k}} v^{\mathrm{IB}}(k)e^{\phi_k}\hat{b}^\dagger_{\boldsymbol{k}} \\
&\qquad + \mathrm{He}⨍_{\boldsymbol{k},\boldsymbol{q}} v^{\mathrm{IB}}(\boldsymbol{k}-\boldsymbol{q})\Big(\cosh(\phi_k+\phi_q)\hat{b}^\dagger_{\boldsymbol{k}}\hat{b}_{\boldsymbol{q}} + \sinh(\phi_k+\phi_q)\hat{b}^\dagger_{\boldsymbol{k}}\hat{b}^\dagger_{-\boldsymbol{q}}\Big)
\end{aligned}$$

where the hermitian part of an operator has been denoted as $\mathrm{He}\,\hat{A} := (\hat{A} + \hat{A}^\dagger)/2$. Neglecting the constant term, this leads to

$$\begin{aligned}
H_{\mathrm{Bog}} = \frac{\left(\boldsymbol{p}_0^2 - ⨍_{\boldsymbol{k}}\, \boldsymbol{k}\hat{b}^\dagger_{\boldsymbol{k}}\hat{b}_{\boldsymbol{k}}\right)^2}{2m_{\mathrm{I}}} &+ ⨍_{\boldsymbol{k}} \omega_k\hat{b}^\dagger_{\boldsymbol{k}}\hat{b}_{\boldsymbol{k}} + 2\,\mathrm{He}\,\sqrt{n_0}⨍_{\boldsymbol{k}} v^{\mathrm{IB}}_k e^{\phi_k}\hat{b}^\dagger_{\boldsymbol{k}} \\
&+ \mathrm{He}⨍_{\boldsymbol{k},\boldsymbol{q}} v^{\mathrm{IB}}_{\boldsymbol{k}-\boldsymbol{q}}\Big(\cosh(\phi_k+\phi_q)\hat{b}^\dagger_{\boldsymbol{k}}\hat{b}_{\boldsymbol{q}} + \sinh(\phi_k+\phi_q)\hat{b}^\dagger_{\boldsymbol{k}}\hat{b}^\dagger_{-\boldsymbol{q}}\Big).
\end{aligned} \tag{6.1}$$

There exist many works that have discussed the impurity-BEC problem in Bogoliubov theory. However, the above Hamiltonian appears, in this form, in none of them. Instead, there are a number of different further steps that are in common use and lead to further simplifications. The form (6.1) serves as a common basis to these various approaches.

BB Local Born Approximation Bogoliubov theory can capture features of the BB potential up to the second term in the Born series, as detailed in appendix A of [Lie+05]. In the majority of applications, however, Lee-Huang-Yang pseudo-potential is applied, which

corresponds to a first-order Born approximation. This is consistent with the experimental parameter values and with the assumptions of Bogoliubov theory itself. This applies to most of the literature on the Bose polaron as well, even though the results of the next chapter suggest that it might have some interest to go beyond the Born approximation.

IB Contact Interaction Due to the separation of scales in ultracold gases, it is natural to expect that results depend universally on the scattering lengths. A contact potential is usually the most convenient choice of model potential and is employed in the vast majority of the literature.

Fröhlich Hamiltonian The first line in equation (6.1), in which the interaction term is linear in $\hat{b}, \hat{b}^\dagger$ is of the same form as the well-known Fröhlich Hamiltonian, which has first been introduced for the solid-state polaron and was subsequently applied to other polaronic situations as well. For the Bose polaron, it may be obtained when the impurity-boson interaction is weak. Then, one can expand the quadratic terms in the last line around a c-field and set $\hat{b}_k = \beta_k^0 + \hat{\delta b}_k$, neglecting quadratic terms in $\hat{\delta b}, \hat{\delta b}^\dagger$. This yields additional constant and linear terms that are to be combined with the first line, and therefore a Fröhlich Hamiltonian but with a coupling constant different from g_Λ^{IB}:

$$H_{\mathrm{Fr}} = \frac{\left(\boldsymbol{p}_0^2 - \int_{\boldsymbol{k}}^{\Lambda} \boldsymbol{k} \hat{b}_{\boldsymbol{k}}^\dagger \hat{b}_{\boldsymbol{k}}\right)^2}{2m_{\mathrm{I}}} + \int_{\boldsymbol{k}}^{\Lambda} \omega_k \hat{b}_{\boldsymbol{k}}^\dagger \hat{b}_{\boldsymbol{k}} + \sqrt{n_0} g_{\mathrm{Fr}}^{\mathrm{IB}} \int_{\boldsymbol{k}}^{\Lambda} e^{\phi_k} (\hat{b}_{\boldsymbol{k}}^\dagger + \hat{b}_{\boldsymbol{k}}) + \mathcal{E}$$

Various choices for the c-field β_k lead to slightly different values that can be found across the literature. The simplest is to take the zero-energy scattering solution (2.13) of the two-body problem (but without the δ-peak, since the zero-mode is excluded), transformed by the Bogoliubov rotation: $\beta_k = -e^{-\phi_k} 4\pi a \sqrt{n_0} \,/\, k^2$. This leads to the same coupling constant that appears in a local Born approximation:

$$g_{\mathrm{Fr}}^{\mathrm{IB}} = \frac{2\pi a}{m_{\mathrm{red}}}$$

$$\mathcal{E} = n_0 g_{\mathrm{Fr}}^{\mathrm{IB}} - \sqrt{n_0} {g_{\mathrm{Fr}}^{\mathrm{IB}}}^2 \int_{\boldsymbol{k}}^{\Lambda} \frac{2m_{\mathrm{red}}}{k^2} \,.$$

Note that $\mathcal{E}$ is UV-divergent. Such a divergence of the potential energy is normal in the limit of a point interaction and cancelled by a corresponding divergence in the kinetic energy. A slightly more detailed version uses the stationary solution of H_{Fr} for β_k, thereby taking into account the bose-bose interaction. This leads to a shift in the inverse scattering length, $g_{\mathrm{Fr}}^{\mathrm{IB}} = 2\pi \,/\, m_{\mathrm{red}}(a^{-1} - a_+^{-1})$, and to the same mean-field ground state energy as for the full quadratic Hamiltonian.

Quadratic Approximation in kinetic term Consistently with dropping the fourth order terms in the bose-bose interaction, one may do the same in the impurity kinetic term, i.e. in the *effective* interaction introduced by a moving impurity. While this simplification has been made in the first treatment of the impurity-BEC problem [Gir61], it is absent in current works. The reason for this is that the relevant term does not scale with the (small) BB coupling strength, and turns out necessary when the impurity is moving fast.

6.2 Methods

The methods we shall employ in this chapter are of variational type, investigating the Hamiltonian on a reduced submanifold $|\alpha\rangle$ of the Hilbert space, parameterised by some parameters α_i. Projecting the Schrödinger equation onto this submanifold is equivalent to requiring stationarity of the functional $\int \mathcal{L}(\alpha, \dot{\alpha})\,\mathrm{d}t = \int \langle\alpha|(i\partial_t - H)|\alpha\rangle\,\mathrm{d}t$. When the parameters α are complex, it is convenient to write the Euler-Lagrange equations in terms of the two Wirtinger derivatives ∂_α, $\partial_{\overline{\alpha}}$ instead of $\partial_{\mathrm{Re}\,\alpha}$, $\partial_{\mathrm{Im}\,\alpha}$: Since $\mathcal{L}$ is real, the two equations are equivalent, so it is sufficient to require

$$\left(\frac{\partial}{\partial\overline{\alpha}_i} - \frac{\mathrm{d}}{\mathrm{d}t}\frac{\partial}{\partial\dot{\overline{\alpha}}_i}\right)\mathcal{L} = 0.$$

6.2.1 Few-Excitation Approach

Within the context of the problem, it is natural to describe any variational state in terms of phononic excitations of the ground state without impurity $|0\rangle_b$. A simple choice is to restrict the number of such excitations while allowing arbitrary quantum fluctuations between them. This approach was taken in [LPB15; SZC17; Shi+18; Yos+18]. For instance, with up to two excitations such an ansatz might read

$$|\alpha\rangle = |0\rangle_b + \int_{\boldsymbol{k}} \alpha^{(1)}_{\boldsymbol{k}} \hat{b}^\dagger_{\boldsymbol{k}} |0\rangle_b + \int_{\boldsymbol{k},\boldsymbol{q}} \alpha^{(2)}_{\boldsymbol{k},\boldsymbol{q}} \hat{b}^\dagger_{\boldsymbol{k}} \hat{b}^\dagger_{\boldsymbol{q}} |0\rangle_b .$$

For the Fermi polaron, such approaches have indeed turned out to be an efficient choice. However, the boson's increased tendency towards collective behaviour makes them less appealing here than in the fermionic setting. In particular, recall the results of chapter 5, where the exact wave functions were of the form (absorbing the time evolution factors in the alphas)

$$|\phi\rangle = \left(\alpha_0\hat{\psi}^\dagger_0 + \alpha_B(t)\hat{\psi}^\dagger_B + \int_{\mathbb{R}_+} \alpha_k(t)\hat{\psi}^\dagger_k\,\mathrm{d}k\right)^N |0\rangle .$$

On the repulsive side, the bound state proved important for the qualitative dynamics. To compare with above variational ansatz, we may imagine to expand $|\phi\rangle$ in powers of $\hat{\psi}^\dagger_B$ to obtain the weight of a singly occupied bound state, a doubly occupied bound state etc. Note the difference to the Fermi polaron, where each state can be occupied at most once.

The result is readily obtained: for large N, the product state with fixed particle number can be replaced by a coherent state. Splitting off the coherent factor for the bound state, $\exp(\alpha_B \hat{\psi}_B^\dagger)$, one sees that the occupation of the bound state follows a Poisson distribution, centred around the mean value $|\alpha_B|^2 = 8\pi a_{\mathrm{IB}}^3 n$. In order to capture at least qualitatively the results for the simple case of a heavy impurity in a non-interacting BEC, the maximum number $N_{\max}$ of excitations included in a variational ansatz should therefore be large enough to approximate this Poisson distribution well – or inversely, the coupling strength $a_{\mathrm{IB}} n^{1/3}$ should be significantly smaller than $(N_{\max} \,/\, 8\pi)^{1/3} = 0.34... N_{\max}^{1/3}$. Even though this estimate relied on the bound state, we may expect that a similar reasoning applies to the continuum as well. Unfortunately, these conditions are too restrictive for the parameter regimes in which we are interested here, so we rely instead on approaches with a larger number of excitations.

6.2.2 Coherent States

To allow for an arbitrary number of excitations, we use a coherent state ansatz

$$\begin{aligned} |\beta\rangle &:= \exp\left(\int\!\!\!\!\!\!-_{\boldsymbol{k}} \left(\beta_{\boldsymbol{k}} \hat{b}_{\boldsymbol{k}}^\dagger - \frac{|\beta_{\boldsymbol{k}}|^2}{2} \right) \right) |0\rangle_{\hat{b}} \\ &= D_\beta \, |0\rangle_{\hat{b}} \end{aligned} \tag{6.2}$$

with the unitary *displacement operator*

$$D_\beta := \exp\left(\int\!\!\!\!\!\!-_{\boldsymbol{k}} \left(\beta_{\boldsymbol{k}} \hat{b}_{\boldsymbol{k}}^\dagger - \overline{\beta}_{\boldsymbol{k}} \hat{b}_{\boldsymbol{k}} \right) \right).$$

Within this ansatz, no correlations between different phonon modes are allowed. However, some correlations between *boson* modes are nonetheless present within the phonon vacuum state. In this way, the model is different from directly using a coherent state in terms of the boson operators. The coherent state ansatz was first applied to the Fröhlich Hamiltonian in [LLP53] and to the Bose polaron problem in [Sha+14; Shc+16b].

In two limiting cases, the eigenstates are exactly of form (6.2): (*i*) For $m_{\mathrm{I}} = \infty$ and $a_{\mathrm{BB}} = 0$, as shown in chapter 5. (*ii*) For $m_{\mathrm{I}} = \infty$ and the Fröhlich model. For the latter, the ansatz has first been used in ref. [LLP53]; the same, that introduced the LLP transformation.

Since the phonon operators and the exponent $\ln D_\beta$ are second-commuting, the transformed operators are given by

$$\begin{aligned} D_\beta^{-1} \hat{b}_{\boldsymbol{k}} D_\beta &= \hat{b}_{\boldsymbol{k}} - [\ln D_\beta, \hat{b}_{\boldsymbol{k}}] = \hat{b}_{\boldsymbol{k}} + \beta_{\boldsymbol{k}} \\ D_\beta^{-1} \hat{b}_{\boldsymbol{k}}^\dagger D_\beta &= \hat{b}_{\boldsymbol{k}}^\dagger - [\ln D_\beta, \hat{b}_{\boldsymbol{k}}^\dagger] = \hat{b}_{\boldsymbol{k}}^\dagger + \overline{\beta_{\boldsymbol{k}}}. \end{aligned}$$

The transformation thus shifts the operators by the c-numbers $\beta, \overline{\beta}$. In particular, taking the expectation value of a normal-ordered expression with respect to $|\beta\rangle$ results in replacing $\hat{b}$ and $\hat{b}^\dagger$ by β and $\overline{\beta}$.

6.2.3 Squeezed States

For infinite mass, or when the Bogoliubov approximation is applied to the impurity-induced interaction as well, Hamiltonian (6.1) is quadratic in the phonon operators, but it contains terms of the form $\hat{b}_{\boldsymbol{k}}\hat{b}_{\boldsymbol{q}}$. This is similar to standard Bogoliubov theory, where terms like $\hat{a}_{\boldsymbol{k}}\hat{a}_{-\boldsymbol{k}}$ appear and the Hamiltonian can be diagonalised by the Bogoliubov transformation $\exp(i \operatorname{Ah} \fint_{\boldsymbol{k}} \phi_k \hat{a}_{\boldsymbol{k}}\hat{a}_{-\boldsymbol{k}})$. Here, the situation is more complicated because all modes are coupled to each other, but the Bogoliubov transformation can be generalised by replacing ϕ by a suitable matrix (we assume in this section that momentum space is finite and the integral is an appropriately scaled summation to keep the discussion simple). Such transformations are known as squeezing transformations in quantum optics, the states obtained when applying them to the vacuum or a coherent state are called squeezed states[1] or (correlated) Gaussian states. They have been applied before to the Bose polaron in [Shc+16a; KL18].

Notation To keep the expressions short, we will employ a notation of "vectors of operators" $\hat{\boldsymbol{a}} = (\hat{a}_{\boldsymbol{k}})_{\boldsymbol{k}\in\mathbb{R}^3}$. The following conventions are used, where $\hat{\boldsymbol{v}}, \hat{\boldsymbol{w}}$ stand for vectors of operators, A, B for matrices and T for a "scalar" operator.

- "Inner adjoint" $\hat{\boldsymbol{v}}^* = (\hat{v}_{\boldsymbol{k}}^\dagger)_{\boldsymbol{k}\in\mathbb{R}^3}$, e.g. $(A\hat{\boldsymbol{v}})^* = \overline{A}\hat{\boldsymbol{v}}^*$
- Transposition $\hat{\boldsymbol{v}}^{\mathrm{T}}$: $\hat{\boldsymbol{v}}^{\mathrm{T}}\hat{\boldsymbol{w}} = \fint_{\boldsymbol{k}} \hat{v}_{\boldsymbol{k}}\hat{w}_{\boldsymbol{k}}$
- "Full adjoint" $\hat{\boldsymbol{v}}^\dagger = \hat{\boldsymbol{v}}^{*\mathrm{T}}$, e.g.

$$\hat{\boldsymbol{a}}^\dagger A\hat{\boldsymbol{a}} = \fint_{\boldsymbol{k},\boldsymbol{q}} A_{\boldsymbol{k},\boldsymbol{q}}\hat{a}_{\boldsymbol{k}}^\dagger\hat{a}_{\boldsymbol{q}}$$
$$(\hat{\boldsymbol{v}}^{\mathrm{T}} A\hat{\boldsymbol{w}})^\dagger = \hat{\boldsymbol{w}}^\dagger A^\dagger\hat{\boldsymbol{v}}^*$$

- Elementwise commutation with scalar operator: $[T, \hat{\boldsymbol{v}}] = ([T, \hat{v}_{\boldsymbol{k}}])_{\boldsymbol{k}\in\mathbb{R}^3}$, in particular

$$[T, A\hat{\boldsymbol{v}}] = A[T, \hat{\boldsymbol{v}}]$$
$$e^T\hat{\boldsymbol{v}}e^{-T} = \sum_n \frac{[T, \hat{\boldsymbol{v}}]_n}{n!}$$
$$[\hat{\boldsymbol{a}}^\dagger A\hat{\boldsymbol{a}}^*, \hat{\boldsymbol{a}}] = -(A + A^{\mathrm{T}})\hat{\boldsymbol{a}}^*$$

Squeezing Operator The squeezing operator with a *squeezing matrix* Ξ' is now defined as

$$S_\Xi := \exp\left(\frac{1}{2}\left(\hat{\boldsymbol{a}}^{\mathrm{T}}\overline{\Xi'}\hat{\boldsymbol{a}} - \hat{\boldsymbol{a}}^\dagger\Xi'\hat{\boldsymbol{a}}^*\right)\right).$$

[1] The rationale for the name is the following: If one measures the observables $\operatorname{He}\hat{a}$ and $\operatorname{Ah}\hat{a}$ of a single mode in a coherent state, the two-dimensional probability distribution takes the form of a circle. The squeezing operator squeezes this circle to an ellipsis. Note that if $\hat{a}, \hat{a}^\dagger$ are the ladder operators of a particle in a harmonic oscillator, then $\operatorname{He}\hat{a}$, $\operatorname{Ah}\hat{a}$ are simply position and momentum in oscillator units.

Since Ξ' is multiplied with the same vector from left and right in both cases, it can be chosen symmetric and therefore decomposed as $\Xi' = U'^{\mathrm{T}}\Phi U'$ with a unitary matrix U' and a real diagonal positive matrix Φ. Note that this corresponds to first transforming $\hat{\boldsymbol{a}}$ into a suitable basis before squeezing the resulting modes individually. It will be more convenient though to write this in terms of the hermitian (instead of symmetric) $\Xi := U'^{\mathrm{T}}\Phi\overline{U'}$ and the unitary symmetric $U := U'^{\mathrm{T}}U'$, such that $\Xi' = \Xi U$. Then,

$$\begin{aligned}\overline{U}U = U^\dagger U = 1\\ U\overline{\Xi} = \Xi U\\ S_\Xi = \exp\left(\frac{1}{2}\left(\hat{\boldsymbol{a}}^{\mathrm{T}}\overline{U}\Xi\hat{\boldsymbol{a}} - \hat{\boldsymbol{a}}^\dagger\Xi U\hat{\boldsymbol{a}}^*\right)\right).\end{aligned}$$

For the commutators of the exponent with $\hat{\boldsymbol{a}}, \hat{\boldsymbol{a}}^*$, we find with the commutator relations above

$$\begin{aligned}[\ln S_\Xi, \hat{\boldsymbol{a}}\ ] &= \Xi U\hat{\boldsymbol{a}}^*\\ [\ln S_\Xi, \hat{\boldsymbol{a}}^*] &= \overline{U}\Xi\hat{\boldsymbol{a}}\\ \Rightarrow [\ln S_\Xi, \hat{\boldsymbol{a}}]_n &= \begin{cases}\Xi^n\hat{\boldsymbol{a}} & \text{if } n \text{ even}\\ \Xi^n U\hat{\boldsymbol{a}}^* & \text{if } n \text{ odd.}\end{cases}\end{aligned}$$

The transformed operators $\hat{\boldsymbol{c}} := S_\Xi\hat{\boldsymbol{a}}S_\Xi^{-1}$ thus read

$$\begin{aligned}\hat{\boldsymbol{c}}\ &= \cosh(\Xi)\,\hat{\boldsymbol{a}}\ + \sinh(\Xi)U\hat{\boldsymbol{a}}^*\\ \hat{\boldsymbol{c}}^* &= \cosh(\overline{\Xi})\,\hat{\boldsymbol{a}}^* + \sinh(\overline{\Xi})\overline{U}\hat{\boldsymbol{a}},\end{aligned}$$

with the inverse transformation

$$\begin{aligned}\hat{\boldsymbol{a}}\ &= \cosh(\Xi)\,\hat{\boldsymbol{c}}\ - \sinh(\Xi)U\hat{\boldsymbol{c}}^*\\ \hat{\boldsymbol{a}}^* &= \cosh(\overline{\Xi})\,\hat{\boldsymbol{c}}^* - \sinh(\overline{\Xi})\overline{U}\hat{\boldsymbol{c}}.\end{aligned}$$

6.3 Application of Coherent State Approach

We will now apply the coherent state approach to Hamiltonian (6.1) with a contact interaction and study both the resulting energy functional and, in particular, the dynamics that evolves when the impurity is quenched from a non-interacting state into an interacting state.

Energy Functional The only expression in equation (6.1) which is not normal ordered is the impurity kinetic term. Normal-ordering it yields an additional $⨍_{\boldsymbol{k}}(k^2/2m_{\mathrm{I}})\hat{b}_{\boldsymbol{k}}^\dagger\hat{b}_{\boldsymbol{k}}$. Thus

$$\begin{aligned}E[\beta] :=\ & \langle\beta|H_{\mathrm{Bog}}|\beta\rangle\\ =\ & \frac{\left(\boldsymbol{p}_0 - ⨍_{\boldsymbol{k}}\,\boldsymbol{k}|\beta_{\boldsymbol{k}}|^2\right)^2}{2m_{\mathrm{I}}} + ⨍_{\boldsymbol{k}}\Omega_k|\beta_{\boldsymbol{k}}|^2 + 2\,\mathrm{Re}\,\sqrt{n_0}⨍_{\boldsymbol{k}}v_k^{\mathrm{IB}}e^{\phi_k}\beta_{\boldsymbol{k}}\\ &+ \mathrm{Re}⨍_{\boldsymbol{k},\boldsymbol{q}}v_{\boldsymbol{k}-\boldsymbol{q}}^{\mathrm{IB}}\Big(\cosh(\phi_k+\phi_q)\overline{\beta_{\boldsymbol{k}}}\beta_{\boldsymbol{q}} + \sinh(\phi_k+\phi_q)\beta_{\boldsymbol{k}}\beta_{-\boldsymbol{q}}\Big).\end{aligned}$$

where $\Omega_k = k^2 \,/\, 2m_\mathrm{I} + \omega_k$.

When V^IB is a contact potential, the last line can be simplified because the prefactor to $\beta_{-\boldsymbol{q}}$ becomes symmetric in $\boldsymbol{q}$:

$$\begin{aligned}
&g_\Lambda^\mathrm{IB} \fint_{\boldsymbol{k},\boldsymbol{q}}^\Lambda \mathrm{Re}\Big(\cosh(\phi_k+\phi_q)\overline{\beta}_{\boldsymbol{k}}\beta_{\boldsymbol{q}} + \sinh(\phi_k+\phi_q)\beta_{\boldsymbol{k}}\beta_{\boldsymbol{q}}\Big) \\
&= g_\Lambda^\mathrm{IB} \fint_{\boldsymbol{k},\boldsymbol{q}}^\Lambda \Big(e^{\phi_k+\phi_q}\,\mathrm{Re}\,\beta_{\boldsymbol{k}}\,\mathrm{Re}\,\beta_{\boldsymbol{q}} + e^{-\phi_k-\phi_q}\,\mathrm{Im}\,\beta_{\boldsymbol{k}}\,\mathrm{Im}\,\beta_{\boldsymbol{q}}\Big) \\
&= g_\Lambda^\mathrm{IB}\Big(\fint_{\boldsymbol{k}}^\Lambda e^{\phi_k}\,\mathrm{Re}\,\beta_{\boldsymbol{k}}\Big)^2 + g_\Lambda^\mathrm{IB}\Big(\fint_{\boldsymbol{k}}^\Lambda e^{-\phi_k}\,\mathrm{Im}\,\beta_{\boldsymbol{k}}\Big)^2.
\end{aligned}$$

We can thus write the energy functional as

$$E[\beta] = \frac{\boldsymbol{p}_\mathrm{I}[\beta]^2}{2m_\mathrm{I}} + \fint_{\boldsymbol{k}}^\Lambda \Omega_k|\beta_{\boldsymbol{k}}|^2 + {g_\Lambda^\mathrm{IB}}^{-1}(C_1[\beta]^2 + C_2[\beta]^2) \tag{6.3}$$

where

$$\begin{aligned}
\Omega_k &= \frac{k^2}{2m_\mathrm{I}} + \frac{k^2}{2m_\mathrm{B}}e^{-\phi_k} \\
\boldsymbol{p}_\mathrm{I}[\beta] &= \boldsymbol{p}_0 - \fint^\Lambda \boldsymbol{k}|\beta_{\boldsymbol{k}}|^2 \\
C_1[\beta] &= g_\Lambda^\mathrm{IB}\Big(\fint_{\boldsymbol{k}}^\Lambda e^{\phi_k}\,\mathrm{Re}\,\beta_{\boldsymbol{k}} + \sqrt{n_0}\Big) \\
C_2[\beta] &= g_\Lambda^\mathrm{IB}\fint_{\boldsymbol{k}}^\Lambda e^{-\phi_k}\,\mathrm{Im}\,\beta_{\boldsymbol{k}}.
\end{aligned}$$

These quantities are UV convergent: The contact condition requires β to have a tail like k^{-2}, which is, however, spherically symmetric because the contact potential acts only on s-wave states. Therefore, the momentum integral is not affected due to anti-symmetry in the integrand. For $C_{1,2}$, note that $\exp(\phi_k) = 1 + \mathcal{O}(k^{-2})$, such that $C_{1,2} = g_\Lambda^\mathrm{IB}\mathcal{O}(\Lambda) = \mathcal{O}(1)$. Together with the prefactor ${g_\Lambda^\mathrm{IB}}^{-1}$, however, the potential energy is $\mathcal{O}(\Lambda)$ and cancels the divergence of the kinetic energy.

Dynamics From the first line in equation (6.2) we see

$$\begin{aligned}
\langle\beta|i\partial_t|\beta\rangle &= \langle\beta|i\fint_{\boldsymbol{k}}\left(\dot\beta_{\boldsymbol{k}}\hat b_{\boldsymbol{k}}^\dagger - \frac{\dot\beta_{\boldsymbol{k}}\overline{\beta}_{\boldsymbol{k}} + \beta_{\boldsymbol{k}}\dot{\overline{\beta}}_{\boldsymbol{k}}}{2}\right)|\beta\rangle \\
&= \frac{i}{2}(\dot\beta_{\boldsymbol{k}}\overline{\beta}_{\boldsymbol{k}} - \beta_{\boldsymbol{k}}\dot{\overline{\beta}}_{\boldsymbol{k}}) \\
\Rightarrow \quad \left(\frac{\partial}{\partial\overline{\beta}_{\boldsymbol{k}}} - \frac{\mathrm{d}}{\mathrm{d}t}\frac{\partial}{\partial\dot{\overline{\beta}}_{\boldsymbol{k}}}\right)\langle\beta|i\partial_t|\beta\rangle &= i\dot\beta_{\boldsymbol{k}} = \frac{\partial}{\partial\overline{\beta}_{\boldsymbol{k}}}E[\beta],
\end{aligned}$$

thus

$$i\dot\beta_{\boldsymbol{k}} = \Big(-\boldsymbol{k}\cdot\boldsymbol{v}_\mathrm{I}[\beta] + \Omega_k\Big)\beta_{\boldsymbol{k}} + e^{\phi_k}C_1[\beta] + ie^{-\phi_k}C_2[\beta] \tag{6.4}$$

where $\boldsymbol{v}_\mathrm{I} = \boldsymbol{p}_\mathrm{I}/m_\mathrm{I}$. Most of the dynamical results in this chapter will be obtained by solving this equation numerically. Note that it is cubic is β. If, however, $\boldsymbol{p}_0 = 0$ and the initial state is spherically symmetric, then the symmetry cannot be broken and we have $\boldsymbol{p}_\mathrm{I} = 0$ for all times. In this case, the equation becomes linear in $\mathrm{Re}\,\beta$ and $\mathrm{Im}\,\beta$, but not complex linear. The same would always hold if we had used the quadratic approximation in the impurity kinetic term as well, which would then read $-\boldsymbol{k}\cdot\boldsymbol{v}_0$ in the differential equation.

6.3.1 Stationary Coherent State

By requiring $\dot{\beta}_k = 0$, we obtain the stationary solution β^s:

$$\beta^\mathrm{s}_{\boldsymbol{k}} = -\frac{e^{\phi_k} C_1^\mathrm{s} + i e^{-\phi_k} C_2^\mathrm{s}}{\Omega_k - \boldsymbol{k}\cdot\boldsymbol{v}_\mathrm{I}^\mathrm{s}}.$$

C_1^s, C_2^s and $\boldsymbol{v}_\mathrm{I}^\mathrm{s}$ are to be determined self-consistently. The equations read

$$\begin{aligned}
C_1^\mathrm{s} &= -g_\Lambda^\mathrm{IB} \int_{\boldsymbol{k}}^\Lambda \frac{e^{2\phi_k}}{\Omega_k - \boldsymbol{k}\cdot\boldsymbol{v}_\mathrm{I}^\mathrm{s}} C_1^\mathrm{s} + g_\Lambda^\mathrm{IB}\sqrt{n_0} \\
C_2^\mathrm{s} &= -g_\Lambda^\mathrm{IB} \int_{\boldsymbol{k}}^\Lambda \frac{e^{-2\phi_k}}{\Omega_k - \boldsymbol{k}\cdot\boldsymbol{v}_\mathrm{I}^\mathrm{s}} C_2^\mathrm{s} \\
\boldsymbol{p}_\mathrm{I}^\mathrm{s} &= \boldsymbol{p}_0 - \int_{\boldsymbol{k}} \boldsymbol{k} \frac{e^{2\phi_k} {C_1^\mathrm{s}}^2 + e^{-2\phi_k} {C_2^\mathrm{s}}^2}{(\Omega_k - \boldsymbol{k}\cdot\boldsymbol{v}_\mathrm{I}^\mathrm{s})^2}.
\end{aligned}$$

The second line implies $C_2^\mathrm{s} = 0$ unless

$$\int_{\boldsymbol{k}}^\Lambda \frac{e^{-2\phi_k}}{\Omega_k - \boldsymbol{k}\cdot\boldsymbol{v}_\mathrm{I}^\mathrm{s}} = -{g_\Lambda^\mathrm{IB}}^{-1} = \int_{\boldsymbol{k}}^\Lambda \frac{2m_\mathrm{red}}{k^2} - \frac{m_\mathrm{red}}{2\pi a_\mathrm{IB}},$$

in which case C_2^s is arbitrary. There exists two critical scattering lengths $a_\pm(v_\mathrm{I}^\mathrm{s})$, defined by

$$\frac{m_\mathrm{red}}{2\pi a_\pm(v_\mathrm{I}^\mathrm{s})} := \int_{\boldsymbol{k}} \left(\frac{2m_\mathrm{red}}{k^2} - \frac{e^{\pm 2\phi_k}}{\Omega_k - \boldsymbol{k}\cdot\boldsymbol{v}_\mathrm{I}^\mathrm{s}} \right). \tag{6.5}$$

In particular, the value for $\boldsymbol{v}_\mathrm{I}^\mathrm{s} = 0$ is important, which can be computed directly without a self-consistency requirement. It will be simply denoted by $a_\pm := a_\pm(0)$. $C_{1,2}^\mathrm{s}$ can now be written as

$$\begin{aligned}
C_1^\mathrm{s} &= \frac{2\pi\sqrt{n_0}}{m_\mathrm{red}(a_\mathrm{IB}^{-1} - a_+(v_\mathrm{I}^\mathrm{s})^{-1})} \\
C_2^\mathrm{s} &= 0 \qquad \text{unless } a = a_-(v_\mathrm{I}^\mathrm{s}).
\end{aligned}$$

For the energy one finds

$$E^\mathrm{s} = \frac{2\pi n_0}{m_\mathrm{red}(a_\mathrm{IB}^{-1} - a_+(v_\mathrm{I}^\mathrm{s})^{-1})} + \frac{\boldsymbol{p}_0\cdot\boldsymbol{p}_\mathrm{I}^\mathrm{s}}{m_\mathrm{I}} - \frac{{\boldsymbol{p}_\mathrm{I}^\mathrm{s}}^2}{2m_\mathrm{I}}.$$

Two remarks are in order.

- The solution need not be unique: By choosing $\boldsymbol{p}_\mathrm{I}^\mathrm{s}$, it may be possible to adjust $a_-(v_\mathrm{I}^\mathrm{s})$ to match a_IB. Then, C_2^s can be determined such that the chosen $\boldsymbol{p}_\mathrm{I}^\mathrm{s}$ is self-consistent.
- For small k, $\Omega_k \sim ck$ with the Landau critical velocity c. If we had $v_\mathrm{I}^\mathrm{s} > c$, then β^s would have a pole and some of the integrals would diverge. This is consistent with Landau's theory: By momentum and energy balance, collision processes between phonons and an impurity at sub-critical velocity are impossible unless there is also a change in potential energy. A stationary state with $v_\mathrm{I}^\mathrm{s} < c$, in which the impurity moves freely, is thus possible. For $v_\mathrm{I} > c$, however, collisions always take place and the impurity is slowed down further.

6.4 Expansion around Stationary Solution

Let us now focus on the case $\boldsymbol{p}_\mathrm{I} = 0$ where the system is linear, and investigate the eigenvalues of the dynamics to obtain the qualitative behaviour. By setting $\beta = \beta^\mathrm{s} + \delta\beta$, the equation for $\delta\beta$ becomes homogeneous:

$$i\dot{\delta\beta}_{\boldsymbol{k}} = \Omega_k \delta\beta_{\boldsymbol{k}} + e^{\phi_k}\tilde{C}_1[\delta\beta] + ie^{-\phi_k}C_2[\delta\beta]$$

where

$$\tilde{C}_1[\delta\beta] = g_\Lambda^\mathrm{IB} \fint_{\boldsymbol{k}}^\Lambda e^{\phi_k} \operatorname{Re}\delta\beta_{\boldsymbol{k}}.$$

This can be written as

$$\begin{pmatrix} \operatorname{Re}\dot{\delta\beta} \\ \operatorname{Im}\dot{\delta\beta} \end{pmatrix} = \begin{pmatrix} 0 & H_- \\ -H_+ & 0 \end{pmatrix} \begin{pmatrix} \operatorname{Re}\delta\beta \\ \operatorname{Im}\delta\beta \end{pmatrix}$$
$$H_\pm = \Omega + g_\Lambda^\mathrm{IB} e^{\pm\phi}(e^{\pm\phi})^\mathrm{T}$$

where Ω means a multiplication operator, exp is understood pointwise and w^T is defined by $w^\mathrm{T}v := \fint_{\boldsymbol{k}}^\Lambda w_{\boldsymbol{k}} v_{\boldsymbol{k}}$ as before. For the remainder of this section, integrals will be abbreviated as $\langle wv\rangle := \fint_{\boldsymbol{k}}^\Lambda w_{\boldsymbol{k}} v_{\boldsymbol{k}}$.

6.4.1 Equations for Eigenvalues

The characteristics of the dynamics are determined by the eigenvalues of above matrix. To determine them, we consider the squared matrix, that yields decoupled second-order equations

$$\begin{pmatrix} \operatorname{Re}\ddot{\delta\beta} \\ \operatorname{Im}\ddot{\delta\beta} \end{pmatrix} = \begin{pmatrix} -H_-H_+ & 0 \\ 0 & -H_+H_- \end{pmatrix} \begin{pmatrix} \operatorname{Re}\delta\beta \\ \operatorname{Im}\delta\beta \end{pmatrix}.$$

The operators H_-H_+ and H_+H_- are adjoints of each other and we may use either of them. They consist of a multiplication operator and a rank-2 perturbation:

$$H_-H_+ = \Omega^2 + g_\Lambda^\mathrm{IB}\Omega e^\phi(e^\phi)^\mathrm{T} + g_\Lambda^\mathrm{IB} e^{-\phi}(e^{-\phi})^\mathrm{T}\Omega + {g_\Lambda^\mathrm{IB}}^2 \langle 1\rangle\, e^\phi(e^{-\phi})^\mathrm{T}.$$

We wish to solve the eigenvalue equation

$$H_- H_+ v = \chi v.$$

If an eigenvalue $\chi < 0$ exists, then $\delta\beta$ has exponentially decaying and growing modes. This would mean that the system is dynamically unstable, which is not expected on physical grounds. If, on the other hand, we find a $\chi > 0$, then $\delta\beta$ will oscillate with frequency $\sqrt{|\chi|}$. From the results of chapter 5, such oscillations are expected for $a_{\mathrm{IB}} > 0$, with a frequency corresponding to the two-body binding energy. If no eigenvalue exists, the dynamics is fully governed by the continuous spectrum, which is $\mathbb{R}_+$, since the rank-2 perturbation does not alter it. In this case, the generalised eigenstates themselves are oscillatory, but these oscillations dephase for a normalisable state and the system is expected to show convergence towards the stationary state. This is the behaviour, which we have found for $a_{\mathrm{IB}} < 0$ for the ideal BEC.

The invertibility of $\Omega^2 - \chi$ depends on the sign of χ, so we distinguish these two cases.

Case 1: $\boldsymbol{\chi < 0}$. In this case we can invert $\Omega^2 - \chi$ and obtain

$$v = \frac{-g_\Lambda^{\mathrm{IB}}}{\Omega^2 - \chi}\left[\Omega e^{\phi}\left\langle e^{\phi} v\right\rangle + e^{-\phi}\left\langle e^{-\phi}\Omega v\right\rangle + g_\Lambda^{\mathrm{IB}}\left\langle 1\right\rangle e^{-\phi}\left\langle e^{\phi} v\right\rangle\right]. \tag{6.6}$$

There appear two different integrals involving v on the right-hand side. By integrating both sides with appropriate prefactors, we obtain a two-dimensional linear equation system for them.

$$\left\langle e^{\phi} v\right\rangle = -g_\Lambda^{\mathrm{IB}}\left\langle \frac{\Omega e^{2\phi} + \langle g_\Lambda^{\mathrm{IB}}\rangle}{\Omega^2 - \chi}\right\rangle\left\langle e^{\phi} v\right\rangle - \left\langle \frac{g_\Lambda^{\mathrm{IB}}}{\Omega^2 - \chi}\right\rangle\left\langle e^{-\phi}\Omega v\right\rangle \tag{6.7a}$$

$$\left\langle e^{-\phi}\Omega v\right\rangle = -g_\Lambda^{\mathrm{IB}}\left\langle \frac{\Omega^2 + \langle g_\Lambda^{\mathrm{IB}}\rangle\,\Omega e^{-2\phi}}{\Omega^2 - \chi}\right\rangle\left\langle e^{\phi} v\right\rangle - \left\langle \frac{g_\Lambda^{\mathrm{IB}}\Omega e^{-2\phi}}{\Omega^2 - \chi}\right\rangle\left\langle e^{-\phi}\Omega v\right\rangle \tag{6.7b}$$

For this to be a solvable system, the determinant of the corresponding matrix must be zero. One finds, after some rearrangements,

$$\left(g_\Lambda^{\mathrm{IB}\,-1} + \left\langle \frac{\Omega e^{2\phi}}{\Omega^2 - \chi}\right\rangle\right)\left(g_\Lambda^{\mathrm{IB}\,-1} + \left\langle \frac{\Omega e^{-2\phi}}{\Omega^2 - \chi}\right\rangle\right) = \chi\left\langle \frac{1}{\Omega^2 - \chi}\right\rangle^2.$$

The negative eigenvalues of $H_- H_+$ can thus be obtained from solving this equation for χ, which is numerically easy. It is convenient to write the equation in a UV convergent way. With the definitions of g_Λ^{IB} and $a_\pm$, one obtains

$$\left(\Delta_+ + \chi\left\langle \frac{e^{2\phi}}{\Omega(\Omega^2 - \chi)}\right\rangle\right)\left(\Delta_- + \chi\left\langle \frac{e^{-2\phi}}{\Omega(\Omega^2 - \chi)}\right\rangle\right) = \chi\left\langle \frac{1}{\Omega^2 - \chi}\right\rangle^2 \tag{6.8}$$

$$\Delta_\pm = \frac{m_{\mathrm{red}}}{2\pi}(a_{\mathrm{IB}}^{-1} - a_\pm^{-1}).$$

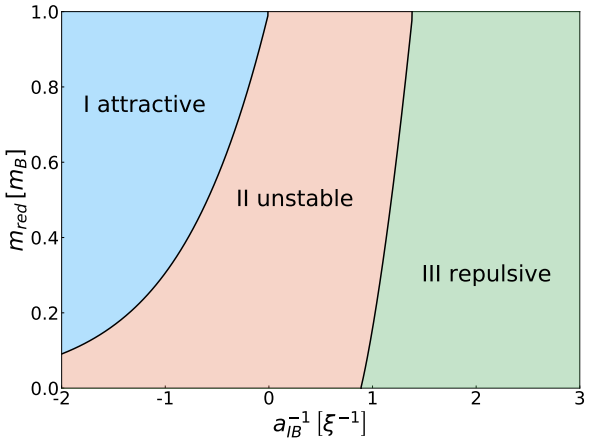

Figure 6.1: The three regimes of qualitatively different behaviour of the system in Bogoliubov theory. The boundaries are given by the curves $a_\pm$ (equation (6.5)).

Case 2: $\chi > 0$. In this case, there is a k_0 such that $\Omega_{k_0}^2 = \chi$. Therefore, $\Omega^2 - \chi$ is not invertible as an operator, but (6.6) must still hold pointwise for every $k \neq k_0$. The resulting v may thus have a pole at k_0. The formal solutions to the eigenvalue equation can be given, similarly to equation (6.6), as $v = \mathcal{P}\frac{1}{\Omega^2-\chi}[\dots] + \gamma\delta_{k_0}$ where γ is determined such that the equation is self-consistent. These are, however, no normalisable states and simply form the continuum of H_-H_+. For a true eigenvalue, the pole must vanish by the square bracket being zero at k_0:

$$\Omega_{k_0} e^{\phi_{k_0}} \left\langle e^{\phi} v \right\rangle + e^{-\phi_{k_0}} \left\langle e^{-\phi} \Omega v \right\rangle + g_\Lambda^{\mathrm{IB}} \langle 1 \rangle e^{-\phi_{k_0}} \left\langle e^{\phi} v \right\rangle = 0. \tag{6.9}$$

This is a third linear equation for $\left\langle e^{\phi} v \right\rangle$ and $\left\langle e^{-\phi} \Omega v \right\rangle$ in addition to eqs. (6.7). The result (6.8) can be derived in the same way as before, even though the splitting up of integrals over sums into sums of integrals in (6.7) requires using principal value integrals. The positive eigenvalues are thus given by the simultaneous solution of (6.8) with principal value integrals and (6.9)[2].

6.4.2 Solutions for Eigenvalues

By solving equations (6.8) and (6.9) numerically, we find three qualitatively different regions:

I. $a_{\mathrm{IB}} < a_-$: No solution.

II. $a_- < a_{\mathrm{IB}} < a_+$: One solution $\chi < 0$.

III. $a_+ < a_{\mathrm{IB}}$: One solution $\chi > 0$.

These are shown in figure 6.1. Regions I and III correspond to the behaviour of convergence or oscillations for $a < 0$ or $a > 0$, respectively, that was found in chapter 5 for $a_{\mathrm{BB}} = 0$ and $m_{\mathrm{I}} = \infty$. The strong-coupling region II, on the other hand, presents a dynamical instability, which is

[2] An equivalent condition to equation (6.9), which we have given in [DSE19], is that (6.8) holds for "different principal value integrals", i.e. for arbitrary $\mathcal{P}_s \int_{\mathbb{R}} := \lim_{\epsilon \searrow 0} (\int_{-\infty}^{k_0 - \epsilon} + \int_{k_0 + s\epsilon}^{\infty})$.

not expected and absent in the setting of chapter 5. It is not physically plausible that the inclusion of a boson repulsion should destabilise the system. Rather, we must assume that one of the approximations made in the derivation fails at strong coupling. These were:

(i) The Bogoliubov approximation, that dropped third- and fourth-order terms in the BB interaction. This assumes that the majority of bosons is in the zero-mode, around which the higher-momentum terms represent fluctuations. In particular, the condensate density should be sufficiently homogeneous.

(ii) The coherent state variational ansatz, which neglects correlations beyond the unperturbed BEC. This, as well, assumes that the number of excited modes is limited, such that the correlations are small corrections.

A number of arguments indicate that it is Bogoliubov theory itself that fails.

- The instability corresponds to an unbounded growth of the number of bosons in a vicinity of the impurity. When both interactions are quadratic in the boson operators, one may outweigh the other irrespective of the boson number, since both scale with n. But if boson repulsion was included to fourth order, it would scale as n^2. Thus, it would become dominant when the boson density gets too large at one point and prevent unbounded growth.
- Bogoliubov theory is based on the assumption that the density is sufficiently homogeneous. This is not the case in presence of a strong local impurity potential.
- When taking $a_{\mathrm{BB}} \to 0$, the Bogoliubov approximation becomes exact while the coherent state approach does not. Nonetheless, the unstable region vanishes since $a_{\pm} \to 0$.

The failure of Bogoliubov theory is an important point, because many theoretical investigations are based on applying different methods to one or another Hamiltonian obtained from it. While these can produce excellent results for weak to intermediate coupling, none is able to fully treat arbitrarily strong coupling and the transition from attractive to repulsive coupling across a Feshbach resonance. A promising solution is the use of Gross-Pitaevskii theory, which does include the boson repulsion to full fourth order and is intended to cover non-homogeneous condensates. This will be discussed in chapter 7.

Within the regions I and III, on the other hand, we expect the theory to be accurate: we will see that here, the number of bosons removed from the condensate is only of order one to ten, which makes the approximations plausible.

6.4.3 Oscillation Frequencies

From eqs. (6.8), (6.9), we can obtain the oscillation frequency $\omega = \sqrt{|\chi|}$ and compare it to the ideal-BEC result, which was the binding energy

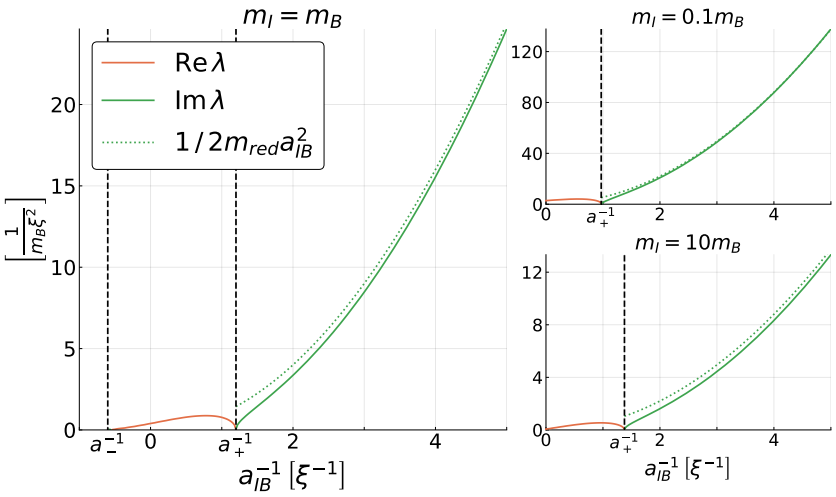

Figure 6.2: Characteristic oscillation frequencies ω on the repulsive side. In comparison, the two-body binding energy $k^2/2m_{\mathrm{red}}$, which is the exact result from chapter 5 for a heavy impurity in an ideal BEC. Calculations were carried out at a gas parameter of $n_0 a_{\mathrm{BB}}^3 = 10^{-5}$ and a momentum cutoff of $\Lambda = 1000\xi^{-}1$.

$1/2m_{\mathrm{red}}a_{\mathrm{IB}}^2$. The result is shown in fig. 6.2. The agreement is excellent for weak impurity-boson coupling. In particular, the result generalises perfectly for the finite-mass case. As a_{IB} approaches the critical value a_+, the frequency decreases until the oscillations vanish.

In chapter 5, we have conjectured that oscillations will eventually decay due to the BB interaction. But, surprisingly, the oscillatory modes are still eigenmodes of the coefficients β and hence continue for arbitrarily long times. A decay can therefore only come from beyond-Bogoliubov terms. Close to the unstable region, we may suspect that the higher-order coupling terms are still more important than initially thought. Further away, however, where the distortion of the BEC by the impurity gets smaller, the higher-order terms are less important, such that the oscillations are indeed very long-lived.

6.5 Results of Dynamical Simulation

We now turn to the numerical solution of the time evolution equation (6.4) with an initially non-interacting impurity being quenched into an interacting state at $t = 0$. From the resulting wave function, the following observables are computed:

- The impurity velocity $\boldsymbol{v}_{\mathrm{I}}(t)$ and position $\boldsymbol{x}_{\mathrm{I}}(t) = \langle \hat{\boldsymbol{x}}_{\mathrm{I}}(t) - \hat{\boldsymbol{x}}_{\mathrm{I}}(0)\rangle$, which, according to Ehrenfest's theorem, is simply $\boldsymbol{x}_{\mathrm{I}}(t) = \int_0^t \boldsymbol{v}_{\mathrm{I}}(t)\,\mathrm{d}t$.
- The bosonic density profile $n_{\mathrm{B}}(\boldsymbol{x}, t)$ at a distance $\boldsymbol{x}$ from the impurity. While in the lab frame, it would be obtained from the correlation function $n_{\mathrm{B}} = \langle \hat{n}_{\mathrm{B}}(\boldsymbol{x})\hat{n}_{\mathrm{I}}(\boldsymbol{x})\rangle = \langle \hat{n}_{\mathrm{B}}(\boldsymbol{x} + \hat{\boldsymbol{x}}_{\mathrm{I}})\rangle$, in the LLP frame it is simply given by $n_{\mathrm{B}}(\boldsymbol{x}, t) = \langle \hat{n}_{\mathrm{B}}(\boldsymbol{x})\rangle$. In terms of the coherent state, it takes the form

$$n(\boldsymbol{x}) = (\sqrt{n_0} + \mathrm{Re}\,\mathscr{F}^{-1}[\beta e^{\phi}])^2 + (\mathrm{Im}\,\mathscr{F}^{-1}[\beta e^{-\phi}])^2.$$

  With state-of-the-art imaging technologies, a direct observation of

density profiles is within reach of experiments, although challenging due to the small length and time scales involved.

- The number of bosons removed from the condensate and gathered around the impurity. Within Bogoliubov theory, it can be directly obtained from the particle number operator. This excludes the condensate because the zero-mode has been replaced by a c-number and constitutes an essential polaronic property. Its expression is not altered by the LLP transformation and reads

$$\begin{aligned}\Delta N_{\mathrm{B}}(t) &= \langle\psi(t)| \int_{\boldsymbol{k}} \hat{a}_{\boldsymbol{k}}^\dagger \hat{a}_{\boldsymbol{k}} |\psi(t)\rangle - \langle 0| \int_{\boldsymbol{k}} \hat{a}_{\boldsymbol{k}}^\dagger \hat{a}_{\boldsymbol{k}} |0\rangle \\ &= \int_{\boldsymbol{k}} \big(\cosh(2\phi_k) |\beta_{\boldsymbol{k}}|^2 + \sinh(2\phi_k)\, \mathrm{Re}\, \beta_{\boldsymbol{k}} \beta_{-\boldsymbol{k}} \big).\end{aligned}$$

6.5.1 Impurity Trajectories

Solving the equation for different initial velocities and coupling strengths, the results in fig. 6.3 are obtained.

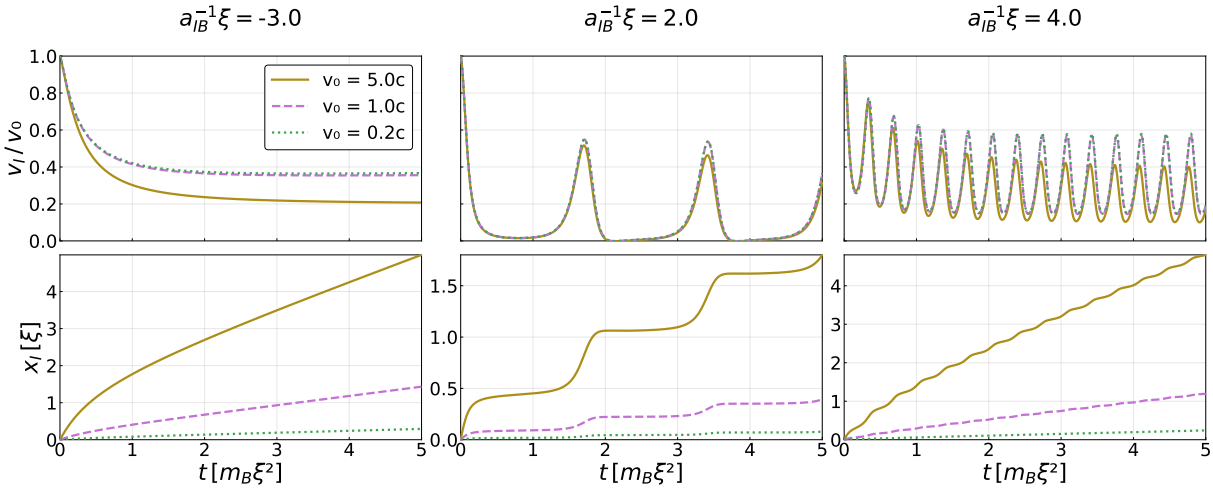

Figure 6.3: Time evolution of velocity and position on both sides of the resonance. The behaviour on the attractive side is characteristic for polarons: the velocity decreases as the polaron forms and reaches a stationary final value. The latter is always below the Landau critical velocity. On the repulsive side, the interplay with the bound state leads to oscillations in the velocity and to remarkable "stop-and-go" trajectories. These become most pronounced near the critical scattering length a_+. Here, the reduced frequency is favourable for experimental observation. Parameters are $n_0 a_{\mathrm{BB}}^3 = 10^{-5}$ and $m_{\mathrm{B}} = m_{\mathrm{I}}$. A soft momentum cutoff e^{-3k^2/Λ^2} with $\Lambda = 100\xi^{-1}$ was used.

Comparison of attractive and repulsive side The different behaviours that were announced for $a_{\mathrm{IB}} < 0$ and $a_{\mathrm{IB}} > 0$ are clearly visible. On the attractive side, the impurity slows down due to scattering with the bosons after switching on interactions, but reaches a non-zero final velocity. On the repulsive side, however, the velocity oscillates with the frequency derived before. Momentum is periodically exchanged back and forth between the impurity and the bosons as it gathers more or less particles around it. This can be understood as a periodically varying effective mass of the polaron. In the trajectories, this leads to remarkable "bumpy" behaviour up to stop-and-go motion when, at strong coupling, the velocity periodically comes close to zero.

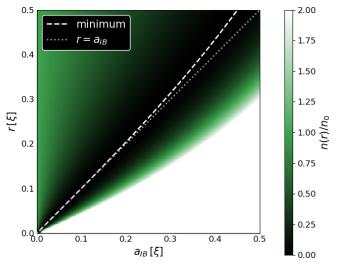

Figure 6.6: Stationary boson density profiles for a range of repulsive coupling strengths. The points of maximal depletion are compared to the IB scattering lengths, where they would lie without BB interaction. Parameters are the same as in fig. 6.3 but with a momentum cutoff $\Lambda = 600\xi^{-1}$ to resolve the short-scale structure at weak coupling.

Sub- vs. supercritical velocity If the impurity is initially slower than Landau's critical velocity c, the slow-down and the final velocity are relative to the initial velocity. Note that the interaction of a sub-critical particle with the BEC is not in contradiction to Landau's theory, since the latter applies only for a stationary state, in which no further change in potential energy occurs. If, on the other hand, the initial velocity is much higher than c, the slow-down is stronger and ensures that the final velocity is no larger than c.

6.5.2 Time Evolution of Density Profiles

Impurity at Rest Fig. 6.4 shows the density profiles for $\boldsymbol{p}_0 = 0$ for scattering lengths from the three regimes. In the last line, the asymptotics for $t = \infty$ is shown together with the profile obtained from the stationary solution.

For $a < a_-$, a peak around the impurity quickly forms and continues to broaden until the stationary shape is reached. The sudden perturbation of the BEC leads to waves being emitted radially in an intuitive way.

In the unstable region $a_- < a_{\mathrm{IB}} < a_+$, the evolution starts qualitatively similar as in the other regions. We may thus expect that the approach continues to describe the physics correctly at short times. However, the growth of the boson cloud around the impurity does not stop and no convergence is reached.

For $a > a_+$, a halo of depletion forms around the impurity in the same way as for the situation in chapter 5. Remarkably, the depth of depletion halos continues to reach zero density despite the boson repulsion, which is expected to act in favour of a more homogeneous condensate. Also, the oscillations in depth and their continuation for arbitrarily long times have not been weakened. The zeros in the wave function are, in fact, present in the stationary solution as well. For the ideal BEC, they occur precisely at $r = a_{\mathrm{IB}}$, as shown in chapter 5. For the stationary state in the interacting case, this is essentially still the case, with a slight correction towards the value of the healing length, as the BB coupling is included, as shown in fig. 6.6. In the dynamics, the stationary profile is not reached precisely and the minima are further shifted outwards. The factor of 1.45 that was obtained in chapter 5 is still valid with good accuracy.

Moving Impurity For an initially moving impurity, the emerging density profiles along the direction of motion are shown in fig. 6.5 (focusing now on the parameter regions where the theory is applicable also for longer times). In comparison to fig. 6.4, the behaviour is similar for velocities up to the critical velocity but different when the impurity is supersonic: here, an asymmetry arises which leads to an increased depletion in front of the impurity. On the attractive side, it persists even for long times when the attractive polaron has formed. On the repulsive side, the impurity moves slowly whenever the depletion halo is most pronounced. This may be unexpected, as there seem to be less bosons around the impurity, such that a lower effective mass should be expected. However, at these time points the attractive core is largest,

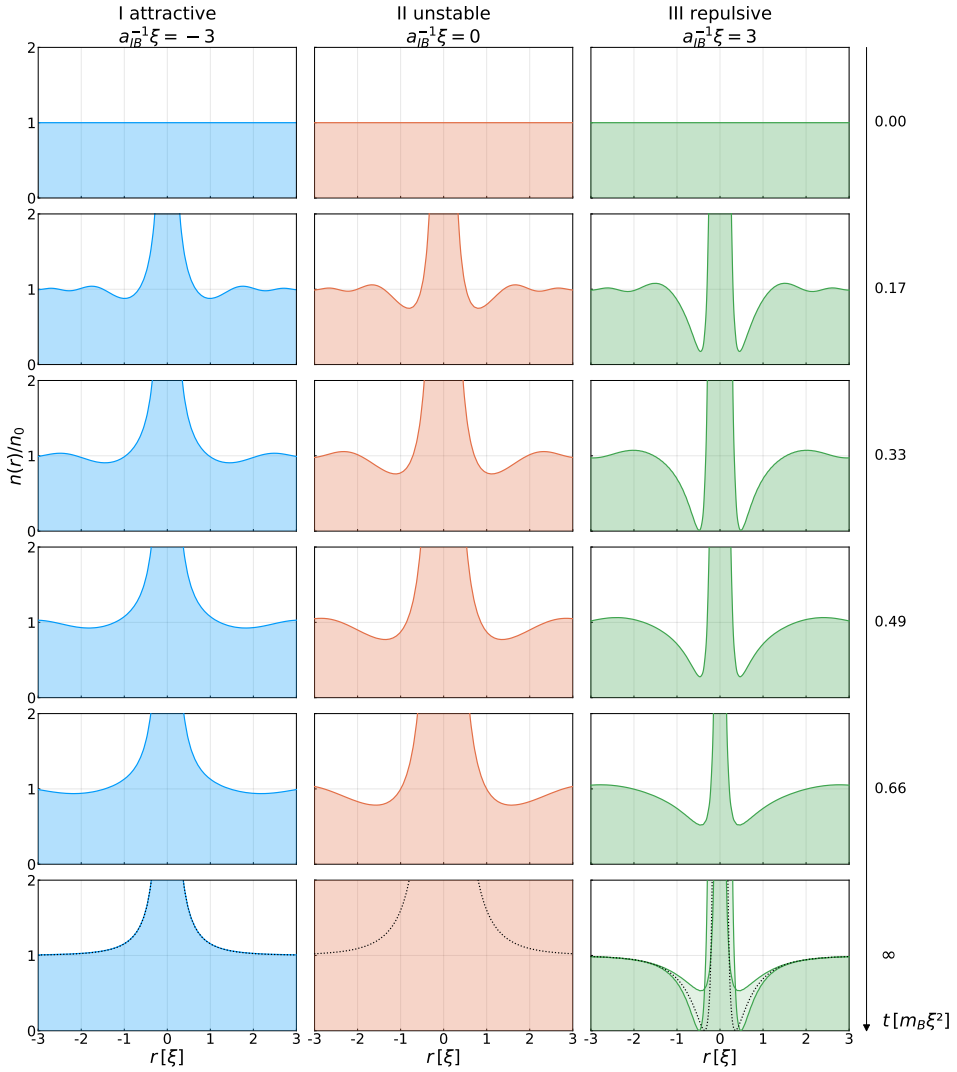

Figure 6.4: Time evolution of boson density $n(r)$ at a distance r from the impurity for $\boldsymbol{p}_0 = 0$. Three qualitatively different behaviours are observed according to the three regimes. For $a_{\mathrm{IB}}^{-1} < a_-^{-1}$, the density rapidly increases locally and the attractive polaron forms. For $a_-^{-1} < a_{\mathrm{IB}}^{-1} < a_+^{-1}$, the profile is similar for short times, but grows without bounds. This is not physical, but due to the dynamical instability in Bogoliubov theory, that manifests itself at long times. For $a_+^{-1} < a_{\mathrm{IB}}^{-1}$, the oscillating behaviour found for the ideal BEC is preserved. In particular, the depletion halos occurring near $r = a_{\mathrm{IB}}$ continue to reach zero density and to not decay at long times. Parameters are like in fig. 6.3 with a soft momentum cutoff e^{-2k^2/Λ^2} and $\Lambda = 80\xi^{-1}$.

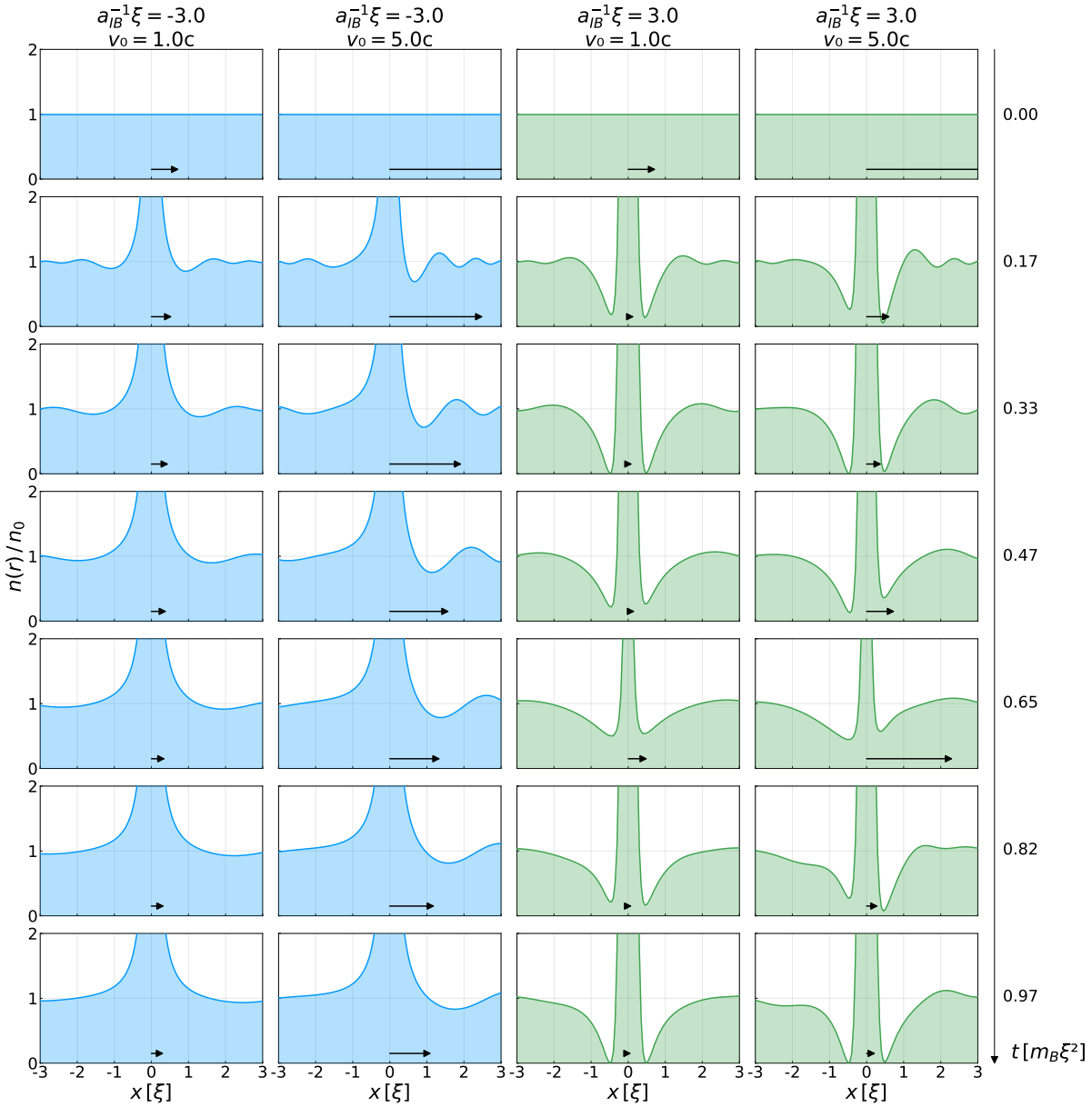

Figure 6.5: Density profiles for an initially moving impurity along the direction of motion. Arrows indicate the impurity velocities. At subsonic speed, the results are similar to those of the stationary impurity (fig. 6.4). At supersonic speed, the profiles become asymmetric with an accumulation of bosons building up in front of the impurity. The parameters are the same as in fig. 6.4.

giving rise to a higher number of attracted boson (cf. the next section) and a larger effective mass. The asymmetry, on the other hand, is largest whenever the impurity is moving and in particular when the velocity changes. The connection between the asymmetry and changes in velocity can be understood intuitively: At times where there are more bosons in front of the impurity, the latter is accelerated due to the attractive interaction, while at times with a higher number of bosons behind it, it is decelerated. Likewise, in the attractive case, the initial asymmetry leads to a deceleration, even though it is not clear why the profile is still asymmetric when the stationary state is reached. Here, internal modes beyond what is visible in the density seem to be important.

6.5.3 Number of Bosons attracted by the Impurity

The results for the boson number are shown in fig. 6.7. The characteristic

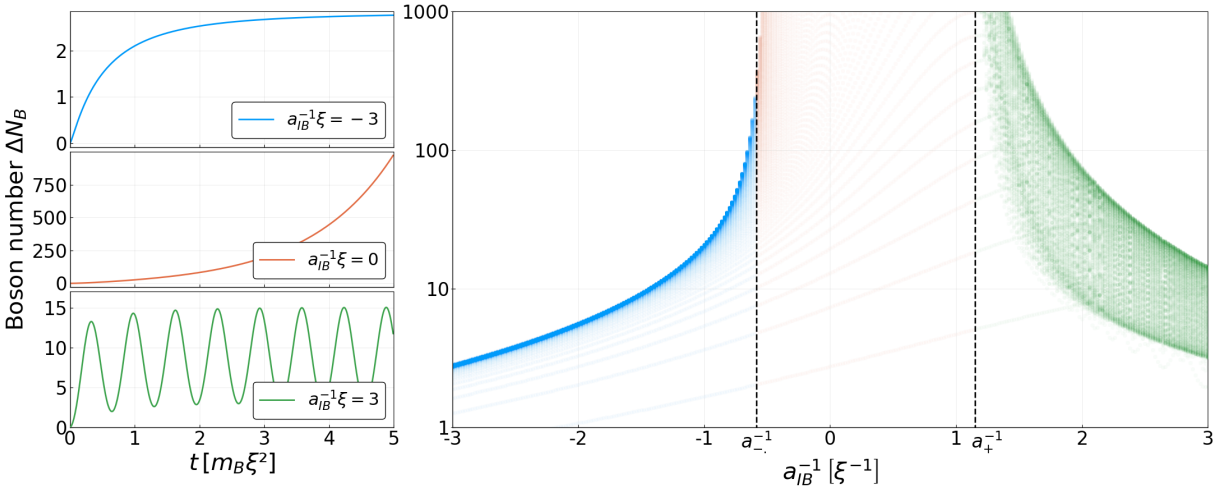

Figure 6.7: Number of bosons attracted by the impurity. On the left: time evolution for three scattering lengths from the three regimes. It converges on the attractive side and oscillates on the repulsive side while close to the resonance, the dynamical instability leads to exponential growth and the results are valid only for short times. On the right: the time evolution is solved for a range of scattering lengths for times up to $t_{\max} = 60 m_B \xi^2$. At each time point a low-opacity point is drawn. Opaque regions indicate convergence or recurrence. The parameters are the same as in fig. 6.4. On the right, a hard momentum cutoff at $\Lambda = 20\xi^{-1}$ was used.

behaviours of the three regimes can be seen clearly: on the attractive side, the number converges to a final value. For strong coupling, the dynamical instability of the Bogoliubov description leads to exponential growth. On the repulsive side, oscillations with the predicted frequency occur, like in the density profiles. The time points of maximum boson number correspond to the density profiles with maximum depletion. This is in accordance with the interpretation of the profiles with non-zero impurity velocity, that at these times the attractive core is most pronounced and the effective mass highest.

The total number of attracted bosons depends strongly on the coupling strength. At weak couplings, it is of order unity. At stronger coupling, it is of order 10 while close to the unstable region, order 100 is reached. At this point, the regularisation of higher-order coupling terms beyond Bogoliubov theory is expected to become important.

Also the time to convergence depends on the coupling strength: at strong coupling, it increases significantly, which can be seen from the fact

that the curves are still washed-out and not yet fully converged.

6.6 Stability of Oscillations

The unexpected finding that the oscillations do not decay despite the BB interaction deserves a separate discussion. In fact, this result can be understood analytically for the case of infinite impurity mass. We had already seen how stable oscillations emerge for the case of an ideal BEC in chapter 5, where we argued in position space. Now, we extend this analysis to include a BB repulsion and this time, we work in momentum space because we employ Bogoliubov theory.

We start with the Hamiltonian after the c-number substitution and neglecting of 3rd and 4th order terms in the BB coupling, but do not yet apply the Bogoliubov transformation.

$$\begin{aligned} H = &\fint_{\boldsymbol{k},\boldsymbol{q}} \left(\left(\frac{k^2}{2m_{\mathrm{B}}} + g^{\mathrm{BB}} n_0 \right) (2\pi)^3 \delta^3_{\boldsymbol{k}-\boldsymbol{q}} + g^{\mathrm{IB}}_\Lambda \right) \hat{a}^\dagger_{\boldsymbol{k}} \hat{a}_{\boldsymbol{q}} \\ &+ g^{\mathrm{BB}} n_0 \fint_{\boldsymbol{k}} \left(\hat{a}^\dagger_{\boldsymbol{k}} \hat{a}^\dagger_{-\boldsymbol{k}} + \hat{a}_{\boldsymbol{k}} \hat{a}_{-\boldsymbol{k}} \right) \\ &+ g^{\mathrm{IB}}_\Lambda \sqrt{n_0} \fint_{\boldsymbol{k}} \left(\hat{a}^\dagger_{\boldsymbol{k}} + \hat{a}_{\boldsymbol{k}} \right) \end{aligned}$$

Diagonalisation The first two lines are quadratic in the boson operators. They can be diagonalised by first applying a squeezing transformation as described in section 6.2.3 to remove terms of the form $\hat{a}_{\boldsymbol{k}} \hat{a}_{-\boldsymbol{k}}$, followed by a diagonalisation of the resulting terms involving $\hat{a}^\dagger_{\boldsymbol{q}} \hat{a}_{\boldsymbol{k}}$ by a unitary matrix V:

$$\begin{aligned} \hat{\boldsymbol{c}} &= A\hat{\boldsymbol{a}} + B\hat{\boldsymbol{a}}^* \\ \hat{\boldsymbol{a}} &= C\hat{\boldsymbol{c}} + D\hat{\boldsymbol{c}}^* \end{aligned}$$

where $A = V\cosh(\Xi)$, $B = V\sinh(\Xi)U$, $C = \cosh(\Xi)V^{-1}$ and $D = -\sinh(\Xi)U\overline{V}^{-1}$. The usual Bogoliubov transformation is also of this type. The difference is that here, all modes are coupled by g^{IB}_Λ instead of only $\boldsymbol{k}$ and $-\boldsymbol{k}$. With suitable choice of Ξ, U and V, the Hamiltonian then takes the form

$$H = \int_E \rho_E \big(E \hat{c}^\dagger_E \hat{c}_E + v_E \hat{c}^\dagger_E + \overline{v}_E \hat{c}_E \big) + const$$

for some v_E, where we have now parameterised $\hat{c}$ by the energy and introduced the spectral density ρ_E. We shall not need to compute Ξ, U, V, ρ and v explicitly to see how stable oscillations can emerge.

The remaining linear terms can be removed by a displacement transformation (section 6.2.2)

$$\hat{d}_E = \hat{c}_E + \frac{v_E}{E},$$

such that the Hamiltonian is brought to the simple form

$$H = \int_E \rho_E E \hat{d}^\dagger_E \hat{d}_E + const.$$

Time evolution From this Hamiltonian, the time evolution of the mode operators in Heisenberg picture can be obtained.

$$\begin{aligned} & e^{iHt}\hat{d}_E e^{-iHt} = e^{-iEt}\hat{d}_E \\ \Rightarrow \quad & e^{iHt}\hat{c}_E e^{-iHt} = e^{-iEt}\hat{c}_E + \frac{v_E}{E}\left(e^{-iEt}-1\right). \end{aligned}$$

Before moving to $\hat{a}$, let us discuss this intermediate result. (This is related to the ideal-BEC case, where $\hat{a}$ and $\hat{c}$ differ only by the transformation V.) The shift in c compared to d has led to the term $e^{-iEt}-1$, which is responsible for the stable oscillations. Indeed, if we now compute the expectation value of an operator such as $\int_E \rho_E \hat{c}_E^\dagger \hat{c}_E$ in the state $|0_{\hat{c}}\rangle$ – this corresponds to particle number operator and the BEC state if $a_{\mathrm{BB}} = 0$ – we obtain

$$\langle 0_{\hat{c}}| e^{iHt} \int_E \rho_E \hat{c}_E^\dagger \hat{c}_E \; e^{-iHt} |0_{\hat{c}}\rangle = \int_E \rho_E \frac{2|v_E|^2}{E^2}\left(1-\cos(Et)\right).$$

If there is no bound state, ρ is regular and any oscillations between the modes will eventually dephase. But if there is even just a single bound state, an oscillatory term $\sim (2|v_{E_\mathrm{b}}|^2 \,/\, E_\mathrm{b}^2)(1-\cos(E_\mathrm{b}t))$ will remain. Similar considerations hold true for a larger class of operators and states.

For the boson operators $\hat{a}$, the expression is more complicated:

$$\begin{aligned} e^{iHt}\hat{a}_{\boldsymbol{k}} e^{-iHt} = \fint_{\boldsymbol{p}} \int_E \rho_E \Big[\quad & C_{\boldsymbol{k}E}\big(A_{E\boldsymbol{p}}\hat{a}_{\boldsymbol{p}} + B_{E\boldsymbol{p}}\hat{a}_{\boldsymbol{p}}^\dagger\big)e^{-iEt} \\ & + D_{\boldsymbol{k}E}\big(\overline{A}_{E\boldsymbol{p}}\hat{a}_{\boldsymbol{p}}^\dagger + \overline{B}_{E\boldsymbol{p}}a_{\boldsymbol{p}}\big)e^{iEt} \\ & + C_{\boldsymbol{k}E}\frac{v_E}{E}\left(e^{-iEt}-1\right) \\ & + D_{\boldsymbol{k}E}\frac{\overline{v}_E}{E}\left(e^{iEt}-1\right) \qquad \Big]. \end{aligned}$$

The crucial term $e^{-iEt}-1$ is still present. Therefore, the mechanism is still intact for the interacting Bose gas and undamped oscillations occur. In fact, there is even a second term $e^{iEt}-1$, which could theoretically lead to oscillations with frequency $2E_\mathrm{b}$. However, the prefactor D is proportional to $\sinh(\Xi)$, which is small for a weakly interacting Bose gas, and this effect is probably not visible.

6.7 Original Contribution and Relation to Other Works

The material in this chapter was presented in a self-contained way, including both new contributions and results, that were already known to the community. We will now outline, which of the results are new and which have been obtained before. We focus on works concerning the situation in 3D, as the 1D setting is amenable to both techniques and results, that do not carry over to 3D, such as quantum flutter [MZD12]. Exceptions are made when works are particularly related to our study.

The original results of this chapter have been published in [DSE19].

Techniques The following list contains references, which employ techniques related to those used by us.

- The stationary solution already emerges from the Fröhlich Hamiltonian – or, at least, a similar one if the mean-field correction resulting from the second-order terms is not taken into account. It was discussed in particular by Shashi *et al.* [Sha+14] and by Grusdt *et al.* [Gru+17].
- The importance of second-order coupling terms at larger scattering length has first been pointed out by Rath and Schmidt [RS13]. The resulting full Hamiltonian has been used in a number of works [LD14; CLB15; VHZ15; Shc+16b; Shc+16a; Gru+17; GAD17; KL18; Sch+18].
- The coherent state approach was first used in the context of polaron physics by Lee, Low and Pines [LLP53] in the solid-state setting and in [Sha+14] for the Fröhlich description of the Bose polaron. Shchadilova *et al.* [Shc+16b] subsequently applied it to the beyond-Fröhlich Hamiltonian.
- Squeezed states have been used in [Shc+16a] with further approximations and by Kain and Ling [KL18] in an analytical study of the 1D setting.
- The method of obtaining the structure of the time evolution of the mode operators within the framework of coherent and squeezed states is new to our work.

Results The findings of our work are related to other author's contributions as follows.

- The three regimes of different stability and the critical scattering lengths were first obtained in [Gru+17]. The point, that the instability is inherent to the Bogoliubov description and not a consequence of the coherent state approach, was first raised in [KL18] for the 1D case and a stationary impurity and, independently[3], in our work for the general case.
- The coherent oscillations were already visible in figures in [Shc+16b], but this work was focused on the many-body spectrum and did not explain how the stable oscillations emerge from two-body physics. Providing this explanation and solving the paradox, that the oscillations emerge from two-body physics even though there is only one bound state in the two-body spectrum – such that oscillations should be expected to dephase – was a key achievement of our work. In this dissertation, the essential argument has been given in chapter 5 in position space while in the paper, we argued in momentum space and presented the extension of section 6.6 to include BB coupling.

[3]The paper of Kain and Ling was published during the process of writing of our paper.

- The formula for the oscillation frequency and its relation to the two-body binding energy are new findings; an analogous expression for 1D and infinite mass has been obtained in [KL18].

- Static density profiles for the ground state have been obtained by Peña Ardila and Giorgini [PG15] with quantum Monte Carlo methods and, for 1D, in [KL18]. In our paper, we computed dynamical density profiles for the first time, thereby tracking the polaron formation in real space. In particular, the oscillating behaviour on the repulsive side with the depletion halo reaching zero density is a remarkable feature, as well as the asymmetry that arises at supersonic velocities.

- Polaron trajectories had been obtained so far only from the Fröhlich model by Dasenbrook and Komnik [DK13] and in [Sha+14; Gru+18]. In the beyond-Fröhlich model, we were the first to compute the non-spherically symmetrical case $\boldsymbol{p}_0 \neq 0$, which gave us the opportunity to study the interesting behaviour on the repulsive side for a moving impurity, where the interplay with the bound state leads to remarkable results.

6.8 Summary and Outlook

In this chapter, we have discussed the application of Bogoliubov theory to the impurity-BEC problem. We found that the coherent-state approach is an effective description of the system for weak to moderate couplings, while at strong coupling, the deviation of the condensate density from a homogeneous BEC becomes too large for Bogoliubov theory to be applicable.

The oscillations that arise from the interplay of the zero-mode with multiply bound states, as described in chapter 5, are not found to decay in presence of BB interactions. This is remarkable since one should expect that the coupling leads to decay channels, which allow the system to reach its ground state. It is still likely that the real system eventually behaves in this way, but that the relaxation can only be obtained by including the full BB coupling beyond Bogoliubov theory, the latter thus being applicable only for limited time scales on the repulsive side. This time scale, however, is long for a weakly interacting Bose gas and moderate numbers of excited bosons and we expect a large number of oscillations to be observable.

A particularly fascinating result is that these oscillations occur also in the impurity velocity. At strong coupling, this leads to trajectories where the impurity periodically comes to rest and advances in steps of short duration. It will be interesting to see if this can be observed in experiments.

The density profiles are as well most interesting for repulsive coupling. Despite the bosons interacting, they continue to periodically reach zero density at a distance from the impurity.

Experimentally, the high frequency of the oscillation – typically of the order of one oscillation every 10–100 µs – makes an observation challenging but possible. Direct imaging approaches should focus on the region of stronger coupling, where both the time and the length scales are larger. Another promising approach is Ramsey spectroscopy of the contrast.

For further research, the problems arising in Bogoliubov theory at strong coupling necessitate a new approach. In the next chapter, such a theory is developed. Another interesting direction is the investigation of the interplay of multiple impurities and the effective interactions induced between them by the spatial variation in the condensate density.

Chapter 7

The Strong-Coupling Bose Polaron: A Non-Local Extension of Gross-Pitaevskii Theory

In chapter 6, we have seen that Bogoliubov theory becomes unstable when the coupling gets too strong because of the lack of third- and fourth-order terms in the boson coupling. A natural candidate for approaching the strong-coupling regime is therefore Gross-Pitaevskii theory (GPT), which includes fourth-order coupling terms. It can easily be adapted to include an impurity: in the LLP Hamiltonian, the impurity potential plays the role of an external one, which is already present in standard GPT. The impurity kinetic term can be treated by replacing the boson field operators by the collective wave function after normal ordering. The resulting energy functional and nonlinear Schrödinger equation (obtained, as usual, from $i\dot{\phi} = \partial_{\bar{\phi}} E[\phi]$) read

$$E_{\mathrm{GP}}[\phi] = \frac{(\boldsymbol{p}_0 - \int \bar{\phi}\hat{\boldsymbol{p}}\phi)^2}{2m_{\mathrm{I}}} + \int \left(\frac{|\nabla\phi|^2}{2m_{\mathrm{red}}} + V^{\mathrm{IB}}|\phi|^2 + \frac{2\pi a_{\mathrm{BB}}}{m_{\mathrm{B}}}|\phi|^4 \right)$$

$$i\dot{\phi} = \left(\frac{\boldsymbol{p}_0 - \int \bar{\phi}\hat{\boldsymbol{p}}\phi}{m_{\mathrm{I}}} \cdot i\nabla - \frac{\Delta}{2m_{\mathrm{red}}} + V^{\mathrm{IB}} + \frac{4\pi a_{\mathrm{BB}}}{m_{\mathrm{B}}}|\phi|^2 \right)\phi.$$

Note the reduced mass, which appears due to the normal ordering in the impurity kinetic term.

Unfortunately, these equations are not appropriate for studying the system at hand and the reason for this is the impurity potential, which is very different from the external potential in common applications of GPT. The latter is, after all, of a much longer range than the inter-particle distance. This leads to the condensate wave function varying slowly and a local density approximation being applicable. Here, however, the impurity potential is supposed to act on short length scales and furthermore to be strong, which leads to a spatial variation of the density. The resulting

failure of the local density approximation can be immediately seen by considering the extreme case of a contact potential. Then, ϕ must diverge as $1/r$ near zero for the potential to have any effect, but this leads to a divergence of the $|\phi|^4$ term. The process of "integrating out" the two-body physics of boson collisions, that is included in GPT and leads to the local potential term, is thus no longer possible in presence of a strong local deformation. We will therefore, in this chapter, develop a *non-local* extension of GPT, that includes the two-body physics more explicitly.

To conclude the discussion of GPT, there are, in fact, two situations in which it *can* be applied.

- When V^{IB} is long-range, such that it acts on scales large compared to a_{BB}, the original requirements of GPT are fulfilled. This is, however, rather unphysical in the context of atomic mixtures where the interaction ranges are of equal order.
- When *both* interaction potentials are weak, the Lee-Huang-Yang pseudo-potential can be applied to both of them. This leads to a stable theory and was adopted in [AP04; CT06; KB06; BBJ08; BBT13; Tak+19].

7.1 A Theorem on Jastrow Functions

The two-body physics can be accounted for by using a wave function of the form

$$\Psi(\boldsymbol{x}_1, ..., \boldsymbol{x}_N) = \phi_{\boldsymbol{x}_1} \cdots \phi_{\boldsymbol{x}_N} F_{\boldsymbol{x}_1,...,\boldsymbol{x}_N}.$$

Here, ϕ is the same condensate wave function that appears in GPT and represents the collective behaviour of the bosons. F, on the other hand, encodes the two-body BB physics in the following way: it is one when all particles are far-apart from each other, behaves like a low-energy scattering solution as two particles approach each other and like a product of scattering solutions if multiple such pairs appear. In a cluster development, the wave function is thus expected to be accurate to the level of two-clusters, thereby appealing to the intuition that in a low-density gas, only two-body physics is important.

A simple choice of F is

$$F_{\boldsymbol{x}_1,...,\boldsymbol{x}_N} = \prod_{i<j} f(\boldsymbol{x}_i - \boldsymbol{x}_j)$$

where f is the zero-energy solution to the two-boson problem. A wave function of this form was first employed by Dingle [Din49], following a suggestion of Mott, but with a different f. Later, Jastrow [Jas55] treated such wave functions – this time with a choice of f directly motivated by two-body physics – with a cluster expansion and extended the analysis to fermionic systems. The name Jastrow function for this ansatz has persisted and we will use it also here.

A different shape of F, but with the same behaviour on the level of two-clusters, was employed by Dyson [Dys57] to compute an upper

bound to the ground state energy of a hard sphere Bose gas. Later on, Lieb, Seiringer, Yngvason (LSY) generalised his method to include the collective part ϕ in the context of proving the GPE [LSY00].

In this section, we make use of a technique that Dyson invented for his wave function and that LSY adapted to the inhomogeneous case to prove a general theorem on Jastrow functions.

7.1.1 Statement

The purpose of the technique in Dyson's work was to compute upper bounds to terms arising from the kinetic energy of his trial wave function in the context of the hard-sphere Bose gas. Subsequently, LSY treated various terms resulting from the Hamiltonian of the trapped gas in this manner, with the extension that the wave function includes a spatial variation in the form of ϕ. The Dyson wave function is not permutation symmetric and therefore not a valid bosonic state – this was not required in above-mentioned works, because therein, the wave functions served the purpose of computing upper bounds to the ground state energy. Also for this reason, only one-sided bounds for the different terms were computed.

Here, we will show how the method can be generalised to cover a large class of operators, with the additional modification that we use wave functions of Jastrow's type instead of Dyson's. This is not essential but convenient because Jastrow functions are symmetric in the particle coordinates, thereby also representing valid bosonic states. Also, we include bounds from both sides to obtain the precise expectation values of operators. This is, of course, not related to computing lower bounds to the ground state energy, which is a more difficult task that was treated in Dyson's paper with great ideas but unsatisfactory results and completed only forty years later by Lieb, Yngvason [LY98] for the free gas and LSY [LSY00] for the trapped gas.

The theorem is concerned only with expectation values of k-particle multiplication operators

$$\hat{A} = \sum_{\substack{i_1,i_2,\dots,i_k \\ \text{all different}}} A(\boldsymbol{x}_{i_k}, ..., \boldsymbol{x}_{i_k})$$

(wlog, A is symmetric under permutations). This matches typical potential terms, but not kinetic terms, which include derivatives. However, when the derivative terms are applied to the wave function, we will see that they can be written as a sum of effective multiplication operators (with the coefficients A depending on f, ϕ and their derivatives).

Notation and Wave Function We write coordinate arguments as subscripts and often abbreviate them by their indices, as in $A_{1\dots k} := A(\boldsymbol{x}_1, ..., \boldsymbol{x}_k)$ and $\int_{1\dots N} := \int_{\mathscr{V}} \mathrm{d}^3\boldsymbol{x}_1 \cdots \int_{\mathscr{V}} \mathrm{d}^3\boldsymbol{x}_N$. For f, we write $f_{ij} :=$

$f(\boldsymbol{x}_j - \boldsymbol{x}_i)$. The wave function is given by

$$\Psi_{1\dots N} := \phi_1 \cdots \phi_N F_{1\dots N}$$
$$F_{1\dots N} := \prod_{i<j\leq N} f_{ij}.$$

We use the same symbols with fewer indices to denote analogous functions involving less coordinates and denote by $F_{1\dots k|k+1\dots N}$ the part of F, that couples coordinates with indices up to k to those greater than k:

$$\Psi_{1\dots k} := \phi_1 \cdots \phi_k F_{1\dots k}$$
$$F_{1\dots k} := \prod_{i<j\leq k} f_{ij}$$
$$F_{1\dots k|k+1\dots N} := \prod_{\substack{i,j:\\ i\leq k<j\leq N}} f_{ij}.$$

In particular,

$$\Psi_{12} = \phi_1\phi_2 f_{12}$$
$$\Psi_{1\dots N} = \Psi_{1\dots k}\Psi_{k+1\dots N} F_{1\dots k|k+1\dots N}.$$

Theorem 1 *Let $k, N, \mathscr{V}, \Psi$ and $\hat{A}$ be as above with $\phi \in L^2(\mathscr{V}, \mathbb{C})$ normalised as $\int_{\mathscr{V}} |\phi|^2 = N$, $f \in L^1_{\mathrm{loc}}(\mathbb{R}^3, \mathbb{R})$ satisfying $0 \leq f \leq 1$ and $A\colon \mathscr{V}^k \to \mathbb{C}$ such that $A_{1\dots k}|\phi_1 \cdots \phi_k|^2$ is integrable.*

Then, as $N, \mathscr{V} \to \infty$ with $n = N/\mathscr{V} \to 0$,

$$\frac{\langle\Psi|\hat{A}|\Psi\rangle}{\langle\Psi|\Psi\rangle} = \int_{1\dots k} (A_{1\dots k} + kI|A_{1\dots k}|)|\Psi_{1\dots k}|^2(1 + \mathcal{O}(I))$$

where

$$I = \sup_{\boldsymbol{x}\in\mathscr{V}} \int_{\boldsymbol{y}} |\phi_{\boldsymbol{y}}|^2(1 - f^2_{\boldsymbol{xy}})$$

If A has constant sign, this implies

$$\frac{\langle\Psi|\hat{A}|\Psi\rangle}{\langle\Psi|\Psi\rangle} = \int_{1\dots k} A_{1\dots k}|\Psi_{1\dots k}|^2 \ (1 + \mathcal{O}(I)) \,.$$

(We have assumed $\mathcal{O}(I) \geq \mathcal{O}(N^{-1})$, thereby neglecting simple cases such as $f = 1$.)

As the statement suggests, $I \to 0$ in applications, where, typically, $|\phi|^2$ is of order n and $\int(1 - f^2)$ of order $\mathcal{O}(a_{\mathrm{BB}} n^{-2/3})$. This will be detailed later.

The purpose of the theorem is to reduce N-particle integrals to k-particle integrals, leading to simple terms such as $\int V^{\mathrm{ext}}|\phi|^2$ in the GP functional.

7.1.2 Proof

Making use of the permutation symmetry of Ψ, we have to compute

$$\frac{\langle\Psi|\hat{A}|\Psi\rangle}{\langle\Psi|\Psi\rangle} = N\cdots(N-k+1)\frac{\int_{1\ldots N} A_{1\ldots k}|\Psi_{1\ldots N}|^2}{\int_{1\ldots N}|\Psi_{1\ldots N}|^2}.$$

Rationale The function f is supposed to be different from one only when two particles are close to each other. We might be led to assume that, in the low-density limit, this is an unlikely event and that therefore $F = 1$ almost everywhere in configuration space. We could then compute the normalisation of Ψ by $\int|\Psi|^2 \approx (\int|\phi|^2)^N = N^N$ and would merely have to find suitable similar approximations for $\langle\Psi|\hat{A}|\Psi\rangle$.

But the situation is more complicated as a simple argument shows. Let us call two particles close to each other if one is in a fixed volume $\mathscr{V}_1$ around the other. If we assume that the probability of finding a pair is indeed small, we can estimate it to leading order as follows. There are $N(N-1)/2$ possible pairs of particles and each of these occurs with a probability of $\mathscr{V}_1/\mathscr{V}$. Neglecting the possibility of three- and larger clusters – which are even less probable, the assumption granted – we would thus find a pair with a probability of order $N^2\mathscr{V}_1/\mathscr{V}$. But that this be small requires at least $N^2/\mathscr{V} \to 0$ – more, in fact, because $\mathscr{V}_1$ itself must get large to give enough room for the two particles to acquire a small energy. But this is a much stronger requirement than the low-density limit $N/\mathscr{V} \to 0$. We may conclude that the probability of finding a pair is appreciable – perhaps even close to one – and that, consequently, $F < 1$ in a large region of configuration space. This renders the task of computing the norm of Ψ hopeless.

This difficulty notwithstanding, Dyson was able to compute the expectation value of the Hamiltonian. The reasoning may go as follows. If it was possible to decouple in an integral such as $\int A_1|\Psi_{1\ldots N}|^2$ the coordinate $\boldsymbol{x}_1$ from all the others, i.e. obtain $\int_1 A_1|\phi_1|^2\int_{2\ldots N}|\Psi_{2\ldots N}|^2$ with small relative error, and to do the same in the denominator, then the uncomputable term $\int_{2\ldots N}|\Psi_{2\ldots N}|^2$ could be cancelled. And indeed, such an approximation seems possible: Since $\boldsymbol{x}_1$ is just one specific coordinate, the probability of finding it close to another one is of order $N\mathscr{V}_1/\mathscr{V}$, which indeed gets small as $n \to 0$ and allows for $\mathscr{V}_1$ to grow by an intermediate scale $n^{-\alpha}$, $\alpha < 1$.

Decoupling Integrals in the Denominator The task being stated in the previous paragraph, its execution is a matter of computation. We start with $k = 1$ but allow for a reduced number $M \leq N$ of coordinates, which will enable us to obtain the case of general k by induction (note that $\Psi_{1\ldots N}$ depends on N not only by the number of coordinates but

also by the normalisation of ϕ).

$$\begin{aligned}
&\int_{1\dots M} |\Psi_{1\dots M}|^2 \\
&= \int_{1\dots M} |\phi_1|^2 |\Psi_{2\dots M}|^2 F^2_{1|2\dots M} \\
&\quad \Big| \textit{ Write } F = 1-(1-F^2) \textit{ to get a decoupled and an error term.} \\
&= \int_1 |\phi_1|^2 \int_{2\dots M} |\Psi_{2\dots M}|^2 \\
&\qquad\qquad - \int_{1\dots M} |\phi_1|^2 |\Psi_{2\dots M}|^2 (1-F^2_{1|2\dots M}).
\end{aligned}$$

Take $z_i = \exp(-r_i)$ and observe that $1-\exp(-r)$ is subadditive on $\mathbb{R}_+$.

To bound the error term, we make use of the fact that for numbers $0 \le z_i \le 1$ we have $1 - \prod_i z_i \le \sum_i (1-z_i)$. We thus get

$$1 - F^2_{1|2\dots M} \le \sum_{j\ge 2}^{M} (1 - f^2_{1j}).$$

and

$$\begin{aligned}
&\int_{1\dots M} |\phi_1|^2 |\Psi_{2\dots M}|^2 (1-F^2_{1|2\dots M}) \\
&\le (M-1) \int_{1\dots M} |\phi_1|^2 |\Psi_{2\dots M}|^2 (1-f^2_{1M}) \\
&\quad \Big| \textit{ Use } M-1 \le N \textit{ and } 1-f^2_{1M} \le \sup_{\boldsymbol{y}} 1-f^2_{1\boldsymbol{y}}. \\
&\le IN \int_{2\dots M} |\Psi_{2\dots k}|^2.
\end{aligned}$$

Hence, with $\int |\phi|^2 = N$,

$$\int_{1\dots M} |\Psi_{1\dots M}|^2 = N \int_{1\dots M-1} |\Psi_{1\dots M-1}| \; (1+\mathcal{O}(I)). \tag{7.1}$$

For k arbitrary (but fixed as $N\to\infty$), we obtain inductively

$$\langle \Psi | \Psi \rangle = N^k \int_{1\dots N-k} |\Psi_{1\dots N-k}|^2 \; (1+\mathcal{O}(I)). \tag{7.2}$$

Decoupling Integrals in the Numerator The method is the same. We have

$$\begin{aligned}
&\langle \Psi | \hat{A} | \Psi \rangle \\
&= N \cdots (N-k+1) \int_{1\dots N} A_{1\dots k} |\Psi_{1\dots N}|^2 \\
&= N \cdots (N-k+1) \int_{1\dots k} A_{1\dots k} |\Psi_{1\dots k}|^2 \int_{k+1\dots N} |\Psi_{k+1\dots N}|^2 \\
&\qquad -N \cdots (N-k+1) \int_{1\dots N} A_{1\dots k} |\Psi_{1\dots k}|^2 |\Psi_{k+1\dots N}|^2 \\
&\qquad\qquad \cdot (1 - F^2_{1\dots k|k+1\dots N}).
\end{aligned}$$

For the decoupled first line, we may use (7.2) backwards as well as $N \cdots (N-k+1) = N^k(1+\mathcal{O}(1/N))$:

$$N \cdots (N-k+1) \int_{1\dots k} A_{1\dots k} |\Psi_{1\dots k}|^2 \int_{k+1\dots N} |\Psi_{k+1\dots N}|^2$$
$$= \int_{1\dots k} A_{1\dots k} |\Psi_{1\dots k}|^2 \langle \Psi | \Psi \rangle (1+\mathcal{O}(I)).$$

For the error term, we obtain

$$N \cdots (N-k+1) \int_{1\dots N} A_{1\dots k} |\Psi_{1\dots k}|^2 |\Psi_{k+1\dots N}|^2 \ (1 - F^2_{1\dots k|k+1\dots N})$$
$$\Big| \ 1 - F^2_{1\dots k|k+1\dots N} \leq \textstyle\sum_{i\leq k, j>k} (1-f_{ij}^2). \ \textit{Use permutation symmetry of } A \textit{ and } \Psi.$$
$$\leq N^k k(N-k) \int_{1\dots N} |A_{1\dots k}| |\Psi_{1\dots k}|^2 |\Psi_{k+1\dots N}|^2 \ (1 - f^2_{1,k+1})$$
$$\Big| \ \textit{Decouple one more term: } |\Psi_{k+1\dots N}|^2 \leq |\Psi_{k+2\dots N}|^2 |\phi_{k+1}|^2 \textit{ and use } \textstyle\int_{k+1} |\phi_{k+1}|^2 (1-f^2_{1,k+1}) \leq I.$$
$$\leq N^{k+1} kI \int_{1\dots k} |A_{1\dots k}| |\Psi_{1\dots k}|^2 \int_{k+2\dots N} |\Psi_{k+2\dots N}|^2.$$
$$\Big| \ \textit{Apply (7.2) with } k+1.$$
$$= kI \int_{1\dots k} |A_{1\dots k}| |\Psi_{1\dots k}|^2 \langle \Psi | \Psi \rangle (1+\mathcal{O}(I)).$$

Thus, in total,

$$\frac{\langle \Psi | \hat{A} | \Psi \rangle}{\langle \Psi | \Psi \rangle} = \int_{1\dots k} (A_{1\dots k} + kI|A_{1\dots k}|) |\Psi_{1\dots k}|^2 (1+\mathcal{O}(I)),$$

q.e.d.

7.2 Application to Impurity-BEC Problem

We can now apply the general theorem to derive the energy expectation value of the LLP Hamiltonian (4.1). For f, we choose the zero-energy solution of the two-boson problem. For instance, for a hard-sphere potential this amounts to $f(r) = \max(0, 1 - a_{\mathrm{BB}}/r)$. During the calculation, the difference to 1 needs to be restricted to a volume $\mathscr{V}_1$, satisfying $\mathscr{V}_1 \ll \mathscr{V}$ but $\mathscr{V}_1 \to \infty$, as outlined before and discussed in detail in [Dys57; LSY00], because the decay of $1/r$ is too slow. This does, however, not enter in the final formula.

7.2.1 Energy Functional

The computation of the derivatives terms is analogous to [LSY00]. We arrive at the following energy functional $E[\phi] = \langle \Psi | H | \Psi \rangle \,/\, \langle \Psi | \Psi \rangle$ for low

densities:

$$E[\phi] = \frac{\left(\boldsymbol{p}_0 - \int \bar{\phi}\hat{\boldsymbol{p}}\phi\right)^2}{2m_\mathrm{I}} + \int_{\boldsymbol{x}} \left(\frac{|\nabla\phi|^2}{2m_\mathrm{red}} + V^\mathrm{IB}|\phi|^2\right) + \int_{\boldsymbol{x}_1\boldsymbol{x}_2} |\phi_1\phi_2|^2 \left[\frac{f_{12}'^2}{2m_\mathrm{B}} + \frac{V_{12}^\mathrm{BB}}{2} f_{12}^2\right] + \mathrm{Re}\int_{\boldsymbol{x}_1\boldsymbol{x}_2} \frac{\overline{\phi_1}\nabla\phi_1 \cdot \overline{\phi_2}\nabla\phi_2 \left(1 - f_{12}^2\right)}{2m_\mathrm{I}}. \tag{7.3}$$

It differs from the functional obtained from local GPT,

$$E_\mathrm{GP}[\phi] = \frac{(\boldsymbol{p}_0 - \int \bar{\phi}\hat{\boldsymbol{p}}\phi)^2}{2m_\mathrm{I}} + \int \left(\frac{|\nabla\phi|^2}{2m_\mathrm{red}} + V^\mathrm{IB}|\phi|^2 + \frac{2\pi a_\mathrm{BB}}{m_\mathrm{B}}|\phi|^4\right),$$

in two ways:

- The local BB term is replaced by a non-local one (line 2 of (7.3)), that captures features of the two-boson scattering solution f when the density $|\phi|^2$ varies on short length scales. If, instead, $|\phi|^2$ is almost constant on scales of V^BB and f, then the integral over the relative coordinate decouples (square brackets) and yields $2\pi a_\mathrm{BB}/m_\mathrm{B}$, such that the theories come to agree (c.f. the proof of GPT for the Bose gas in a large trap [LSY00]). Note that if ϕ diverges as $1/r$ near zero, as for a contact potential, the double integral remains finite.
- The additional last line is present. It includes effects of backreaction of the medium on the impurity.

GPT is an efficient description of condensates varying on long length scales with numerous applications. We expect that with the non-local extension, the domain of applicability can be expanded even further to include the difficult scenario of short-range density variations.

7.2.2 Dynamics

A dynamical BEC can be described by letting the collective wave function ϕ vary in time. The two-body correlations f, however, must remain fixed because they are a property shared by the condensate across the entire space. This is similar as in local GPT, where it has been proven rigorously that the GPE describes the time evolution correctly [ESY07; ESY09; BS19]. From variation of $E[\phi]$ with respect to $\bar{\phi}$, we obtain

$$\begin{aligned} i\partial_t\phi_1 = &-\frac{\Delta\phi_1}{2m_\mathrm{red}} + V_1^\mathrm{IB}\phi_1 \\ &+ \phi_1 \int_{\boldsymbol{x}_2} |\phi_2|^2 \left[\frac{f_{12}'^2}{m_\mathrm{B}} + V_{12}^\mathrm{BB} f_{12}^2\right] \\ &+ \frac{i\nabla\phi_1}{m_\mathrm{I}} \cdot \left(\boldsymbol{p}_0 - \mathrm{Im}\int_{\boldsymbol{x}_2} \overline{\phi_2}\nabla\phi_2\, f_{12}^2\right) \\ &+ \frac{\phi_1}{m_\mathrm{I}} \int_{\boldsymbol{x}_2} \phi_2\nabla\overline{\phi_2} \cdot f_{12}f_{12}' \frac{\boldsymbol{x}_2 - \boldsymbol{x}_1}{|\boldsymbol{x}_2 - \boldsymbol{x}_1|}. \end{aligned} \tag{7.4}$$

Again, we may compare this to the result from local GPT:

$$i\dot{\phi} = \left(\frac{\boldsymbol{p}_0 - \int \bar{\phi}\hat{\boldsymbol{p}}\phi}{m_{\mathrm{I}}} \cdot i\nabla - \frac{\Delta}{2m_{\mathrm{red}}} + V^{\mathrm{IB}} + \frac{4\pi a_{\mathrm{BB}}}{m_{\mathrm{B}}}|\phi|^2 \right)\phi.$$

Just like in the functional, the local ϕ^3-term is replaced by an integral involving f and V^{BB}. The third line in (7.4) differs from GPT in that a region $\boldsymbol{x}_2 \approx \boldsymbol{x}_1$ is cut out or at least weakened by f_{12}. However, here, also the fourth line contributes, the integrand of which is nonzero only when the coordinates are close to each other.

7.3 Results

We are now able to investigate the behaviour across the resonance as the transition from an attractive to a repulsive polaron occurs. There is a large space of parameters that is worth exploration: Apart from varying the IB scattering length and the properties of the Bose gas in the form of the gas parameter, we can tune the mass ratio and the potential ranges and shapes of both interaction potentials and compare an impurity at rest with one moving at subsonic or supersonic velocities.

The numerical implementation is nonetheless challenging and in the scope of this dissertation, we need to focus on some of the most interesting aspects and leave the remaining to future works. The focus here lies on the transition regime that is inaccessible to Bogoliubov theory, the question whether oscillations decay and the influence of the shape of BB potential, which is included in neither Bogoliubov nor GP theory. To this end, we use Gaussian potentials of different range for the BB interaction,

$$V^{\mathrm{BB}}(\boldsymbol{r}) = \exp(-r^2/\sigma_{\mathrm{BB}}^2).$$

The IB potential is kept fixed. We employ, once again, the contact potential. Here, the analytical forms of the two-body propagator and the time evolution of an ideal BEC are important ingredients for a more efficient numerical implementation. The influence of a finite range in the IB potential is an interesting question for future work; tests indicate that it also has a quantitative effect, but that the following results are qualitatively similar for such a potential.

The choice of mass ratio does not affect the complexity of the equations and can be easily adapted to specific experimental settings. We use $m_{\mathrm{I}} = m_{\mathrm{B}}$. For the velocity, a moving impurity is not necessary to address above questions and so we stick to the simplest case of $\boldsymbol{p}_0 = 0$ where ϕ is spherically symmetric.

Once again, we consider the situation of an initially flat BEC, $\phi(\boldsymbol{x}, t = 0) = \sqrt{n}$, that starts interacting with the impurity at $t = 0$.

7.3.1 Transition from Attractive to Repulsive Polaron

The difference in behaviour between the attractive and repulsive side can be tracked in the time evolution of various observables. Here, we use the impurity-induced Tan contact [Tan08] $C = |4\pi \lim_{r\to 0} r\phi(r)|$. It

quantifies the current amount of interaction at short length scales and serves as a measure of how many bosons are in very close proximity to the impurity. It is also directly relevant to experiments and has been measured in [Yan+20].

The result is shown in fig. 7.1 for three positive scattering lengths and a BB potential range of $\sigma_{\mathrm{BB}} = 0.1 n_0^{-1/3}$. In a), the contact converges

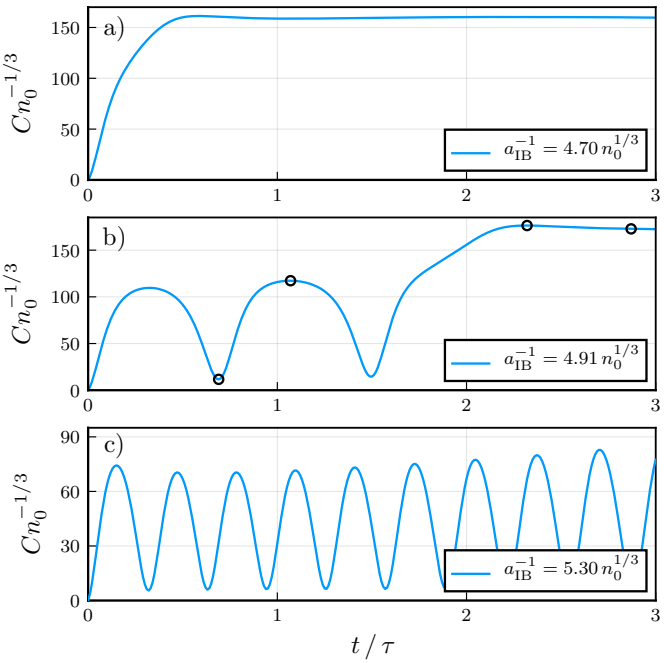

Figure 7.1: Time evolution of impurity-induced Tan contact for three repulsive scattering lengths. In a), the typical behaviour for attractive coupling is observed despite the fact that a_{IB}^{-1} is positive and larger than the mean-field shift from the Bogoliubov description. In b), a dynamical transition from repulsive to attractive behaviour occurs. For larger a_{IB} (c), the typical behaviour for the repulsive side is observed with oscillations being stable for a long time. Calculations were carried out at $a_{\mathrm{BB}} = 0.03 n_0^{-1/3}$, $\sigma_{\mathrm{BB}} = 0.1 n_0^{-1/3}$ and $m_{\mathrm{B}} = m_{\mathrm{I}}$. Time is measured in units of the BEC time scale $\tau = m_{\mathrm{B}} n_0^{-2/3}/\hbar$.

to a final value in the same way as we have observed for number of attracted bosons for an attractive polaron in chapter 6. However, here, the scattering length is positive and even smaller than the mean-field shift a_+, that demarks the region of repulsive behaviour in Bogoliubov theory. The transition point has thus been shifted by the finite-range potential. In b), the scattering length is close to this new critical point. A dynamical transition occurs: first, oscillations are observed, but at some point, they stop and the contact converges to a final value. The decay of oscillations we had expected to occur when higher-order terms in the BB coupling are included is present, but not in the form of a continuously decreasing amplitude, but rather as a qualitative change of behaviour at a critical time point. For lower coupling (c), however, the oscillations continue for long times. We expect also here that there is eventually a time when a transition as in b) occurs. Some additional tests suggest, however, that the number of oscillations before the transition grows very fast as the critical point is crossed.

In order to further investigate the dynamical transition in b), fig. 7.2 shows density profiles at the four time points indicated in fig. 7.1b). Comparison with the profiles obtained from Bogoliubov theory yields a clear picture: at early times (a), oscillations occur with a depletion halo around the impurity, as we have found to be typical on the repulsive

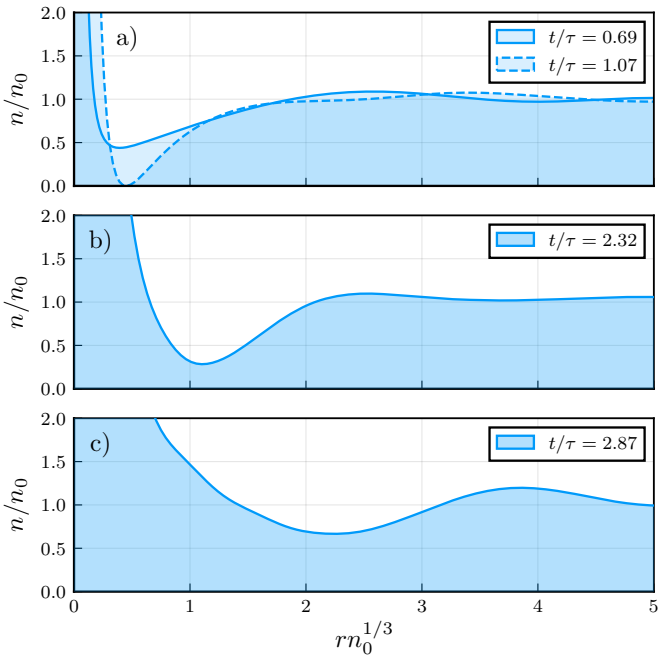

Figure 7.2: Density profiles at four time points for the close-to-critical coupling strength in fig. 7.1b). The first two curves (a) correspond to the typical oscillating profiles that we have found in chapter 6 for repulsive scattering. At a certain point in time, the depletion halo no longer reaches zero density and moves outwards (b). Finally, a profile similar to an attractive polaron is approached (c). Parameters and units are the same as in fig. 7.1b).

side. The depletion reaches zero density at times where the bosons number and the contact are maximal. Near a critical time point (b), the depletion starts to grow again, but no longer reaches zero density. Instead, the minimum starts moving away from the impurity. Finally (c), the depletion gets weaker and the polaron reaches a shape similar to that of an attractive polaron.

7.3.2 Influence of the Potential Shape on the critical Scattering Length

The results for the contact show that for a finite-range BB interaction, the resonance is shifted further into the repulsive regime than predicted by Bogoliubov theory. To investigate this systematically, we solve the time evolution for a range of repulsive IB scattering lengths and three BB potentials with the same scattering length $a_{\mathrm{BB}} = 0.03 n_0^{-1/3}$, but different height and width. Specifically, we use Gaussian potentials of range $\sigma_{\mathrm{BB}} = 0.3 n_0^{-1/3}$, $\sigma_{\mathrm{BB}} = 0.1 n_0^{-1/3}$ and a hard-sphere potential. From the contact $C(t)$, the oscillation frequencies are extracted. Fig. 7.3 shows the results. The dependence of the resonance position on the potential range is significant and different from the value a_+, that emerges in Bogoliubov theory. There, the BB interaction is described by a local term and one might think that fort short ranges, the theories should come to agree. The opposite is the case. The reason for this is the Born approximation, which is inherent to the Bogoliubov description (as well as to GPT). It is, in fact, accurate for soft, but not for narrow potentials, even if they are weak.

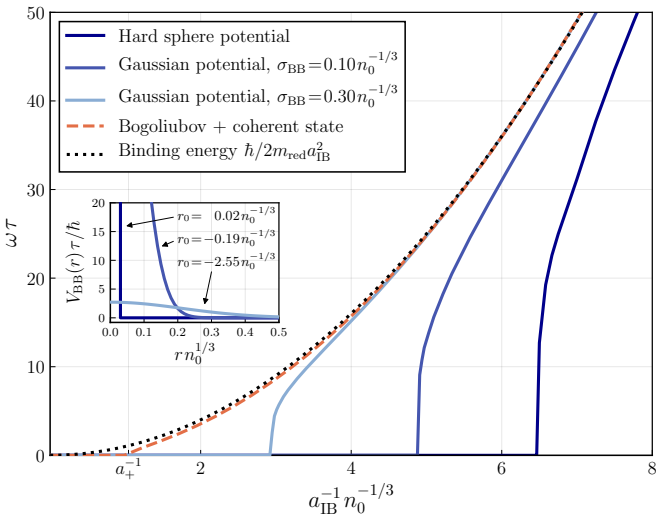

Figure 7.3: Oscillation frequencies on the repulsive side for three BB potentials with the same scattering length but different height and width. The shift of the resonance due to the BEC is found to depend crucially on the potential range. The value from Bogoliubov theory (dashed) is approached as the potential gets softer. In comparison, the two-body binding energy (dotted). Inset: The BB potentials and their effective ranges. Parameters and units are the same as in fig. 7.1.

At weaker IB coupling, the curves agree better. Here, the distortion of the BEC density by the impurity is less important and the local density approximation becomes valid again.

It is an interesting question, if there is a second parameter of the BB potential, that can be used in addition to the scattering length to describe the physics universally. A candidate for this is the effective range, which we have indicated in the inset. An analysis of Yoshida et al. [Yos+18] concerning different *impurity*-boson potentials has shown that here, the effective range does indeed play a central role and leads to a universal description. We expect that the situation is similar for the BB potential.

7.4 Original Contribution and relation to other Works

The method developed and the results obtained in this chapter are new. The Jastrow function method is inspired by the works of LSY and Dyson [LSY00; Dys57] and the resulting theorem is a generalisation of their techniques. A publication on the topic is being planned. The formulae and the results for the Bose polaron problem are published separately [DSE20] and in the process of reviewing at the time of writing.

Jastrow functions have first been introduced by Dingle and Jastrow [Din49; Jas55]. They are in common use in quantum Monte Carlo methods and, in similar form, in mathematical works on the Bose gas [ESY07; ESY09; BS19].

GPT in its local form has been applied by various authors [AP04; CT06; KB06; BBJ08; BBT13; Tak+19] to the Bose polaron problem, usually with a local Born-approximated term in both interaction potentials. This is a valid approach at weak couplings and focuses on different questions than discussed here.

While the discussion of a non-local BB potential is new to our work, insights concerning the role of different IB potentials were obtained in works of Shi *et al.* [Shi+18] and Yoshida *et al.* [Yos+18].

7.5 Summary and Outlook

In this chapter, we have developed a new non-local extension of GPT and applied it to the Bose polaron problem. It is the first theory that can treat arbitrarily strong IB couplings in an interacting Bose gas without becoming unstable and without an *a priori* limitation of the number of excitations from the condensate. The results show that at strong IB coupling, the Born approximation in the BB interaction is no longer valid. The short-scale physics must be taken into account in more detail in order to accurately describe the interplay of the BB repulsion with the IB potential as the latter causes a strong local variation in density. In particular, the shift of the resonance due to the many-body continuum is found to depend sensitively on the BB potential range. Near this critical point, a transition is also observed in time: the behaviour typical for the repulsive side of the resonance transforms into that of an attractive polaron.

The new method and its results open a number of promising directions for future works. More results can be obtained directly within the approach by further exploration of the parameter space. Interesting points are in particular an in-depth investigation of the role of a nonzero range of the impurity potential, the computation of polaron trajectories at strong coupling and properties of the ground state, which can be obtained by minimising the energy functional. Concerning the impurity potential, Shi *et al.* [Shi+18] have found that in an ideal BEC, a two-channel model may deviate from a static potential. Combining our method with a two-channel model could be another interesting approach.

Multiple impurities can be described by deriving an effective interaction between them [CB18]. It will be interesting to see how to what form of interactions the density profiles in particular on the repulsive side lead.

A different direction is the development of modifications to present Bogoliubov approaches, that take into account the importance of the BB potential range. It is not strictly necessary to apply the Born approximation and to use a local interaction term in BT but instead, the full Fourier transform of the potential may be used (this approach was taken in [Gir61]). However, even then, BT makes similar assumptions as the Born approximation (cf. the discussion in appendix A of [Lie+05]) and thus cannot directly be applied to narrow potentials. A solution may be found in Bogoliubov's original paper [Bog47] where he suggests – with credit attributed to Landau – an *a posteriori* inclusion of the two-body scattering states to treat arbitrary potential shapes. This will not resolve the problem of instability at strong coupling, but still be applicable in a parameter regime that is sensitive to the BB potential shape.

Conclusion

We have studied the behaviour of an impurity coupled to a Bose-Einstein condensate close to a scattering resonance and focused on the dynamics after a quench from a non-interacting to an interacting state.

In chapter 5, we have seen that many features could be understood in terms of the two-body eigenstates of one boson and the impurity, which are occupied collectively by the condensate wave function. Multiply occupied bound states were found to be responsible for long-lived coherent oscillations on the repulsive side of the resonance with a frequency given by the binding energy $1/2m_{\mathrm{red}}a_{\mathrm{IB}}^2$. This is an important distinction to the Fermi polaron, where the bound state can be occupied only once. The time evolution for a contact potential was solved analytically and a numerically exact RF spectrum was computed. Its emergence from the two-body spectrum was discussed by separating contributions from the zero-mode, the bound state and the continuum. In chapter 6, we have seen that the findings for the ideal BEC persist when a BB repulsion is present. By an analytical study, a mechanism leading to stable oscillations despite the additional decay channels was found and a formula for the frequencies derived. The real-space formation of Bose polarons has been discussed by means of bosonic density profiles. These converge to the stationary solution for attractive coupling while for repulsive coupling, they periodically reach zero density at a distance close to $1.45a_{\mathrm{IB}}$. The case of a moving impurity was considered and its velocity was found to exhibit the same oscillations that are visible in different other observables. This led to remarkable trajectories in the form of stop-and-go motion near the resonance. Dynamical density profiles feature an asymmetry when the particle is moving at supersonic velocities. It was found that Bogoliubov theory becomes dynamically unstable at strong coupling. In chapter 7, a new theory was derived to be able to describe BECs that are strongly deformed on a short length scale. It includes the two-boson physics explicitly in the form of Jastrow functions and a general method for working with them was developed. The resulting theory allowed to treat the Bose polaron problem across a resonance, including the transition region between the attractive and the repulsive polaron. Here, also a dynamical transition from repulsive to attractive behaviour was observed in the form of finitely many coherent oscillations followed by convergence. At strong coupling, it turned out that the description of the BB potential by a local term in Born approximation is no longer valid. Instead, the potential range becomes important and strongly influences

the position of the resonance in medium.

Inspiration for future investigations can be drawn in particular from the results of the last chapter. More interesting findings can be expected in the strong-coupling region, for instance by investigating the interplay of IB and BB potential ranges and shapes or by considering a non-zero initial velocity. Another route is the combination with works of Efimov physics [Shi+18; Yos+18]: if few-body bound states are described in full detail, the resulting states may yield an effective potential for the remaining condensate, which is subsequently treated by the methods described here. This may provide a route to address the difficult question about the ground state on the repulsive side. At intermediate coupling, the inclusion of a finite-range potential in BT could turn out an efficient approach that is able to describe some features that cannot be obtained with standard BT.

Experimental realisations of the Bose polaron are being achieved at an increasing rate and we hope to have contributed to the awareness of the interest of the repulsive side of a Feshbach resonance. The shift of the resonance that we have found in chapter 7 might be of help here, because the interesting transition region is situated further inside the repulsive region where three-body-losses are less likely than at the resonance. Ramsey experiments and direct imaging are promising techniques and we are particularly curious on results about the time-resolved polaron formation. A first such result concerning the coherence dynamics for attractive coupling was obtained recently [Sko+20].

The Bose polaron is an instance of the general concept of a quantum particle immersed in a medium. We presented techniques to treat the strongly interacting region, which may be of interest also to other systems where strong coupling is accessible. Likewise, the connections between two-body and many-body physics and the influence of bound states are general concepts, which may have their correspondence in other systems.

Acknowledgements

Three and a half years of study and research lie behind me and many great people have contributed to make this a fruitful and enjoyable time.

First of all, I wish to thank my supervisor Priv.-Doz. Dr. Tilman Enss for his support and guidance during the period of my Ph.D. studies. I am particularly grateful for the faith he put in me in giving me the freedom to explore new paths and develop own ideas. A special thanks is devoted to the warm and helpful support in the time of writing my thesis.

I would like to thank Prof. Dr. Thomas Gasenzer for taking the time and effort to referee this thesis. I am also grateful to Prof. Dr. Markus Oberthaler and Prof. Dr. Matthias Bartelmann for being examiners in my oral exam and for the interest in my work.

I very much thank Prof. Dr. Manfred Salmhofer for his faith and support as well as for enlightening and stimulating discussions.

I would also like to thank Prof. Dr. Matthias Weidemüller and the team of project C03 for many interesting discussions in a great atmosphere.

In spite of the fascination that research presents, the everyday work at Philosophenweg would not have been half as enjoyable if it were not for the excellent people that I was lucky to have met there. My warmest thanks therefore go to my friends of the regular lunch group, to the citizens of the Free Cake Kingdom as well as to all present and former colleagues of the adjacent rooms at Philosophenweg 19.

During the long period of research and study there was one constant upon which I could always rely. I consider myself most fortunate to have a family that supports me in all possible ways. For this, it is my deep desire to say: Thank you.

Appendix A

Some integrals

In the context of the continuum states of the contact Hamiltonian, we need the following integrals.

$$\int_{\mathbb{R}} \frac{e^{-ik^2t}}{1+a^2k^2}\,\mathrm{d}k = \frac{\pi}{a} e^{\frac{it}{a^2}} \left(\operatorname{sgn}(a) - \operatorname{erf}\frac{\sqrt{it}}{a}\right) \tag{A.1a}$$

$$\int_{\mathbb{R}} \frac{e^{-ik^2t+ikx}}{ak-i}\,\mathrm{d}k = \frac{i\pi}{a} e^{\frac{it}{a^2}-\frac{x}{a}} \left(\operatorname{sgn}(a) - \operatorname{erf}\left(\frac{\sqrt{it}}{a} - \frac{x}{2\sqrt{it}}\right)\right) \tag{A.1b}$$

$$\mathcal{P}\int_{\mathbb{R}} \frac{e^{-ik^2t+ikx}}{k}\,\mathrm{d}k = -i\pi \operatorname{erf}\left(\frac{x}{2\sqrt{it}}\right) \tag{A.1c}$$

$$\int_{\mathbb{R}_+} e^{ikr}\,\mathrm{d}r = \pi\delta(k) + \mathcal{P}\frac{i}{k} \tag{A.1d}$$

where $\operatorname{Im} t < 0$ in (a)–(c) to ensure convergence of integral and (d) holds in the sense of distributions of a scalar $k \in \mathbb{R}$. The '$\mathcal{P}$' in $\mathcal{P}\frac{1}{k}$ is omitted in the applications in the main text.

Proof

In the following it is always easy to find dominating functions to show holomorphy of integrals.

(a) Consider

$$I_1(\alpha,\gamma) = \int_{\mathbb{R}} \frac{e^{-\alpha k^2}}{k^2+\gamma^2}\,\mathrm{d}k$$

for $\alpha \in \mathbb{C}$, $\operatorname{Re}\alpha > 0$, $\gamma \in \mathbb{R}\setminus\{0\}$. Then

$$\frac{\partial}{\partial\alpha} e^{-\alpha\gamma^2} I_1(\alpha,\gamma) = -e^{-\alpha\gamma^2} \int_{\mathbb{R}} e^{-\alpha k^2}\,\mathrm{d}k = -\sqrt{\frac{\pi}{\alpha}} e^{-\alpha\gamma^2}.$$

Consequently,

$$\begin{aligned} I_1(\alpha,\gamma) &= -e^{\alpha\gamma^2}\int^{\alpha}\sqrt{\frac{\pi}{\alpha'}}e^{-\alpha'\gamma^2}\,\mathrm{d}\alpha' \\ &\quad\Big|\ s=\gamma\sqrt{\alpha'} \\ &= -\sqrt{\pi}e^{\alpha\gamma^2}\int^{\gamma\sqrt{\alpha}} e^{-s^2}\frac{2\,\mathrm{d}s}{\gamma} \\ &= -\frac{\pi}{\gamma}e^{\alpha\gamma^2}(\operatorname{erf}(\gamma\sqrt{\alpha})+C_1(\gamma)) \\ &\quad\Big|\ I_1(+\infty,\gamma)=0 \\ &= \frac{\pi}{\gamma}e^{\alpha\gamma^2}(\operatorname{sgn}(\gamma)-\operatorname{erf}(\gamma\sqrt{\alpha}))\,. \end{aligned}$$

Equation (A.1a) follows with $\alpha = it$, $\gamma = 1/a$.

(b) Now set

$$I_2(\alpha,\beta,\gamma) = \int_{\mathbb{R}}\frac{e^{-\alpha k^2+\beta k}}{k-i\gamma}\,\mathrm{d}k$$

for $\alpha,\beta\in\mathbb{C}$, $\gamma\in\mathbb{R}$, $\operatorname{Re}\alpha>0$. Then

$$\frac{\partial}{\partial\beta}e^{-i\gamma\beta}I_2 = e^{-i\gamma\beta}\int_{\mathbb{R}}e^{-\alpha k^2+\beta k}\,\mathrm{d}k = \sqrt{\frac{\pi}{\alpha}}e^{\frac{\beta^2}{4\alpha}-i\gamma\beta}.$$

Therefore,

$$\begin{aligned} I_2 &= e^{i\beta\gamma}\int^{\beta}\sqrt{\frac{\pi}{\alpha}}e^{\frac{\beta'^2}{4\alpha}-i\gamma\beta'}\,\mathrm{d}\beta' \\ &\quad\Big|\ s=\tfrac{i\beta'}{2\sqrt{\alpha}}+\gamma\sqrt{\alpha} \\ &= \sqrt{\frac{\pi}{\alpha}}e^{i\beta\gamma}\int^{\frac{i\beta}{2\sqrt{\alpha}}+\gamma\sqrt{\alpha}} e^{-s^2+\gamma^2\alpha}\frac{2\sqrt{\alpha}}{i}\,\mathrm{d}s \\ &= -i\pi e^{i\beta\gamma+\gamma^2\alpha}\left(\operatorname{erf}\left(\frac{i\beta}{2\sqrt{\alpha}}+\gamma\sqrt{\alpha}\right)+C_2(\alpha,\gamma)\right). \end{aligned}$$

To evaluate the constant, compute $I_2(\alpha,0,\gamma)$:

$$\begin{aligned} I_2(\alpha,0,\gamma) &= \int_{\mathbb{R}}e^{-\alpha k^2}\frac{k+i\gamma}{k^2+\gamma^2}\,\mathrm{d}k = i\gamma\int_{\mathbb{R}}\frac{e^{-\alpha k^2}}{k^2+\gamma^2} \\ &= i\gamma I_1 = i\pi e^{\alpha\gamma^2}(\operatorname{erf}(\gamma\sqrt{\alpha})-\operatorname{sgn}(\gamma))\,. \end{aligned}$$

Thus,

$$I_2(\alpha,\beta,\gamma) = i\pi e^{\alpha\gamma^2+i\beta\gamma}\left(\operatorname{sgn}(\gamma)-\operatorname{erf}\left(\frac{i\beta}{2\sqrt{\alpha}}+\gamma\sqrt{\alpha}\right)\right).$$

(c) By the Sokhotski-Plemelj theorem,

$$\begin{aligned} \mathcal{P}\int\frac{e^{-\alpha k^2+\beta k}}{k}\,\mathrm{d}k &= \lim_{\gamma\to 0}\frac{I_2(\alpha,\beta,\gamma)+I_2(\alpha,\beta,-\gamma)}{2} \\ &= -i\pi\operatorname{erf}\left(\frac{i\beta}{2\sqrt{\alpha}}\right). \end{aligned}$$

(d) Taking $\beta = ir$ in (c), the limit $\alpha \searrow 0$ can be taken if the integral is understood in the sense of distributions. This yields

$$\begin{aligned} & \int \mathcal{P}\frac{e^{irk}}{k}\,\mathrm{d}k = -i\pi\,\mathrm{sgn}(r) \\ \Rightarrow \quad & 2i\mathscr{F}^{-1}\left[\mathcal{P}\frac{1}{k}\right] = \mathrm{sgn}\ . \end{aligned}$$

Consequently,

$$\int_{\mathbb{R}_+} e^{ikr}\,\mathrm{d}r = \mathscr{F}[\theta](k) = \frac{1}{2}\mathscr{F}[1+\mathrm{sgn}\,](k) = \pi\delta(k) + \mathcal{P}\frac{i}{k}\,.$$

Publications

Used in Dissertation

[DSE19] M. Drescher, M. Salmhofer, and T. Enss. *Real-Space Dynamics of Attractive and Repulsive Polarons in Bose-Einstein Condensates*. Physical Review A 99.2 (Feb. 2019), p. 023601.

[DSE20] M. Drescher, M. Salmhofer, and T. Enss. *Theory of a Resonantly Interacting Impurity in a Bose-Einstein Condensate* (Mar. 2020). arXiv: 2003.01982. Submitted to Physical Review Letters.

Not Used in Dissertation

[DM17] M. Drescher and A. Mielke. *Hard-Core Bosons in Flat Band Systems above the Critical Density*. The European Physical Journal B 90.11 (Nov. 2017), p. 217.

References

[Alb+88] S. Albeverio et al. *Solvable Models in Quantum Mechanics*. Theoretical and Mathematical Physics. Berlin Heidelberg: Springer-Verlag, 1988.

[AP04] G. E. Astrakharchik and L. P. Pitaevskii. *Motion of a Heavy Impurity through a Bose-Einstein Condensate*. Physical Review A 70.1 (July 2004), p. 013608.

[BBJ08] M. Bruderer, W. Bao, and D. Jaksch. *Self-Trapping of Impurities in Bose-Einstein Condensates: Strong Attractive and Repulsive Coupling*. EPL (Europhysics Letters) 82.3 (Apr. 2008), p. 30004.

[BBT13] A. A. Blinova, M. G. Boshier, and E. Timmermans. *Two Polaron Flavors of the Bose-Einstein Condensate Impurity*. Physical Review A 88.5 (Nov. 2013), p. 053610.

[Bla52] J. M. Blatt. *VF Weisskopf Theoretical Nuclear Physics*. John Willey and sons (Seventh edition, 1963) (1952).

[Bog47] N. Bogoliubov. *On the Theory of Superfluidity*. Journal of Physics (USSR) XI.1 (1947), pp. 23–32.

[Bou14] A. Boudjemâa. *Self-Localized State and Solitons in a Bose-Einstein-Condensate–Impurity Mixture at Finite Temperature*. Physical Review A 90.1 (July 2014), p. 013628.

[Boy+19] D. Boyanovsky et al. *Dynamics of Relaxation and Dressing of a Quenched Bose Polaron*. Physical Review A 100.4 (Oct. 2019), p. 043617.

[Bre47] G. Breit. *The Scattering of Slow Neutrons by Bound Protons. I. Methods of Calculation*. Physical Review 71.4 (Feb. 1947), pp. 215–231.

[BS19] C. Brennecke and B. Schlein. *Gross–Pitaevskii Dynamics for Bose–Einstein Condensates*. Analysis & PDE 12.6 (Feb. 2019), pp. 1513–1596.

[Cam+18] F. Camargo et al. *Creation of Rydberg Polarons in a Bose Gas*. Physical Review Letters 120.8 (Feb. 2018), p. 083401.

[Cas+11] W. Casteels et al. *Strong Coupling Treatment of the Polaronic System Consisting of an Impurity in a Condensate*. Laser Physics 21.8 (July 2011), p. 1480.

[Cat+12] J. Catani et al. *Quantum Dynamics of Impurities in a One-Dimensional Bose Gas*. Physical Review A 85.2 (Feb. 2012), p. 023623.

[CB18] A. Camacho-Guardian and G. M. Bruun. *Landau Effective Interaction between Quasiparticles in a Bose-Einstein Condensate*. Physical Review X 8.3 (Aug. 2018), p. 031042.

[CLB15] R. S. Christensen, J. Levinsen, and G. M. Bruun. *Quasiparticle Properties of a Mobile Impurity in a Bose-Einstein Condensate*. Physical Review Letters 115.16 (Oct. 2015), p. 160401.

[CS02] A. Y. Cherny and A. A. Shanenko. *The Kinetic and Interaction Energies of a Trapped Bose Gas: Beyond the Mean Field*. Physics Letters A 293.5 (Feb. 2002), pp. 287–292.

[CT06] F. M. Cucchietti and E. Timmermans. *Strong-Coupling Polarons in Dilute Gas Bose-Einstein Condensates*. Physical Review Letters 96.21 (June 2006), p. 210401.

[CTD12] W. Casteels, J. Tempere, and J. T. Devreese. *Polaronic Properties of an Impurity in a Bose-Einstein Condensate in Reduced Dimensions*. Physical Review A 86.4 (Oct. 2012), p. 043614.

[DA09] J. T. Devreese and A. S. Alexandrov. *Fröhlich Polaron and Bipolaron: Recent Developments*. Reports on Progress in Physics 72.6 (May 2009), p. 066501.

[Din49] R. B. Dingle. *The Zero-Point Energy of a System of Particles*. The London, Edinburgh, and Dublin Philosophical Magazine and Journal of Science 40.304 (May 1949), pp. 573–578.

[DK13] D. Dasenbrook and A. Komnik. *Semiclassical Polaron Dynamics of Impurities in Ultracold Gases*. Physical Review B 87.9 (Mar. 2013), p. 094301.

[DSE19] M. Drescher, M. Salmhofer, and T. Enss. *Real-Space Dynamics of Attractive and Repulsive Polarons in Bose-Einstein Condensates*. Physical Review A 99.2 (Feb. 2019), p. 023601.

[DSE20] M. Drescher, M. Salmhofer, and T. Enss. *Theory of a Resonantly Interacting Impurity in a Bose-Einstein Condensate* (Mar. 2020). arXiv: 2003.01982. Submitted to Physical Review Letters.

[Dys57] F. J. Dyson. *Ground-State Energy of a Hard-Sphere Gas*. Physical Review 106.1 (Apr. 1957), pp. 20–26.

[ESY07] L. Erdős, B. Schlein, and H.-T. Yau. *Derivation of the Cubic Non-Linear Schrödinger Equation from Quantum Dynamics of Many-Body Systems*. Inventiones mathematicae 167.3 (Mar. 2007), pp. 515–614.

[ESY09] L. Erdős, B. Schlein, and H.-T. Yau. *Rigorous Derivation of the Gross-Pitaevskii Equation with a Large Interaction Potential*. Journal of the American Mathematical Society 22.4 (2009), pp. 1099–1156.

[Fer36] E. Fermi. *Sul Moto Dei Neutroni Nelle Sostanze Idrogenate*. Ricerca scientifica 7.2 (1936), pp. 13–52.

[Fey55] R. P. Feynman. *Slow Electrons in a Polar Crystal*. Physical Review 97.3 (Feb. 1955), pp. 660–665.

[Frö54] H. Fröhlich. *Electrons in Lattice Fields*. Advances in Physics 3.11 (July 1954), pp. 325–361.

[GAD17] F. Grusdt, G. E. Astrakharchik, and E. Demler. *Bose Polarons in Ultracold Atoms in One Dimension: Beyond the Fröhlich Paradigm*. New Journal of Physics 19.10 (2017).

[GD16] F. Grusdt and E. Demler. *New Theoretical Approaches to Bose Polarons*. Proceedings of the International School of Physics "Enrico Ferm" 191.Quantum Matter at Ultralow Temperatures (2016), pp. 325–411.

[Gin68] J. Ginibre. *On the Asymptotic Exactness of the Bogoliubov Approximation for Many Boson Systems*. Communications in Mathematical Physics 8.1 (Mar. 1968), pp. 26–51.

[Gir61] M. Girardeau. *Motion of an Impurity Particle in a Boson Superfluid*. The Physics of Fluids 4.3 (Mar. 1961), pp. 279–291.

[Gro61] E. P. Gross. *Structure of a Quantized Vortex in Boson Systems*. Il Nuovo Cimento (1955-1965) 20.3 (May 1961), pp. 454–477.

[Gru+15] F. Grusdt et al. *Renormalization Group Approach to the Fröhlich Polaron Model: Application to Impurity-BEC Problem*. Scientific Reports 5.1 (Dec. 2015), p. 12124.

[Gru+17] F. Grusdt et al. *Strong-Coupling Bose Polarons in a Bose-Einstein Condensate*. Physical Review A 96.1 (July 2017), p. 013607.

[Gru+18] F. Grusdt et al. *Strong-Coupling Bose Polarons out of Equilibrium: Dynamical Renormalization-Group Approach*. Physical Review A 97.3 (Mar. 2018), p. 033612.

[Gru16] F. Grusdt. *All-Coupling Theory for the Fröhlich Polaron*. Physical Review B 93.14 (Apr. 2016), p. 144302.

[Gue+18] N.-E. Guenther et al. *Bose Polarons at Finite Temperature and Strong Coupling*. Physical Review Letters 120.5 (Feb. 2018), p. 050405.

[Hu+16] M.-G. Hu et al. *Bose Polarons in the Strongly Interacting Regime*. Physical Review Letters 117.5 (July 2016), p. 055301.

[HW09] B.-B. Huang and S.-L. Wan. *Polaron in Bose-Einstein-Condensation System*. Chinese Physics Letters 26.8 (July 2009), p. 80302.

[HY57] K. Huang and C. N. Yang. *Quantum-Mechanical Many-Body Problem with Hard-Sphere Interaction*. Physical Review 105.3 (Feb. 1957), pp. 767–775.

[Jas55] R. Jastrow. *Many-Body Problem with Strong Forces*. Physical Review 98.5 (June 1955), pp. 1479–1484.

[Jør+16] N. B. Jørgensen et al. *Observation of Attractive and Repulsive Polarons in a Bose-Einstein Condensate*. Physical Review Letters 117.5 (July 2016), p. 055302.

[KB06] R. M. Kalas and D. Blume. *Interaction-Induced Localization of an Impurity in a Trapped Bose-Einstein Condensate*. Physical Review A 73.4 (Apr. 2006), p. 043608.

[KL16] B. Kain and H. Y. Ling. *Generalized Hartree-Fock-Bogoliubov Description of the Fröhlich Polaron*. Physical Review A 94.1 (July 2016), p. 013621.

[KL18] B. Kain and H. Y. Ling. *Analytical Study of Static Beyond-Fröhlich Bose Polarons in One Dimension*. Physical Review A 98.3 (Sept. 2018), p. 033610.

[Lam+17] A. Lampo et al. *Bose Polaron as an Instance of Quantum Brownian Motion*. Quantum 1 (Sept. 2017), p. 30.

[Lan33] L. D. Landau. *Über Die Bewegung Der Elektronen in Kristallgittern. Electron Motion in Crystal Lattices*. Physikalische Zeitschrift der Sowjetunion 3 (1933), p. 664.

[Lan41] L. Landau. *Theory of the Superfluidity of Helium II*. Physical Review 60.4 (Aug. 1941), pp. 356–358.

[LD14] W. Li and S. Das Sarma. *Variational Study of Polarons in Bose-Einstein Condensates*. Physical Review A 90.1 (July 2014), p. 013618.

[Lev+17] J. Levinsen et al. *Finite-Temperature Behavior of the Bose Polaron*. Physical Review A 96.6 (Dec. 2017), p. 063622.

[Lie+05] E. H. Lieb et al., eds. *The Mathematics of the Bose Gas and Its Condensation*. Oberwolfach Seminars. Basel: Birkhäuser, 2005.

[LLP53] T. D. Lee, F. E. Low, and D. Pines. *The Motion of Slow Electrons in a Polar Crystal*. Physical Review 90.2 (Apr. 1953), pp. 297–302.

[LP48] L. D. Landau and S. I. Pekar. *Effective Mass of a Polaron*. Zhurnal Eksperimentalnoi I Teoreticheskoi Fiziki 18.5 (1948), pp. 419–423.

[LPB15] J. Levinsen, M. M. Parish, and G. M. Bruun. *Impurity in a Bose-Einstein Condensate and the Efimov Effect*. Physical Review Letters 115.12 (Sept. 2015), p. 125302.

[LSY00] E. H. Lieb, R. Seiringer, and J. Yngvason. *Bosons in a Trap: A Rigorous Derivation of the Gross-Pitaevskii Energy Functional*. Physical Review A 61.4 (Mar. 2000), p. 043602.

[LWF18] T. Lausch, A. Widera, and M. Fleischhauer. *Prethermalization in the Cooling Dynamics of an Impurity in a Bose-Einstein Condensate*. Physical Review A 97.2 (Feb. 2018), p. 023621.

[LY98] E. H. Lieb and J. Yngvason. *Ground State Energy of the Low Density Bose Gas*. Physical Review Letters 80.12 (Mar. 1998), pp. 2504–2507.

[Mis+19] S. I. Mistakidis et al. *Quench Dynamics and Orthogonality Catastrophe of Bose Polarons*. Physical Review Letters 122.18 (May 2019), p. 183001.

[MPS05] P. Massignan, C. J. Pethick, and H. Smith. *Static Properties of Positive Ions in Atomic Bose-Einstein Condensates*. Physical Review A 71.2 (Feb. 2005), p. 023606.

[MZD12] C. J. M. Mathy, M. B. Zvonarev, and E. Demler. *Quantum Flutter of Supersonic Particles in One-Dimensional Quantum Liquids*. Nature Physics 8.12 (Dec. 2012), pp. 881–886.

[Nie+19] K. K. Nielsen et al. *Critical Slowdown of Non-Equilibrium Polaron Dynamics*. New Journal of Physics 21.4 (Apr. 2019), p. 043014.

[PD48] S. I. Pekar and M. F. Deigen. *Quantum States and Optical Transitions of Electron in a Polaron and at a Color Center of a Crystal*. Zhurnal Eksperimentalnoi I Teoreticheskoi Fiziki 18.6 (1948), pp. 481–486.

[Pek46a] S. I. Pekar. *Local Quantum States of Electrons in an Ideal Ion Crystal*. Zhurnal Eksperimentalnoi I Teoreticheskoi Fiziki 16.4 (1946), pp. 341–348.

[Pek46b] S. I. Pekar. *Autolocalization of the Electron in a Dielectric Inertially Polarizing Medium*. Zhurnal Eksperimentalnoi i Teoreticheskoi Fiziki 16.4 (1946), pp. 335–340.

[Pek47] S. I. Pekar. *Theory of Colored Crystals*. Zhurnal Eksperimentalnoi i Teoreticheskoi Fiziki 17 (1947), p. 868.

[Pek48] S. I. Pekar. *New View on Electronic Conductivity of Ionic Crystals*. Zhurnal Eksperimentalnoi i Teoreticheskoi Fiziki 18 (1948), p. 105.

[Peñ+19] L. A. Peña Ardila et al. *Analyzing a Bose Polaron across Resonant Interactions*. Physical Review A 99.6 (June 2019), p. 063607.

[PG15] L. A. Peña Ardila and S. Giorgini. *Impurity in a Bose-Einstein Condensate: Study of the Attractive and Repulsive Branch Using Quantum Monte Carlo Methods*. Physical Review A 92.3 (Sept. 2015), p. 033612.

[Pit61] L. P. Pitaevskii. *Vortex Lines in an Imperfect Bose Gas*. Journal of Experimental and Theoretical Physics (U.S.S.R.) 40 (1961), pp. 646–651.

[PS03] L. P. Pitaevskii and S. Stringari. *Bose-Einstein Condensation*. International Series of Monographs on Physics. Oxford, New York: Oxford University Press, Apr. 2003.

[Ren+16] T. Rentrop et al. *Observation of the Phononic Lamb Shift with a Synthetic Vacuum*. Physical Review X 6.4 (Nov. 2016), p. 041041.

[RS13] S. P. Rath and R. Schmidt. *Field-Theoretical Study of the Bose Polaron*. Physical Review A 88.5 (Nov. 2013), p. 053632.

[RS79] M. Reed and B. Simon. *Methods of Modern Mathematical Physics. III. Scattering Theory* (Jan. 1979).

[Sce+13] R. Scelle et al. *Motional Coherence of Fermions Immersed in a Bose Gas*. Physical Review Letters 111.7 (Aug. 2013), p. 070401.

[Sch+18] R. Schmidt et al. *Theory of Excitation of Rydberg Polarons in an Atomic Quantum Gas*. Physical Review A 97.2 (Feb. 2018), p. 022707.

[Sha+14] A. Shashi et al. *Radio-Frequency Spectroscopy of Polarons in Ultracold Bose Gases*. Physical Review A 89.5 (May 2014), p. 053617.

[Shc+16a] Y. E. Shchadilova et al. *Polaronic Mass Renormalization of Impurities in Bose-Einstein Condensates: Correlated Gaussian-Wave-Function Approach*. Physical Review A 93.4 (Apr. 2016), p. 043606.

[Shc+16b] Y. E. Shchadilova et al. *Quantum Dynamics of Ultracold Bose Polarons*. Physical Review Letters 117.11 (Sept. 2016), p. 113002.

[Shi+18] Z.-Y. Shi et al. *Impurity-Induced Multibody Resonances in a Bose Gas*. Physical Review Letters 121.24 (Dec. 2018), p. 243401.

[Sko+20] M. G. Skou et al. *Non-Equilibrium Dynamics of Quantum Impurities* (May 2020). arXiv: 2005.00424.

[SL15] R. Schmidt and M. Lemeshko. *Rotation of Quantum Impurities in the Presence of a Many-Body Environment*. Physical Review Letters 114.20 (May 2015), p. 203001.

[SSD16] R. Schmidt, H. R. Sadeghpour, and E. Demler. *Mesoscopic Rydberg Impurity in an Atomic Quantum Gas*. Physical Review Letters 116.10 (Mar. 2016), p. 105302.

[ST06] K. Sacha and E. Timmermans. *Self-Localized Impurities Embedded in a One-Dimensional Bose-Einstein Condensate and Their Quantum Fluctuations*. Physical Review A 73.6 (June 2006), p. 063604.

[SZC17] M. Sun, H. Zhai, and X. Cui. *Visualizing the Efimov Correlation in Bose Polarons*. Physical Review Letters 119.1 (July 2017), p. 013401.

[Tak+19] J. Takahashi et al. *Bose Polaron in Spherical Trap Potentials: Spatial Structure and Quantum Depletion*. Physical Review A 100.2 (Aug. 2019), p. 023624.

[Tan08] S. Tan. *Energetics of a Strongly Correlated Fermi Gas*. Annals of Physics 323.12 (Dec. 2008), pp. 2952–2970.

[Tem+09] J. Tempere et al. *Feynman Path-Integral Treatment of the BEC-Impurity Polaron*. Physical Review B 80.18 (Nov. 2009), p. 184504.

[Thi13] W. Thirring. *Lehrbuch der Mathematischen Physik: Band 3: Quantenmechanik von Atomen und Molekülen*. Springer-Verlag, Mar. 2013.

[VH17] A. G. Volosniev and H.-W. Hammer. *Analytical Approach to the Bose-Polaron Problem in One Dimension*. Physical Review A 96.3 (Sept. 2017), p. 031601.

[VHZ15] A. G. Volosniev, H.-W. Hammer, and N. T. Zinner. *Real-Time Dynamics of an Impurity in an Ideal Bose Gas in a Trap*. Physical Review A 92.2 (Aug. 2015), p. 023623.

[Vli+15] J. Vlietinck et al. *Diagrammatic Monte Carlo Study of the Acoustic and the Bose–Einstein Condensate Polaron*. New Journal of Physics 17.3 (Mar. 2015), p. 033023.

[Yan+20] Z. Z. Yan et al. *Bose Polarons near Quantum Criticality*. Science 368.6487 (Apr. 2020), pp. 190–194.

[Yng14] J. Yngvason. *Topics in the Mathematical Physics of Cold Bose Gases* (Feb. 2014). arXiv: 1402.0706.

[Yos+18] S. M. Yoshida et al. *Universality of an Impurity in a Bose-Einstein Condensate*. Physical Review X 8.1 (Feb. 2018), p. 011024.

[Zwe12] W. Zwerger, ed. *The BCS-BEC Crossover and the Unitary Fermi Gas*. Lecture Notes in Physics 836. Heidelberg: Springer, 2012.